ECSS-E-HB-31-01 Part 3A
5 December 2011

Space engineering

Thermal design handbook - Part 3: Spacecraft Surface Temperature

ECSS Secretariat
ESA-ESTEC
Requirements & Standards Division
Noordwijk, The Netherlands

Foreword

This Handbook is one document of the series of ECSS Documents intended to be used as supporting material for ECSS Standards in space projects and applications. ECSS is a cooperative effort of the European Space Agency, national space agencies and European industry associations for the purpose of developing and maintaining common standards.

The material in this Handbook is a collection of data gathered from many projects and technical journals which provides the reader with description and recommendation on subjects to be considered when performing the work of Thermal design.

The material for the subjects has been collated from research spanning many years, therefore a subject may have been revisited or updated by science and industry.

The material is provided as good background on the subjects of thermal design, the reader is recommended to research whether a subject has been updated further, since the publication of the material contained herein.

This handbook has been prepared by ESA TEC-MT/QR division, reviewed by the ECSS Executive Secretariat and approved by the ECSS Technical Authority.

Disclaimer

Published by: ESA Requirements and Standards Division
ESTEC, P.O. Box 299,
2200 AG Noordwijk
The Netherlands

Table of contents

Figures

Tables

1 Scope

Factors affecting the equilibrium temperature of a spacecraft surface are described in this Part 3 using simple geometrical configurations and basic assumptions.

Methods for conducting calculations on the affect of Solar, planetary and albedo radiation are given taking into consideration the internal and immediate environmental factors and incorporating the various configurations and dimensions of the constituent parts.

The Thermal design handbook is published in 16 Parts

ECSS-E-HB-31-01 Part 1	Thermal design handbook – Part 1: View factors
ECSS-E-HB-31-01 Part 2	Thermal design handbook – Part 2: Holes, Grooves and Cavities
ECSS-E-HB-31-01 Part 3	Thermal design handbook – Part 3: Spacecraft Surface Temperature
ECSS-E-HB-31-01 Part 4	Thermal design handbook – Part 4: Conductive Heat Transfer
ECSS-E-HB-31-01 Part 5	Thermal design handbook – Part 5: Structural Materials: Metallic and Composite
ECSS-E-HB-31-01 Part 6	Thermal design handbook – Part 6: Thermal Control Surfaces
ECSS-E-HB-31-01 Part 7	Thermal design handbook – Part 7: Insulations
ECSS-E-HB-31-01 Part 8	Thermal design handbook – Part 8: Heat Pipes
ECSS-E-HB-31-01 Part 9	Thermal design handbook – Part 9: Radiators
ECSS-E-HB-31-01 Part 10	Thermal design handbook – Part 10: Phase – Change Capacitors
ECSS-E-HB-31-01 Part 11	Thermal design handbook – Part 11: Electrical Heating
ECSS-E-HB-31-01 Part 12	Thermal design handbook – Part 12: Louvers
ECSS-E-HB-31-01 Part 13	Thermal design handbook – Part 13: Fluid Loops
ECSS-E-HB-31-01 Part 14	Thermal design handbook – Part 14: Cryogenic Cooling
ECSS-E-HB-31-01 Part 15	Thermal design handbook – Part 15: Existing Satellites
ECSS-E-HB-31-01 Part 16	Thermal design handbook – Part 16: Thermal Protection System

2 References

ECSS-S-ST-00-01	ECSS System - Glossary of terms

All other references made to publications in this Part are listed, alphabetically, in the **Bibliography**.

3 Terms, definitions and symbols

3.1 Terms and definitions

For the purpose of this Standard, the terms and definitions given in ECSS-S-ST-00-01 apply.

3.2 Symbols

A_E	emitting area of the spacecraft, [m²]
A_I	area of the spacecraft projected from the sun, [m²]
B_i	parameters of the truncated power series development of F_{SP}, see clause 6.1
F	Albedo view factor from spacecraft to planet
F_{SP}	view factor from spacecraft to planet
R_P	mean radius of the planet, [m]
S	solar flux, [W.m^{-4}] $S = S_0.d^{-2}$
S_0	solar constant, $S_0 = 1353$ W.m^{-2}
T	temperature, [K]
T_A	Albedo temperature, [K] $T_A = [aS_0/\sigma d^2]^{1/4}$
T_R	radiation equilibrium temperature of the infinitely conductive spacecraft, [K]
T_{RA}	radiation equilibrium temperature of the infinitely conductive spacecraft under Albedo radiation, [K]
T_{RP}	radiation equilibrium temperature of the infinitely conductive spacecraft under planetary radiation, [K]
T_P	equivalent planet temperature, [K] $T_P = (e/\sigma)^{1/4}$
T_s	equivalent surrounding temperature, [K]
a	mean Albedo of the planet

b	wall thickness, [m]
c	specific heat, [J.kg^{-1}.K^{-1}]
d	Clause 5: distance from the sun center to the spacecraft, [AU]
e	mean emissive power of the planet per unit area, [W.m^{-2}]
h	distance from the spacecraft to the planet surface, [m]
k	thermal conductivity, [W.m^{-1}.K^{-1}]
γ	dimensionless specific heat in the spinning thin-walled spacecraft, $\gamma = (\rho b c \omega)/(\varepsilon \sigma T_R^3)$
α	hemispherical absorptance
α_s	solar absorptance
ε	hemispherical total emittance
μ	dimensionless thermal conductance in the thin-walled spacecraft, $\mu = (kb)/(\varepsilon \sigma T_R^3 R^2)$, where R is the characteristic length of the spacecraft surface
ρ	density, [kg.m^{-3}]
σ	Stefan-Boltzmann constant, $\sigma = 5{,}6697\text{x}10^{-8}$ W.m^{-2}.K^{-4}
τ	dimensionless temperature, $\tau = T/T_R$.
ω	angular velocity of the spinning spacecraft

Other symbols, mainly used to define the geometry of the configuration, are introduced when required

4
Solar radiation

4.1 General

Data on the equilibrium temperature of a satellite, heated by the Sun, and cooled by radiation to the outer space, are presented in this Clause. Fairly simple geometrical configurations are considered. The temperature field within the satellite corresponds to either of the following two simplifying assumptions.

1. Infinitely conductive satellite. The satellite is constituted by a homogeneous solid body, exhibiting large thermal conductivity. The temperature of the satellite is uniform. This temperature is usually named Spacecraft Radiation Equilibrium Temperature, and is represented by T_R. The following additional assumptions have been used for the calculations:

   (a) The heat addition is by parallel radiation from the Sun.

   (b) The Equivalent Surrounding temperature, T_S, is assumed to be zero.

   (c) Emittance and solar absorptance of the satellite surface are independent of both temperature and wavelength.

   (d) Absorptance is independent of the angle between the surface normal and the direction of the incoming radiation.

The Spacecraft Radiation Equilibrium Temperatures, T_R, is given by

$$T_R = \left(\frac{\alpha_s}{s} \frac{A_I}{A_E} \frac{S_o}{\sigma d^2} + T_s^4 \right)^{1/4} \qquad [4\text{-}1]$$

where T_s is assumed to be zero as it has been indicated > above.

1. Satellites of finite thermal conductivity. A limited amount of the data presented in this Clause concerns bodies of finite thermal conductivity. Some knowledge of the internal structure of the satellite is required to evaluate the temperature field. Here it is assumed that the satellite is a thin-walled body with no internal conductive structure, furthermore, in most cases the gas contained within the body is assumed to be opaque and non conducting.

The data presented are based on the following assumptions:

   (a) The heat addition is by parallel radiation from the Sun.

   (b) The Equivalent Surrounding Temperature, T_s, is assumed to be zero.

(c) The configuration has an axis of symmetry, solar radiation being parallel to this axis.

(d) Emittance and solar absorptance of the satellite surface are independent of both temperature and wavelength.

(e) Thermal conductivity is temperature independent.

(f) Lambert's law is assumed to govern reflection and emission.

(g) The body is filled with an opaque non-conducting gas.

The results are presented in terms of the local temperature, T, made dimensionless with the Spacecraft Radiation Equilibrium Temperature, T_R.

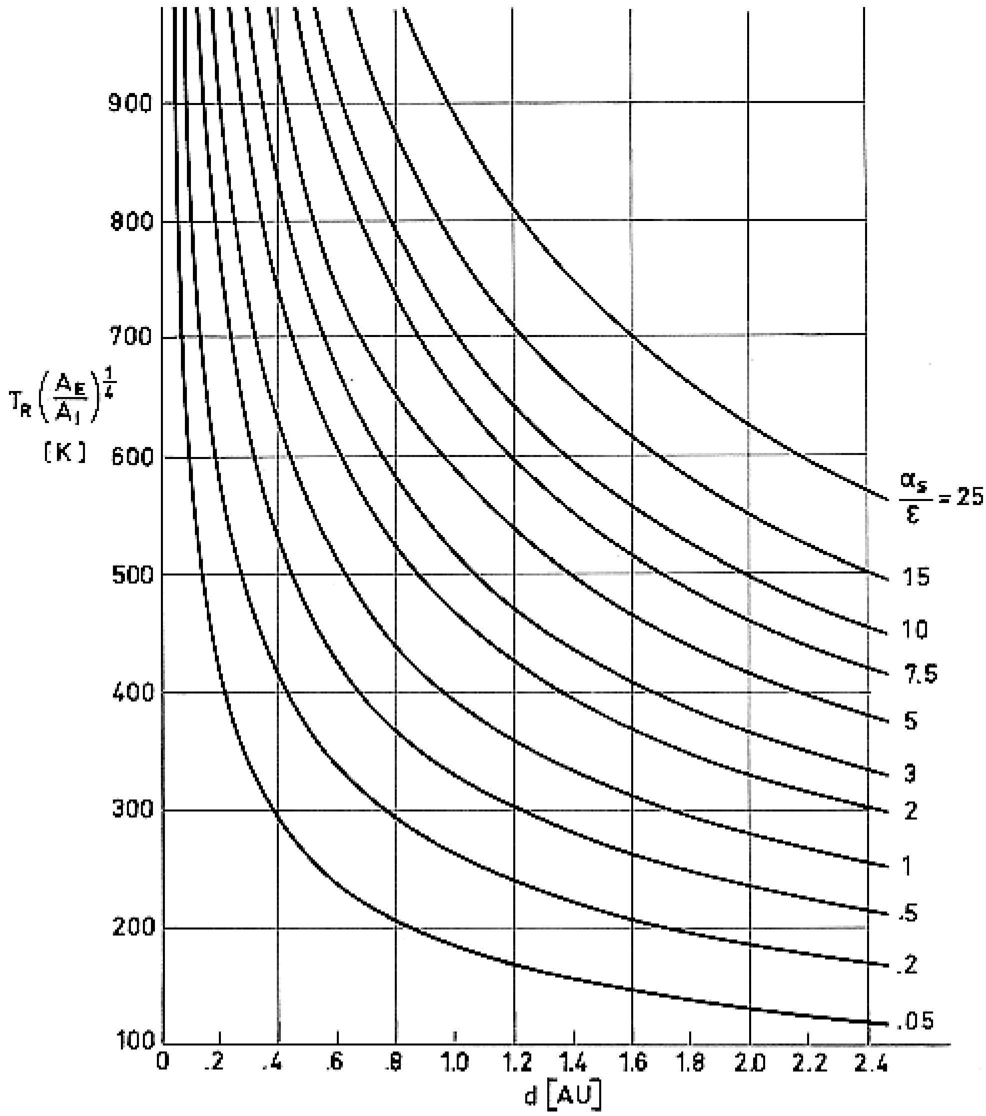

Note: non-si units are used in this figure

Figure 4-1: The function $T_R(A_E/A_I)^{1/4}$ vs. the distance to the Sun. Calculated by the compiler.

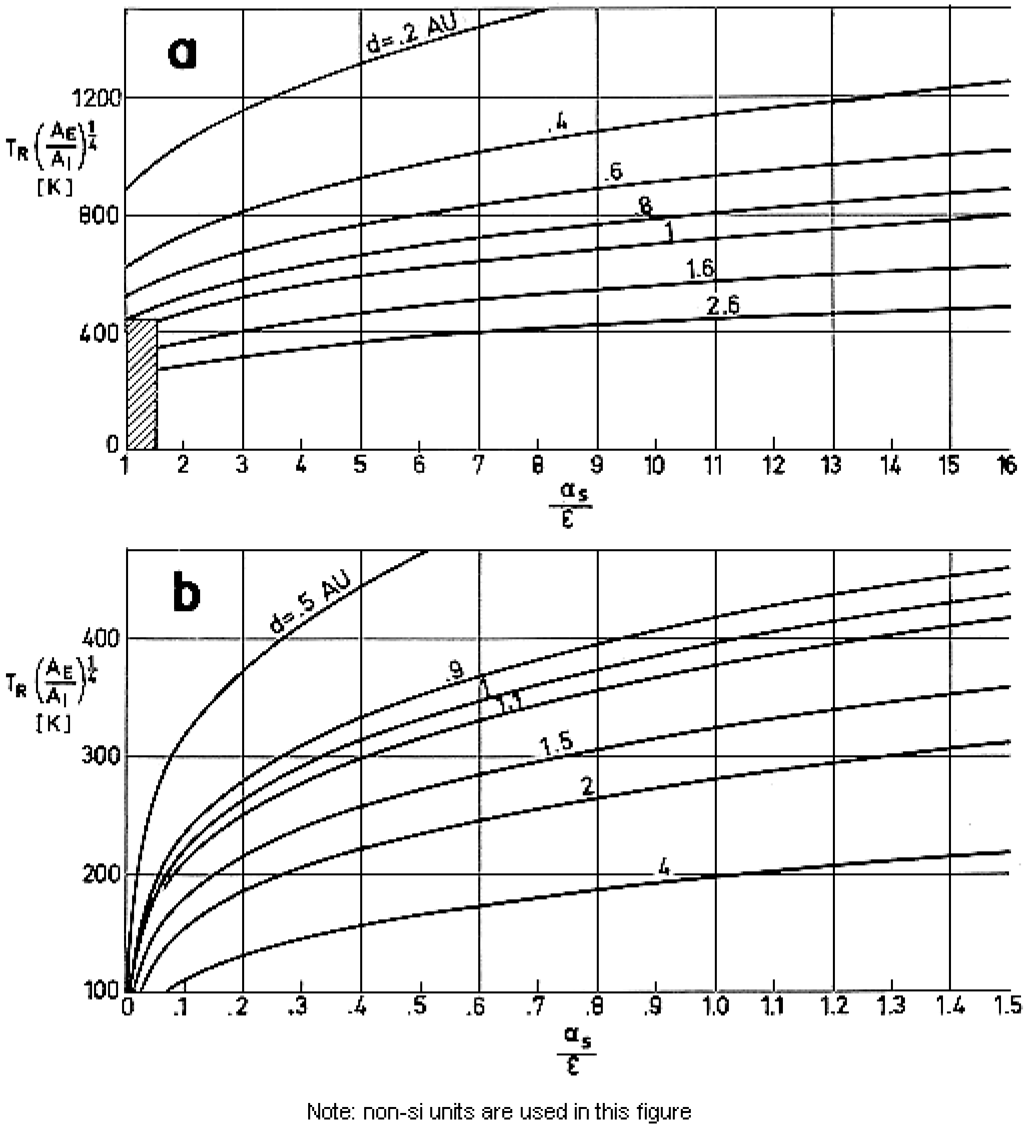

Figure 4-2: The function $T_R(A_E/A_I)^{1/4}$ vs. the optical characteristics of the surface. Shaded zone of *a* is enlarged in *b*. Calculated by the compiler.

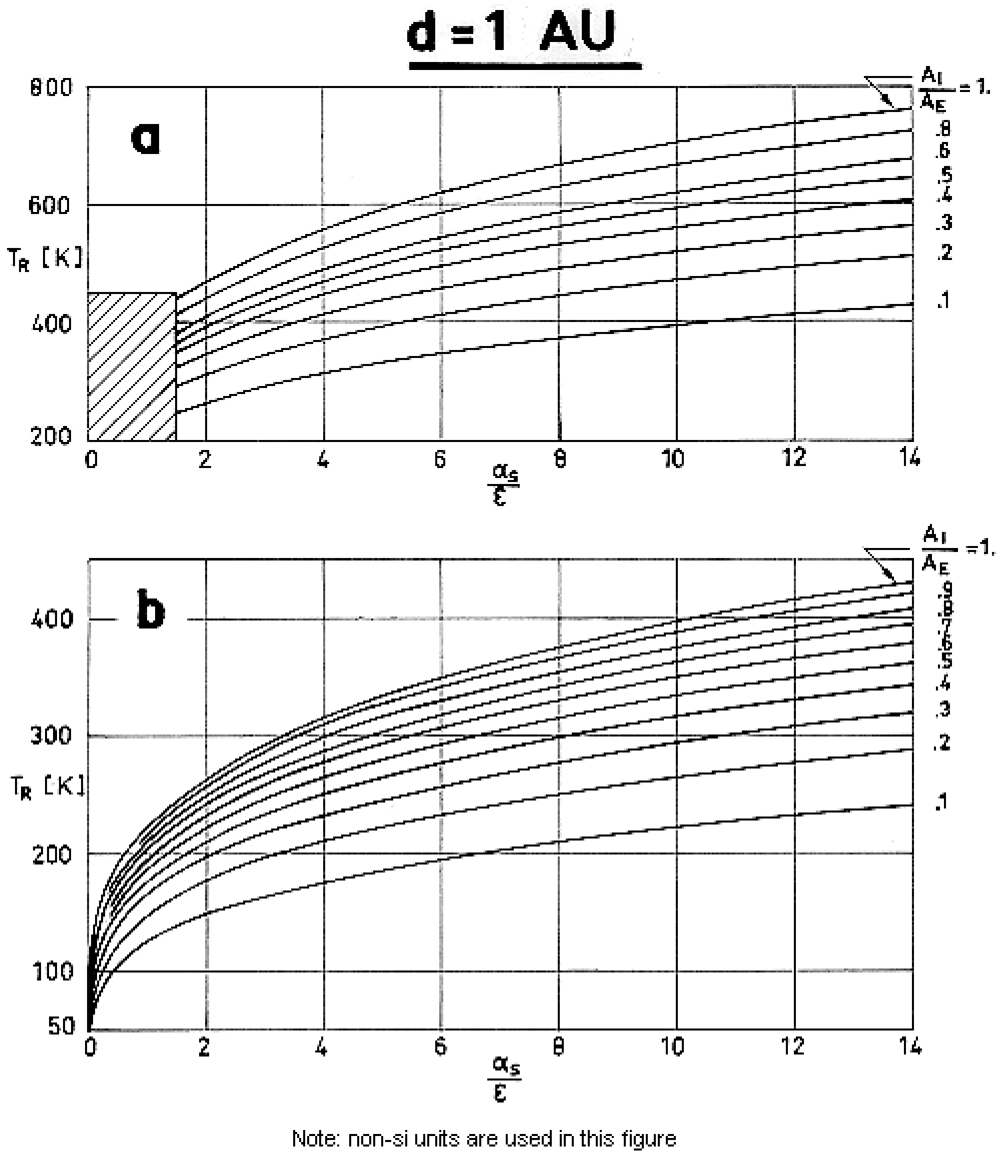

Figure 4-3: Temperature T_R as a function of α_s / ε and A_I/A_E for d = 1 AU. Shaded zone of *a* is enlarged in *b*. Calculated by the compiler.

4.2 Infinitely conductive planar surfaces

4.2.1 Flat plate emitting on one or both sides

I.- FLAT PLATE EMITTING ON ONE SIDE.

Sketch:

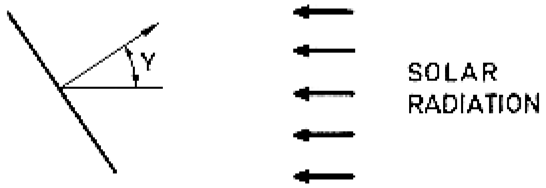

Formula:

$(A_I/A_E) = \cos\gamma$

II.- FLAT PLATE EMITTING ON BOTH SIDES.

Sketch:

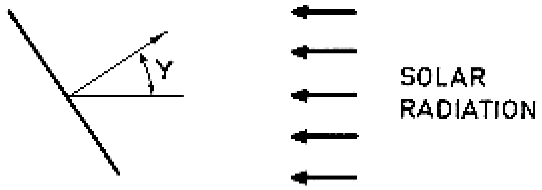

Formula:

$(A_I/A_E) = (\cos\gamma)/2$

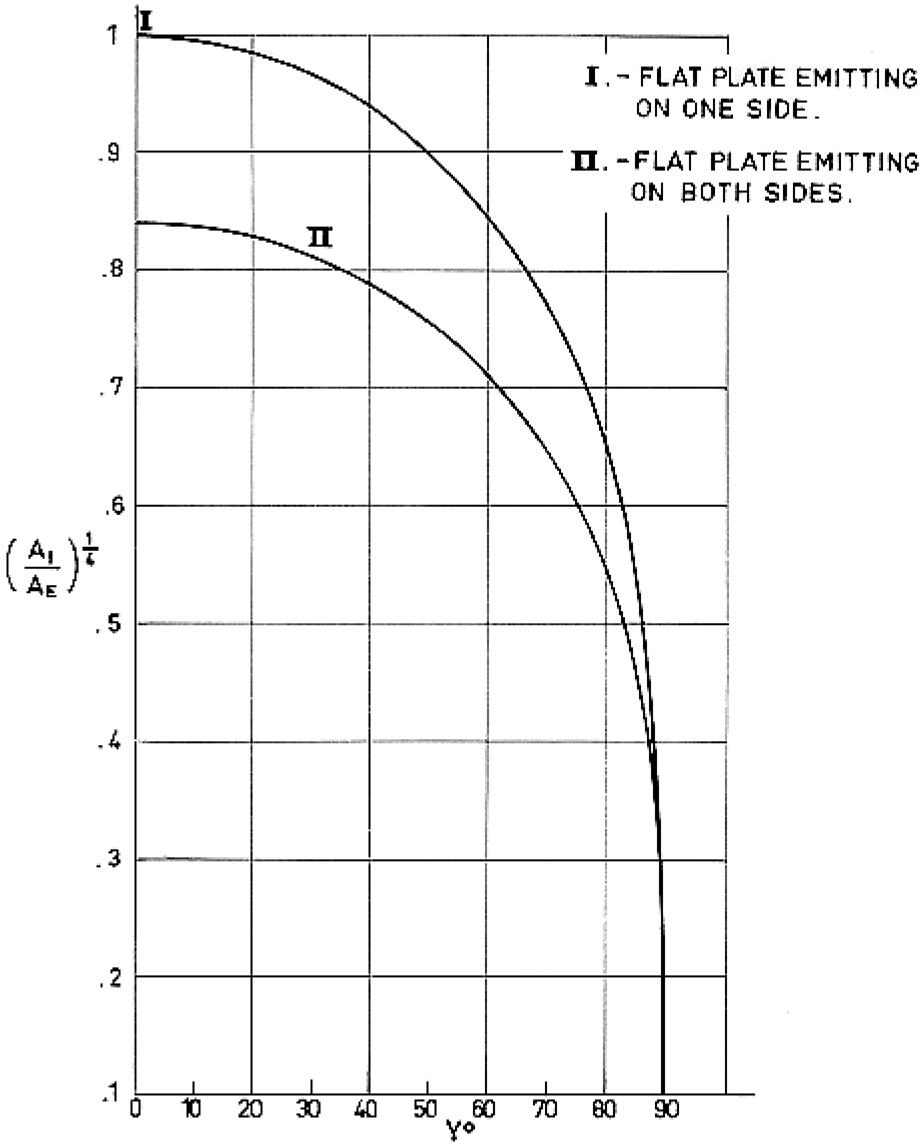

Note: non-si units are used in this figure

Figure 4-4: Ration (A_I/A_E)$^{1/4}$ as a function of γ, in the case of a flat plate. Calculated by the compiler.

4.3 Infinitely conductive spherical surfaces

4.3.1 Sphere

Sketch:

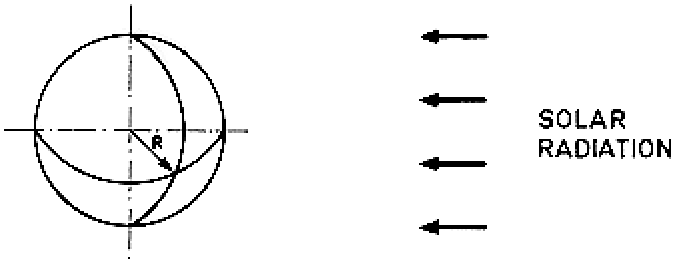

Area Projected from the Sun, A_I:

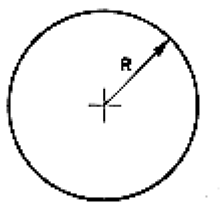

Formula:

$(A_I/A_E) = 1/4$

$(A_I/A_E)^{1/4} = 0,707$

4.4 Infinitely conductive cylindrical surfaces

4.4.1 Two-dimensional circular cylinder

Sketch:

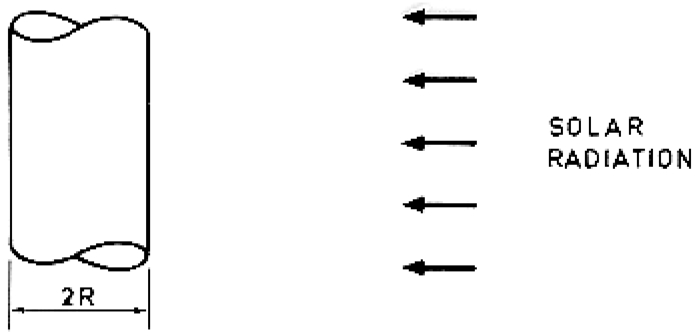

Area Projected from the Sun, A_I:

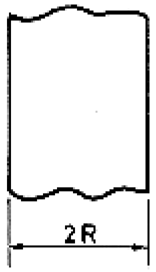

Formula:

$(A_I/A_E) = 1/\pi$

$(A_I/A_E)^{1/4} = 0{,}751$

Comments: This expression can be also applied to the finite circular cylinder with isolated bases.

4.4.2 Three-dimensional circular cylinder

Sketch:

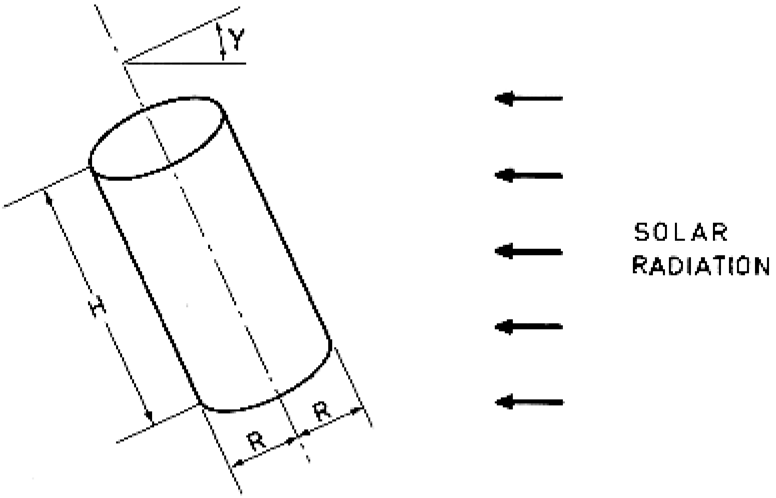

Area Projected from the Sun, A_I:

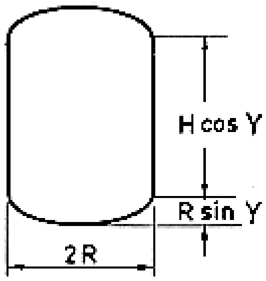

Formula:

$$\frac{A_I}{A_E} = \frac{\pi \sin\gamma + 2\frac{H}{R}\cos\gamma}{2\pi\left(1+\frac{H}{R}\right)} \qquad [4\text{-}2]$$

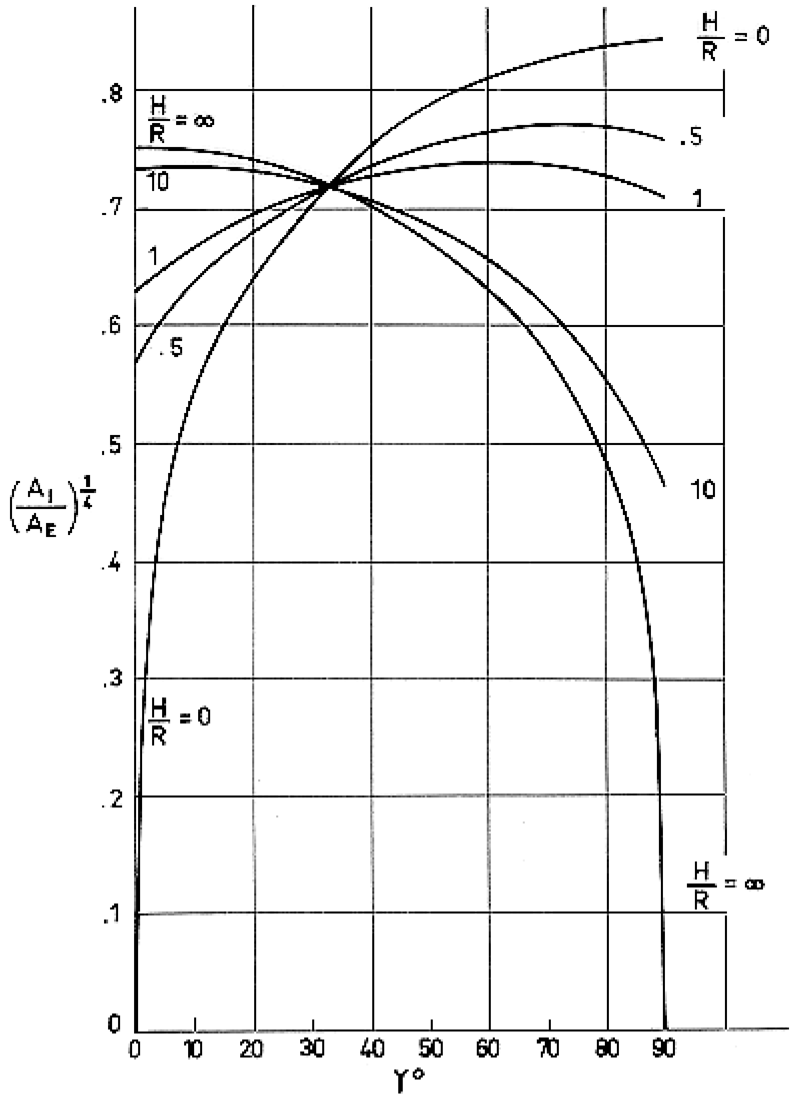

Note: non-si units are used in this figure

Figure 4-5: Ratio $(A_I/A_E)^{1/4}$ as a function of γ and H/R, in the case of a finite height circular cylinder. Calculated by the compiler.

4.5 Infinitely conductive conical surfaces

4.5.1 Semi-infinite circular cone

Sketch:

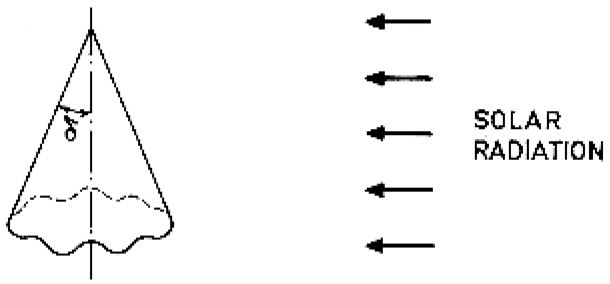

Area Projected from the Sun, A_I:

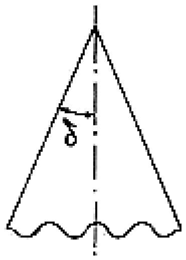

Formula:

$A_I/A_E = (\cos\,\delta)/\pi$

Comments: This expression can be also applied to the finite circular cone with isolated base provided that the incoming radiation is normal to the cone axis.

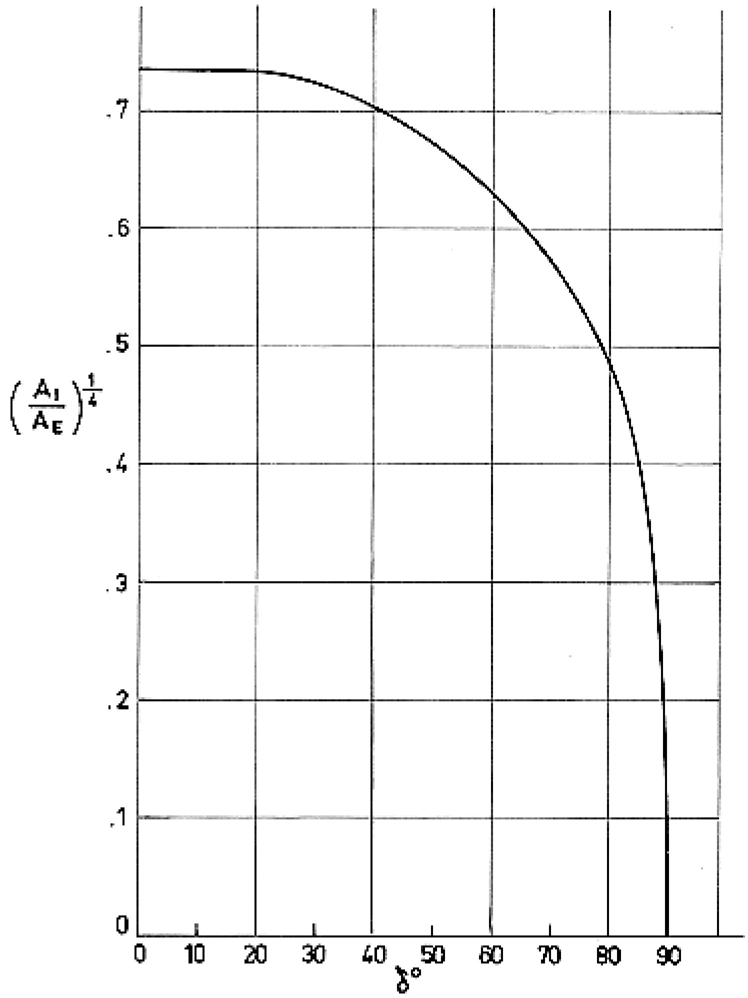

Note: non-si units are used in this figure

Figure 4-6: Ratio $(A_I/A_E)^{1/4}$ as a function of δ, in the case of a semi-infinite circular cone. Calculated by the compiler.

4.5.2 Finite circular cone with insulated base. (axial configuration)

Sketch:

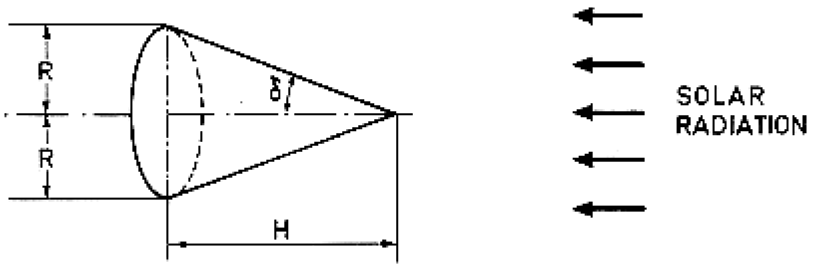

Area Projected from the Sun, A_I:

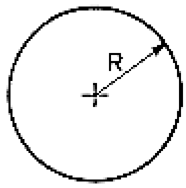

Formula:

$A_I/A_E = \sin\delta$

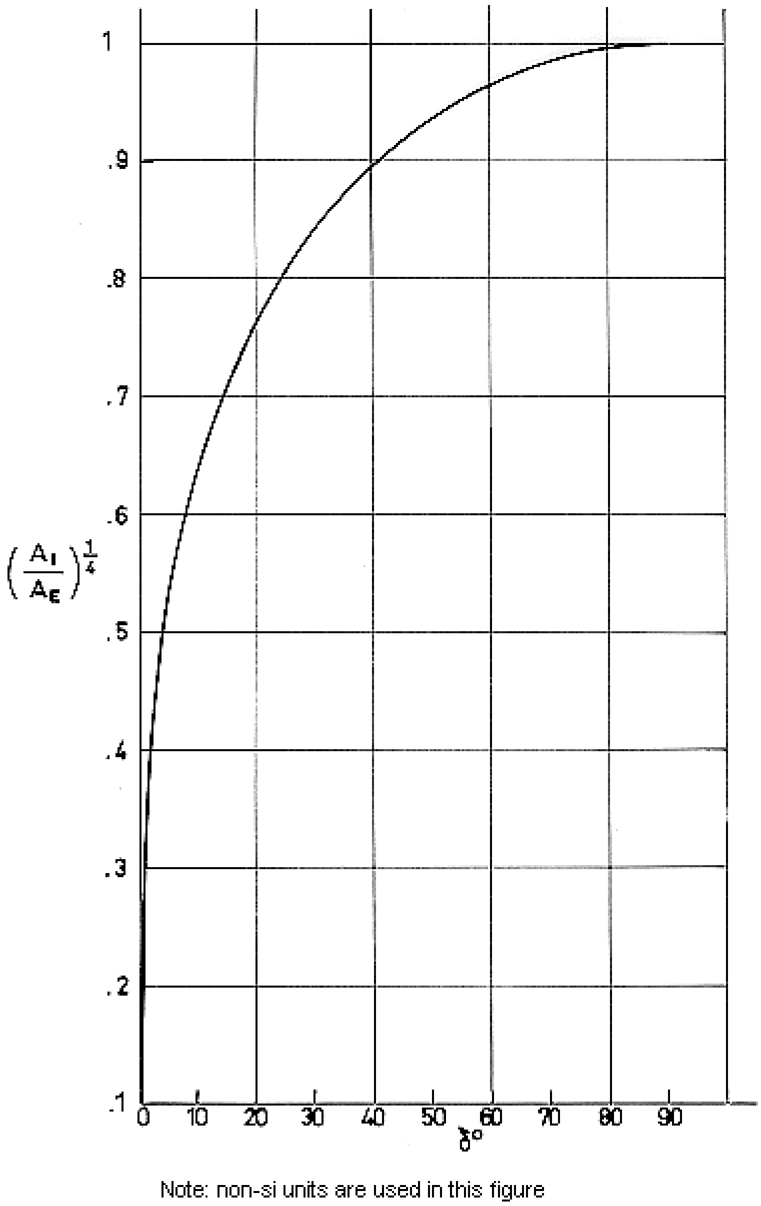

Figure 4-7: Ratio $(A_I/A_E)^{1/4}$ as a function of δ, in the case of a finite circular cone with insulated base (axial configuration). Calculated by the compiler.

4.5.3 Finite height circular cone

Sketch:

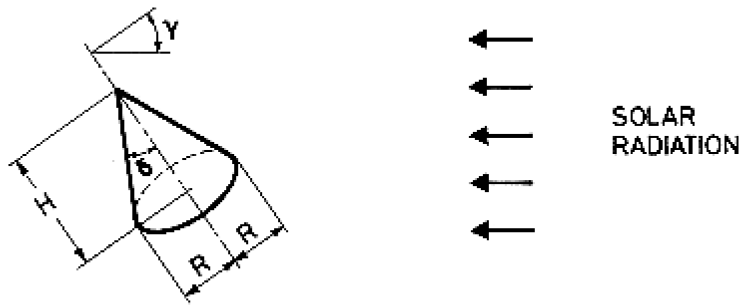

Area Projected from the Sun, A_I:

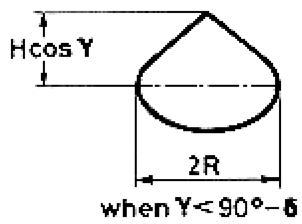

Formula:

a. when $0 \le \gamma \le 90° - \delta$,

$$\frac{A_I}{A_E} = \frac{\sin\gamma \sin\delta}{\pi(1+\sin\delta)}\left(\pi + \frac{\sqrt{1-\tan^2\gamma \tan^2\delta}}{\tan\gamma \tan\delta} - \sin^{-1}\sqrt{1-\tan^2\gamma \tan^2\delta}\right) \quad [4\text{-}3]$$

when $\gamma = 0$ the above expression becomes

$$\frac{A_I}{A_E} = \frac{\cos\delta}{\pi(1+\sin\delta)} \quad [4\text{-}4]$$

b. when $\gamma \ge 90° - \delta$,

$$\frac{A_I}{A_E} = \frac{\sin\delta \sin\gamma}{1+\sin\delta} \quad [4\text{-}5]$$

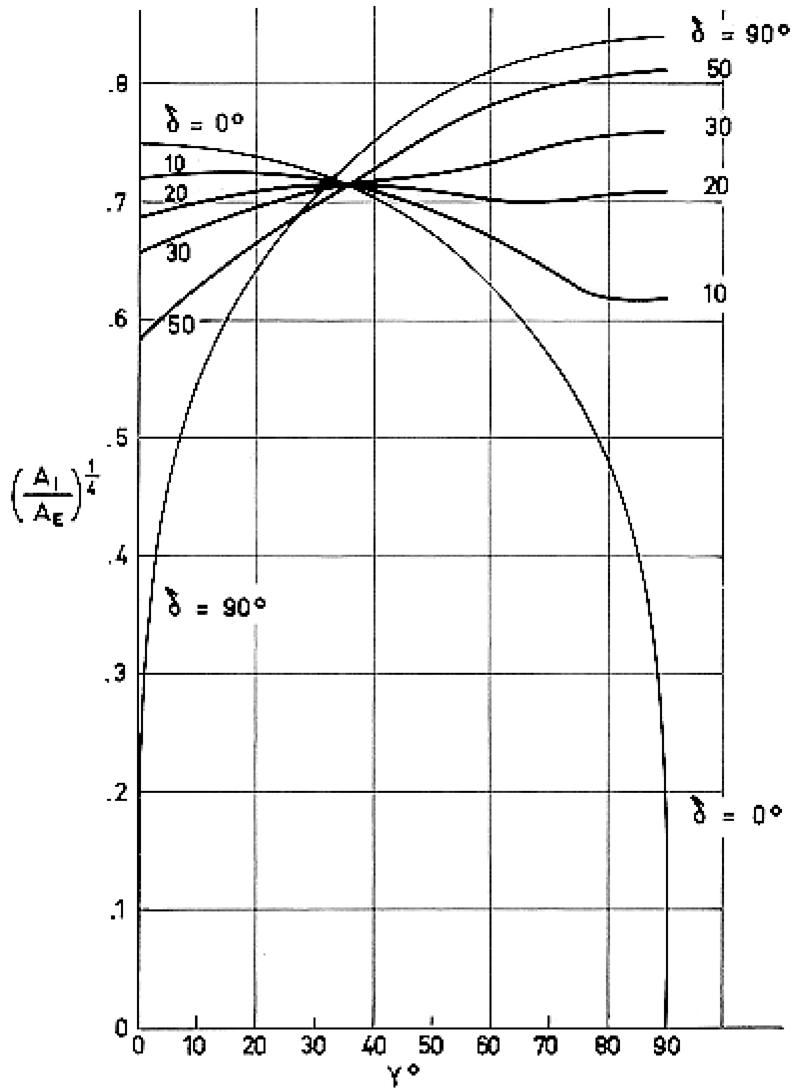

Note: non-si units are used in this figure

Figure 4-8: Ratio $(A_I/A_E)^{1/4}$ as a function of γ and δ, in the case of a finite height cone. Calculated by the compiler.

4.6 Infinitely conductive cylindrical-conical surfaces

4.6.1 Cone-cylinder-cone

Sketch:

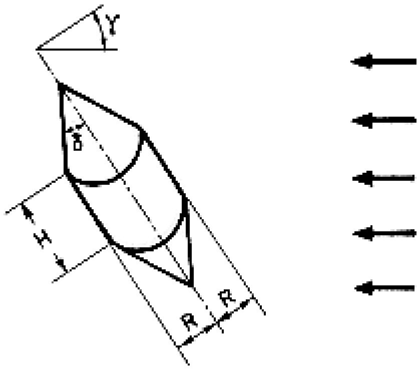

Area Projected from the Sun, A_I:

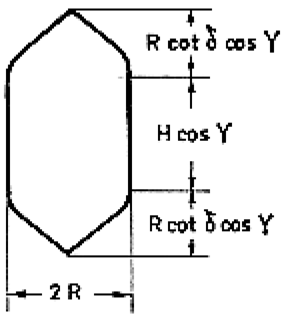

Formula:

a. When $\gamma \leq 90° - \delta$

$$\frac{A_I}{A_E} = \frac{\sin\gamma \sin\delta\left(\frac{\pi}{2} - \sin^{-1}\sqrt{1-\tan^2\gamma\tan^2\delta}\right) + \cos\gamma\left(\frac{H}{R}\sin\delta + \cos\delta\sqrt{1-\tan^2\gamma\tan^2\delta}\right)}{\pi\left(1+\frac{H}{R}\sin\delta\right)} \quad [4\text{-}6]$$

b. when $\gamma \geq 90° - \delta$,

$$\frac{A_I}{A_E} = \frac{\sin\delta\left(\sin\gamma + \frac{2H}{\pi R}\cos\gamma\right)}{\pi\left(1+\frac{H}{R}\sin\delta\right)} \quad [4\text{-}7]$$

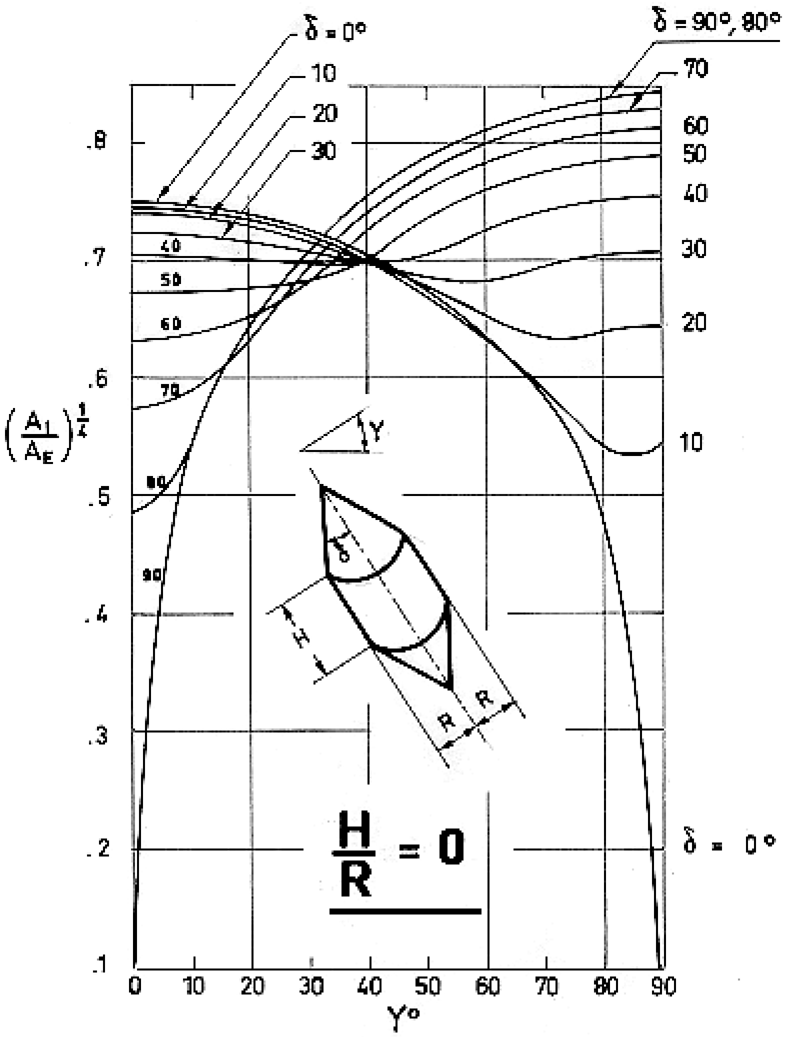

Note: non-si units are used in this figure

Figure 4-9: Ratio (A_I/A_E)$^{1/4}$ as a function of γ and δ, in the case of a cone-cylinder-cone. Calculated by the compiler.

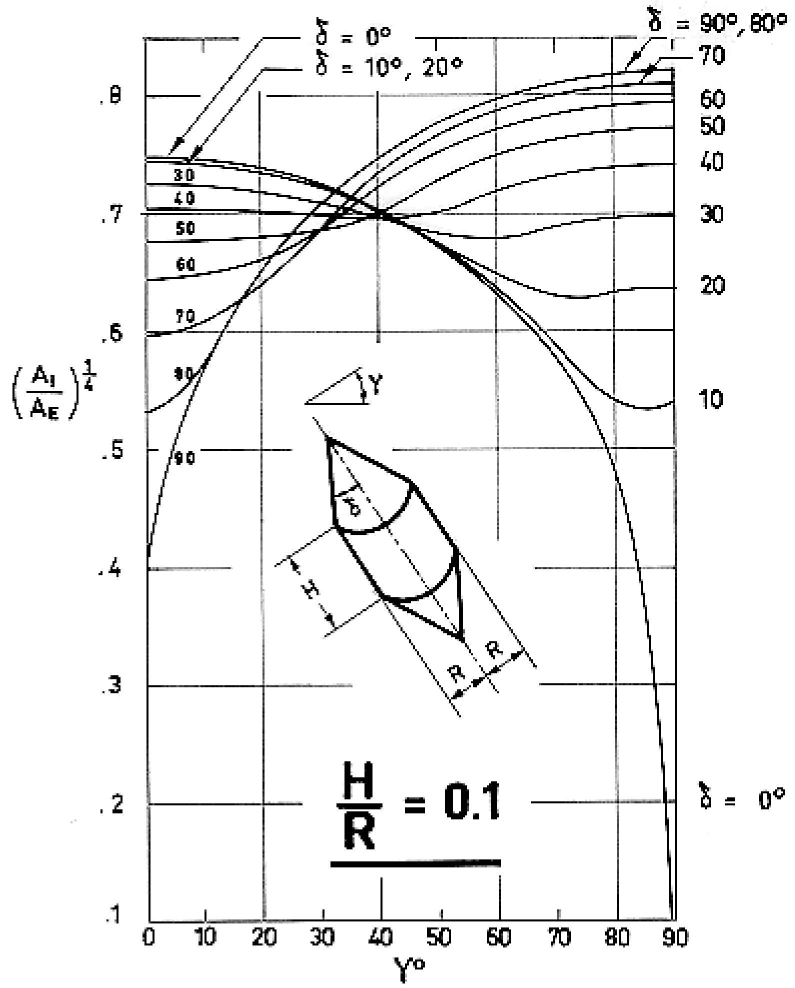

Note: non-si units are used in this figure

Figure 4-10: Ratio $(A_I/A_E)^{1/4}$ as a function of γ and δ, in the case of a cone-cylinder-cone. Calculated by the compiler.

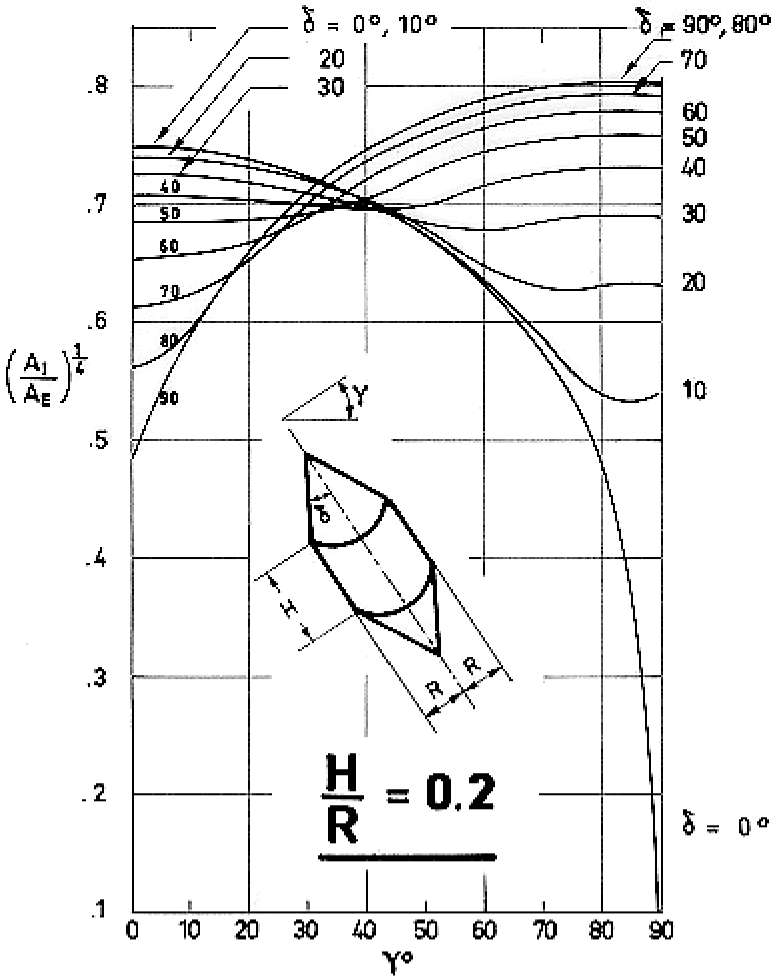

Note: non-si units are used in this figure

Figure 4-11: Ratio $(A_I/A_E)^{1/4}$ as a function of γ and δ, in the case of a cone-cylinder-cone. Calculated by the compiler.

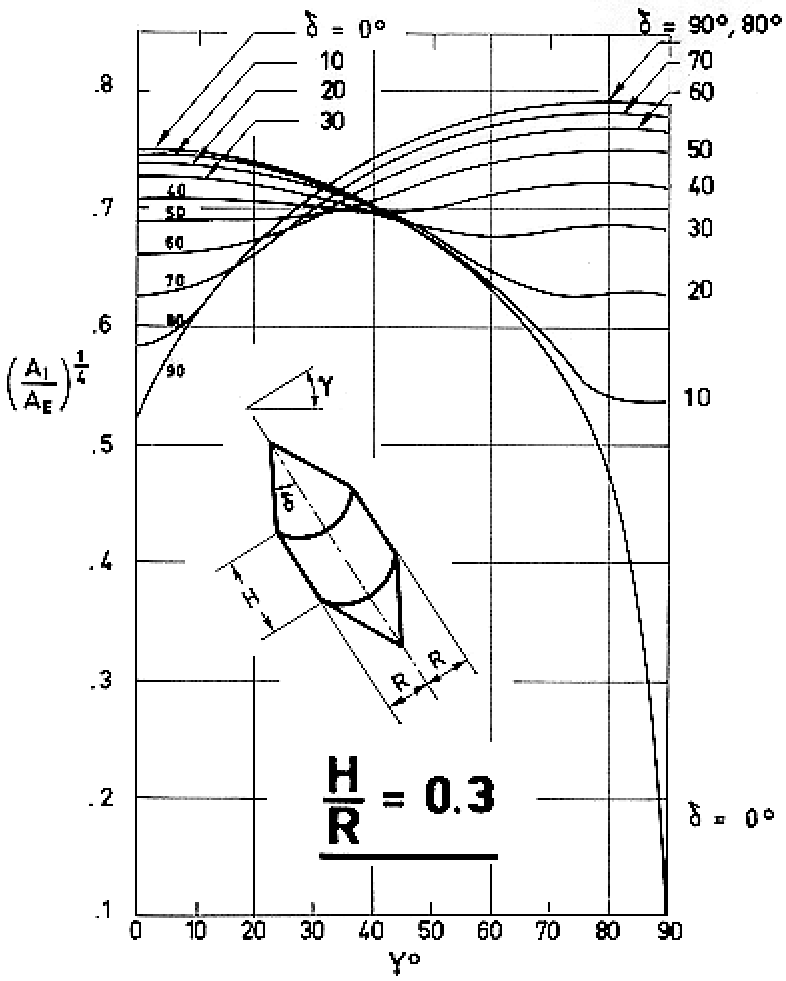

Note: non-si units are used in this figure

Figure 4-12: Ratio $(A_I/A_E)^{1/4}$ as a function of γ and δ, in the case of a cone-cylinder-cone. Calculated by the compiler.

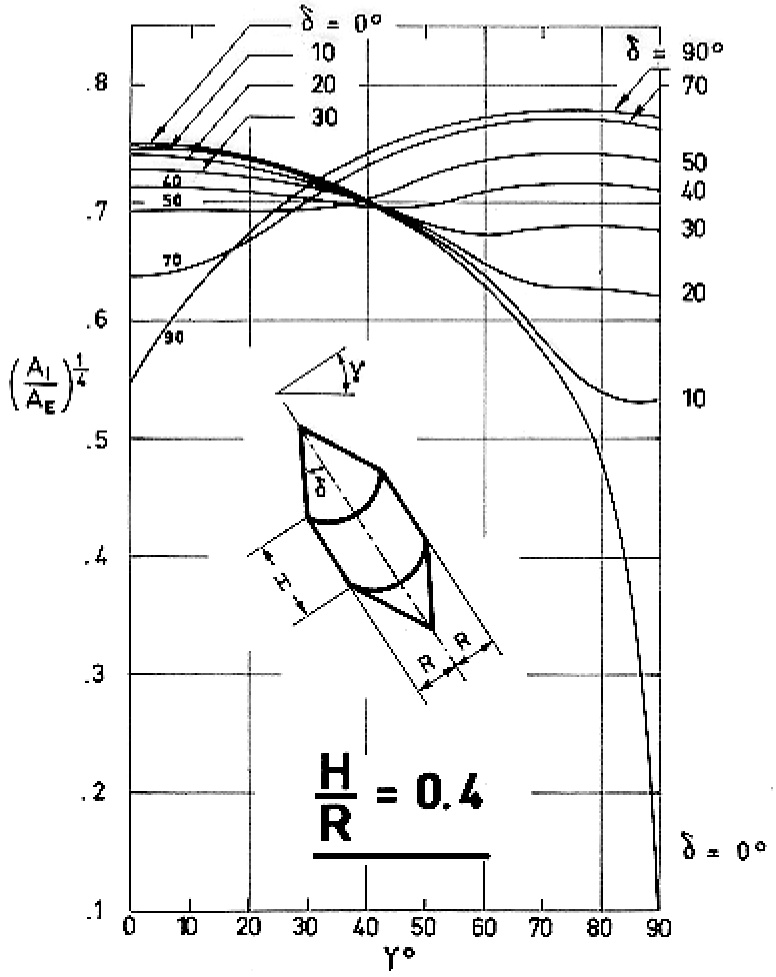

Figure 4-13: Ratio $(A_I/A_E)^{1/4}$ as a function of γ and δ, in the case of a cone-cylinder-cone. Calculated by the compiler.

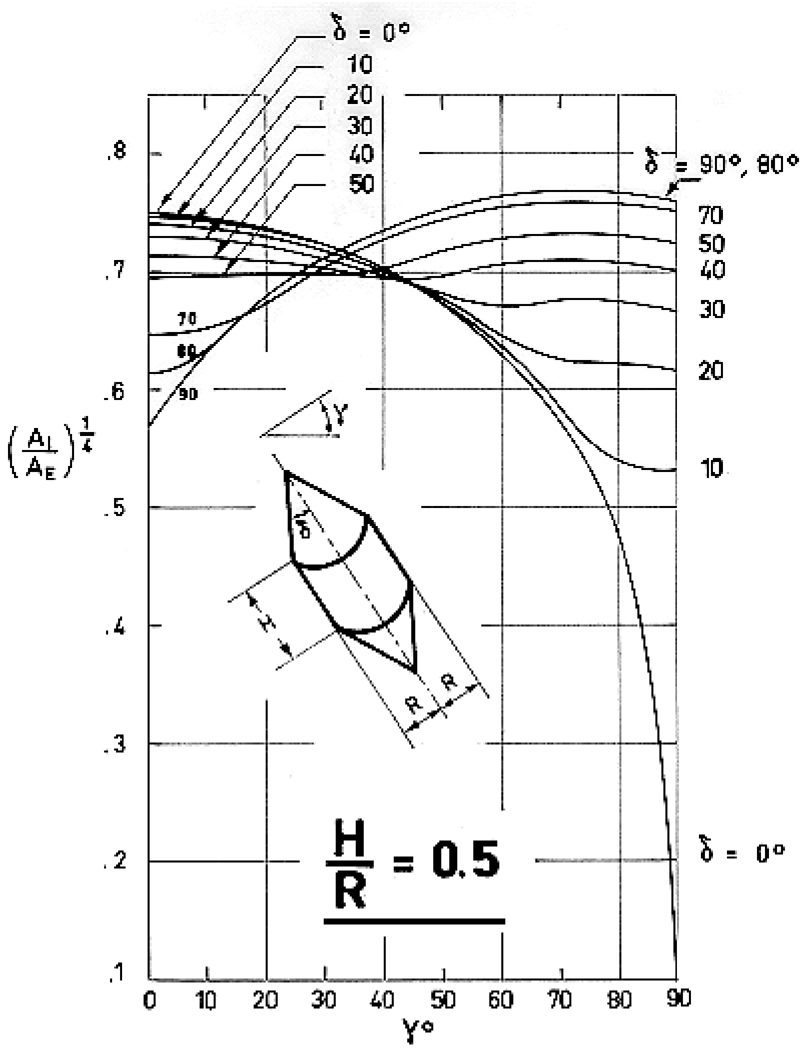

Note: non-si units are used in this figure

Figure 4-14: Ratio $(A_I/A_E)^{1/4}$ as a function of γ and δ, in the case of a cone-cylinder-cone. Calculated by the compiler.

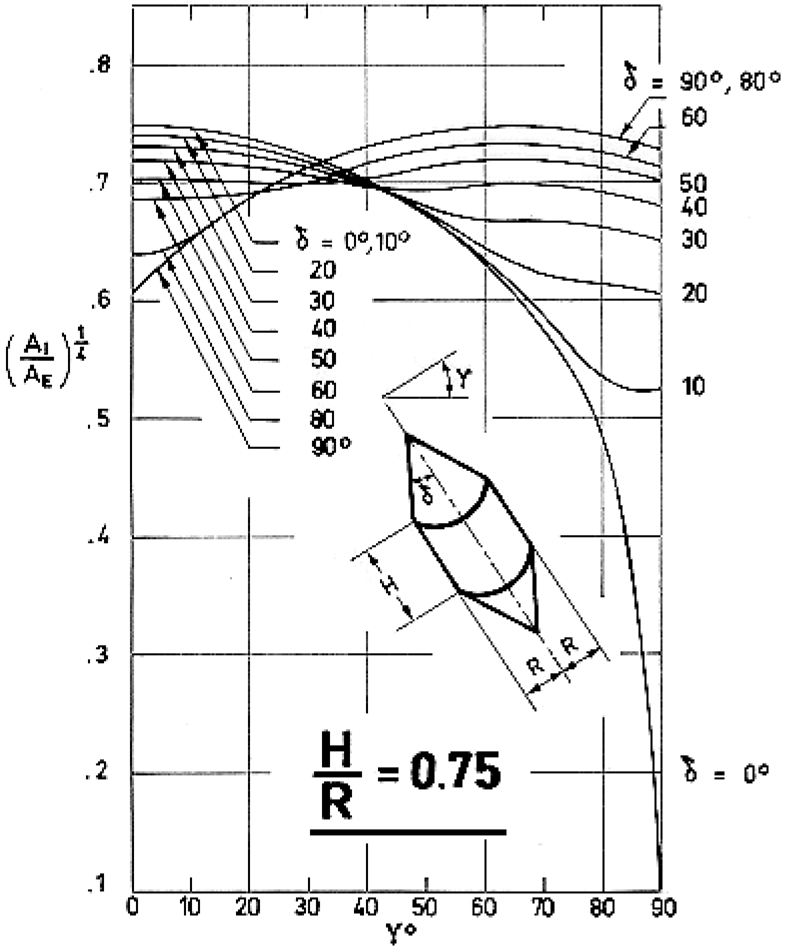

Note: non-si units are used in this figure

Figure 4-15: Ratio $(A_I/A_E)^{1/4}$ as a function of γ and δ, in the case of a cone-cylinder-cone. Calculated by the compiler.

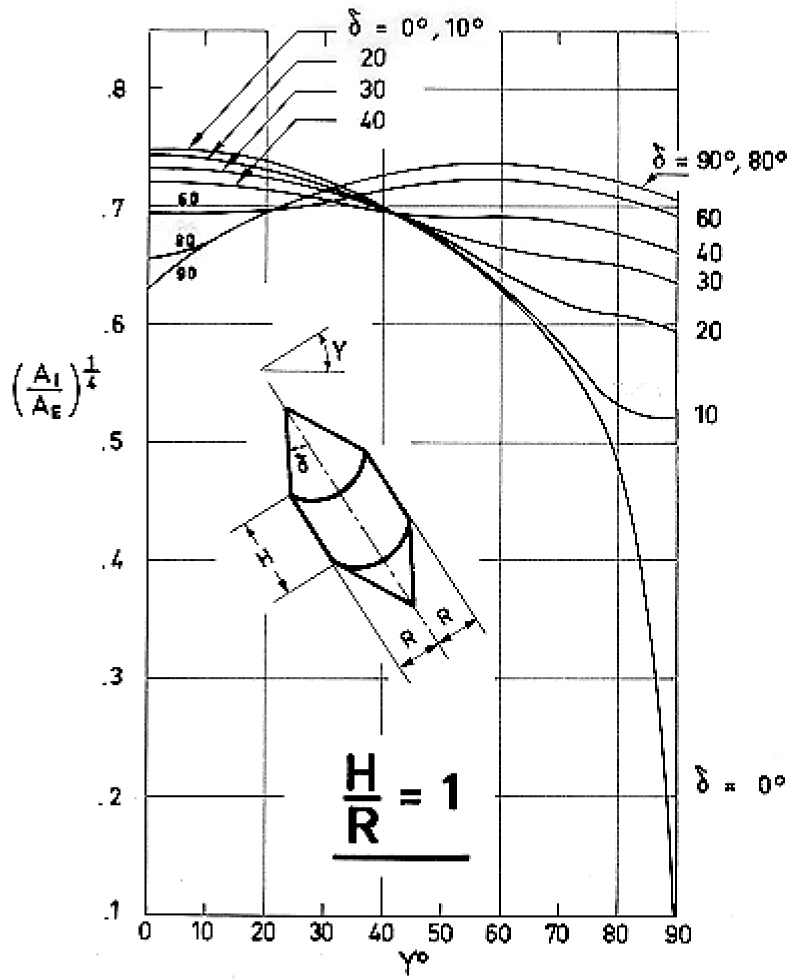

Note: non-si units are used in this figure

Figure 4-16: Ratio $(A_I/A_E)^{1/4}$ as a function of γ and δ, in the case of a cone-cylinder-cone. Calculated by the compiler.

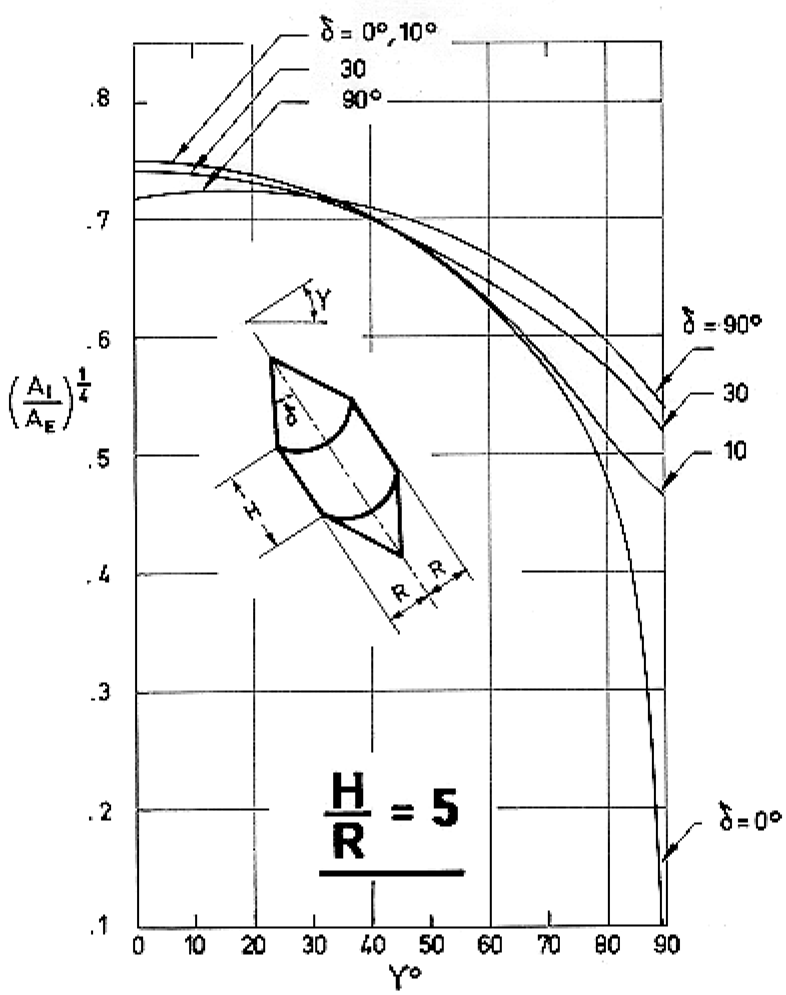

Note: non-si units are used in this figure

Figure 4-17: Ratio $(A_I/A_E)^{1/4}$ as a function of γ and δ, in the case of a cone-cylinder-cone. Calculated by the compiler.

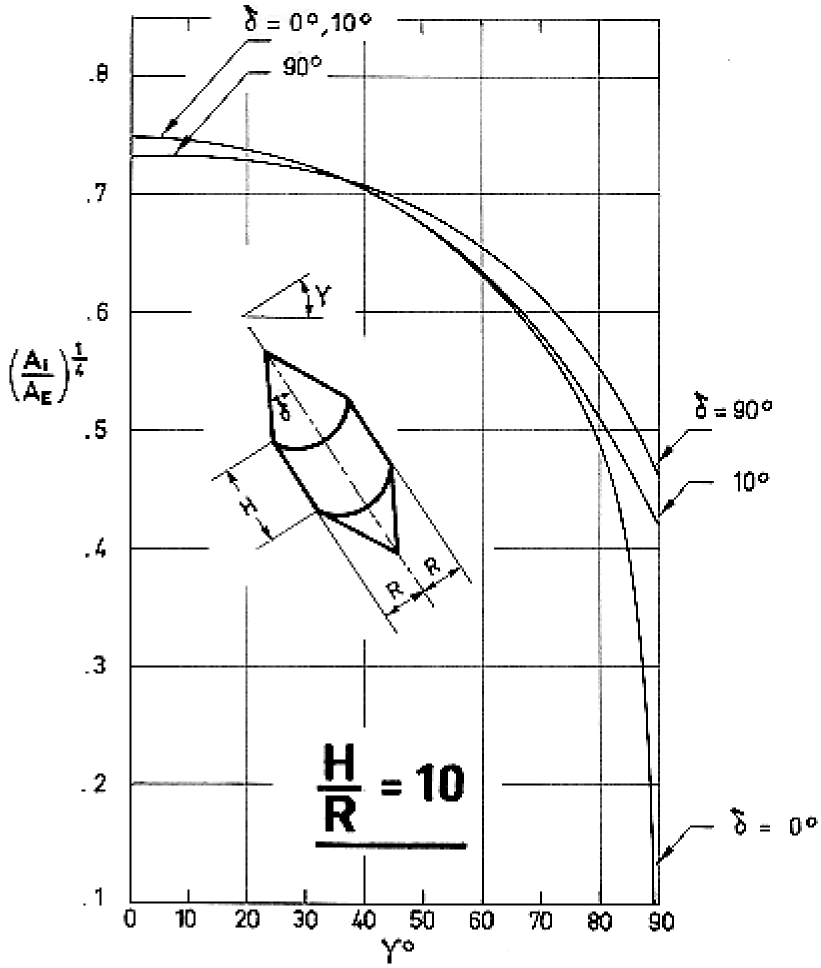

Note: non-si units are used in this figure

Figure 4-18: Ratio $(A_I/A_E)^{1/4}$ as a function of γ and δ, in the case of a cone-cylinder-cone. Calculated by the compiler.

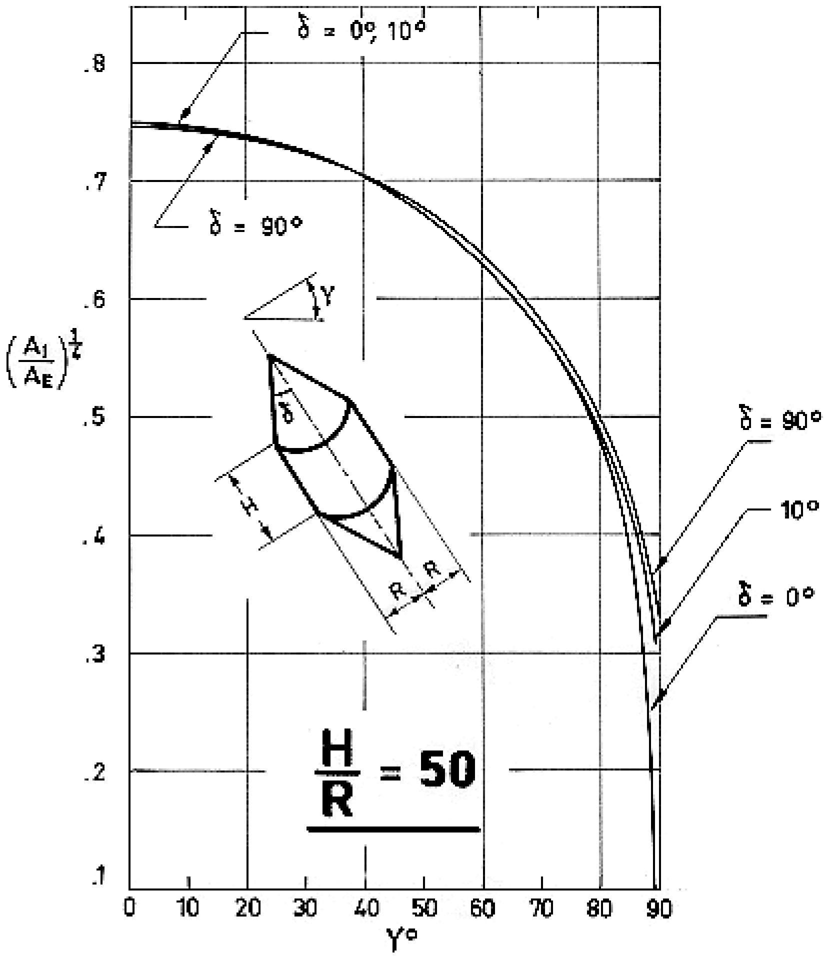

Note: non-si units are used in this figure

Figure 4-19: Ratio (A_I/A_E)$^{1/4}$ as a function of γ and δ, in the case of a cone-cylinder-cone. Calculated by the compiler.

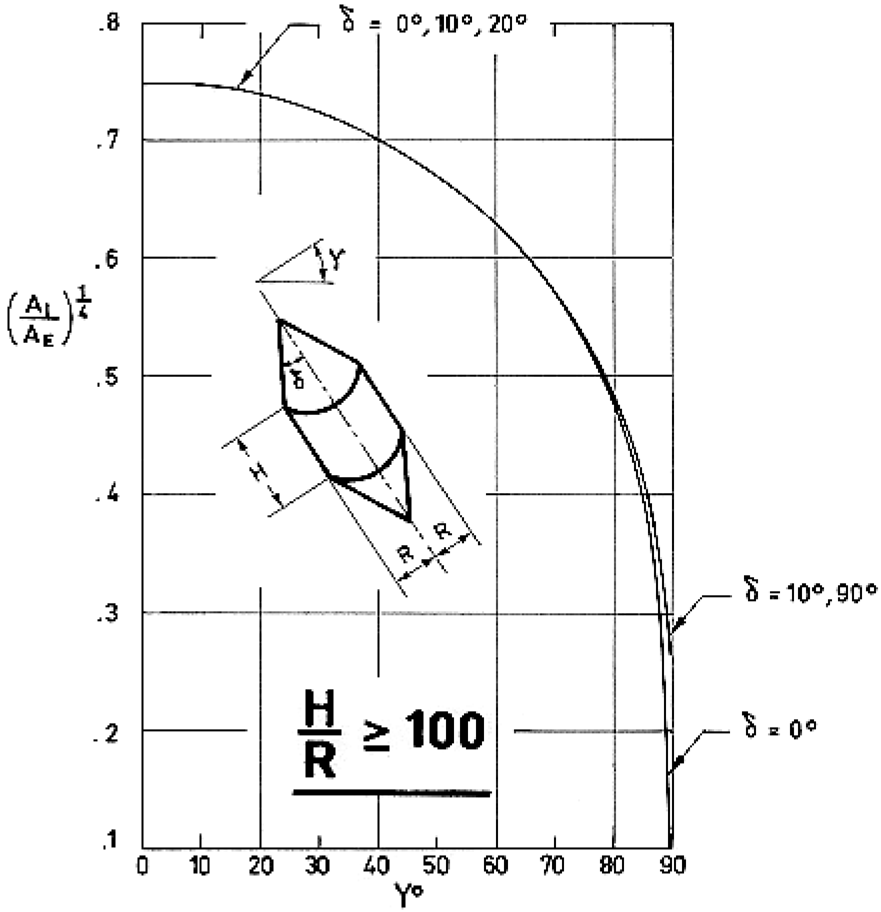

Note: non-si units are used in this figure

Figure 4-20: Ratio (A_l/A_E)$^{1/4}$ as a function of γ and δ, in the case of a cone-cylinder-cone. Calculated by the compiler.

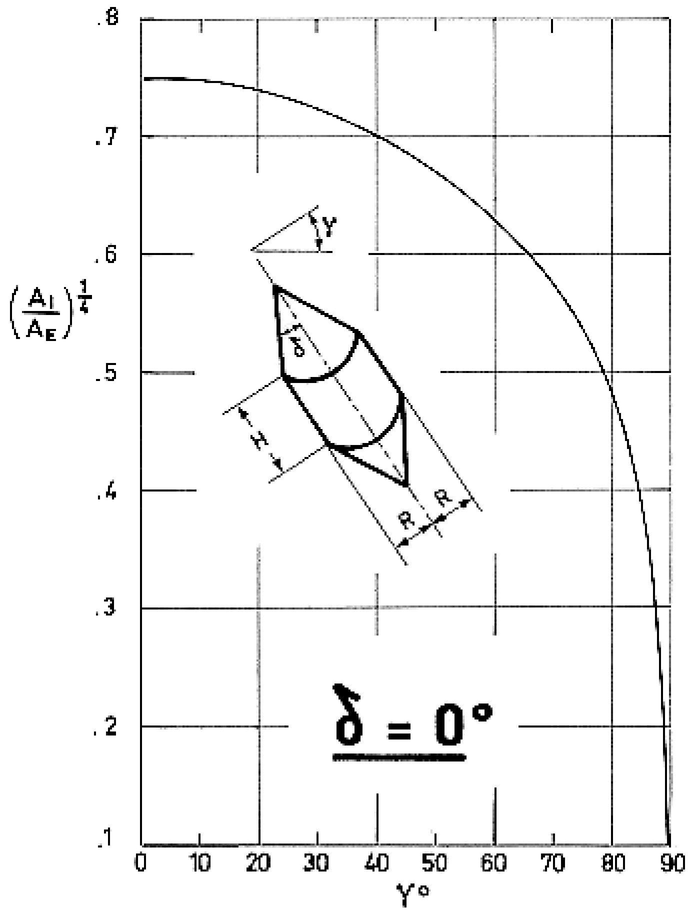

Note: non-si units are used in this figure

Figure 4-21: Ratio $(A_I/A_E)^{1/4}$ as a function of γ for any value of H/R, in the case of a cone-cylinder-cone. Calculated by the compiler.

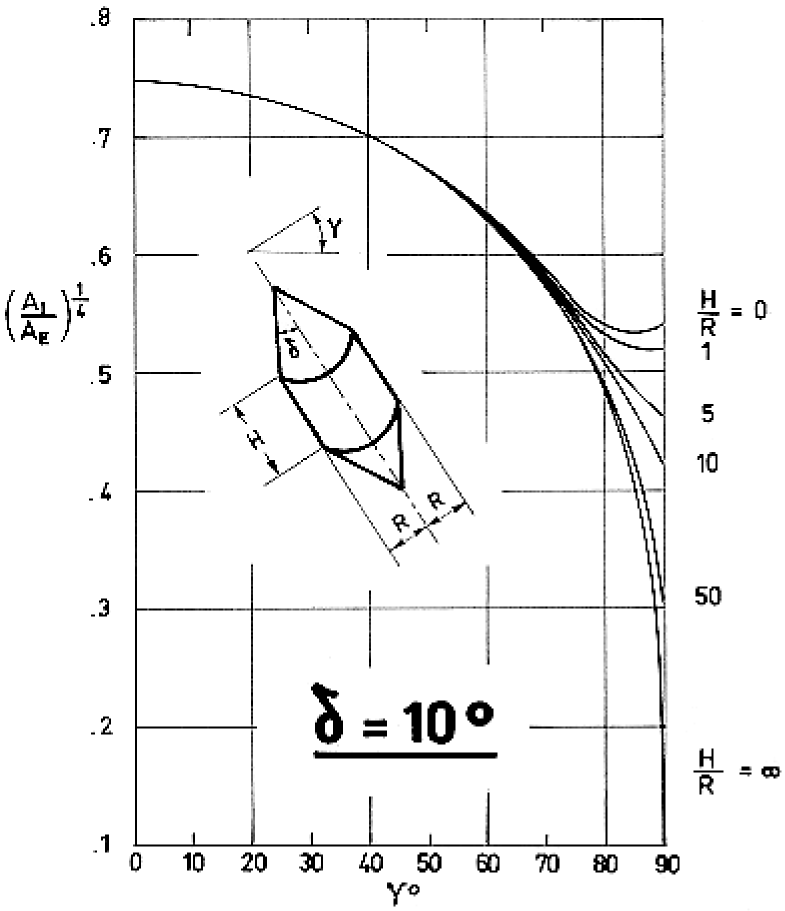

Note: non-si units are used in this figure

Figure 4-22: Ratio $(A_I/A_E)^{1/4}$ as a function of γ and H/R, in the case of a cone-cylinder-cone. Calculated by the compiler.

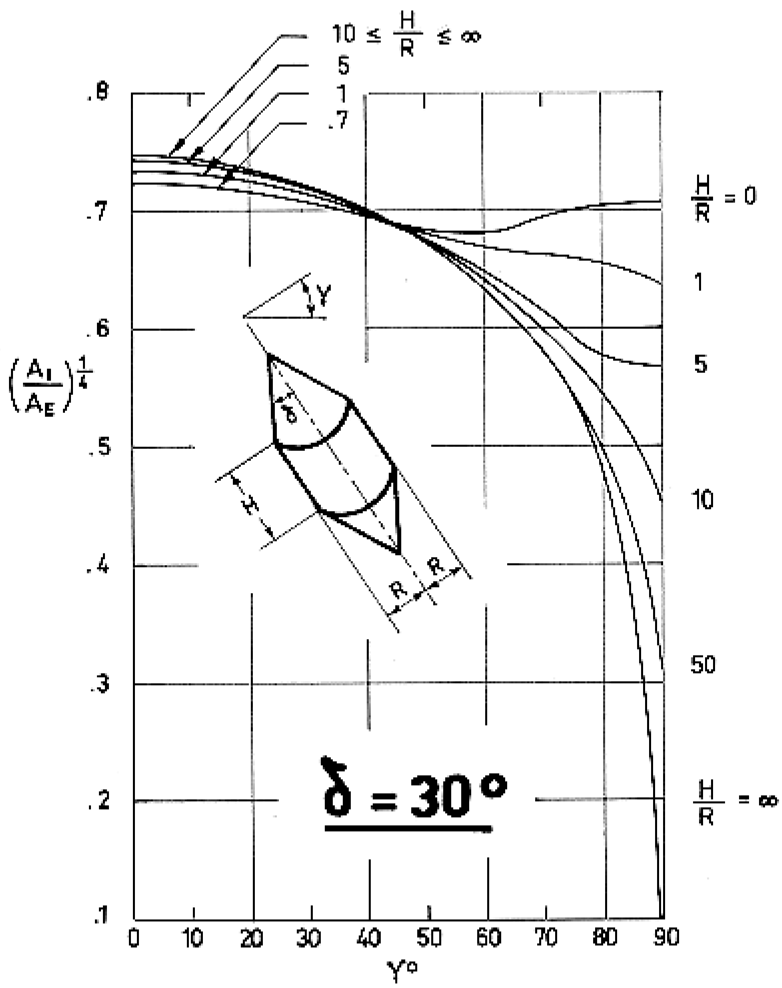

Note: non-si units are used in this figure

Figure 4-23: Ratio $(A_I/A_E)^{1/4}$ as a function of γ and H/R, in the case of a cone-cylinder-cone. Calculated by the compiler.

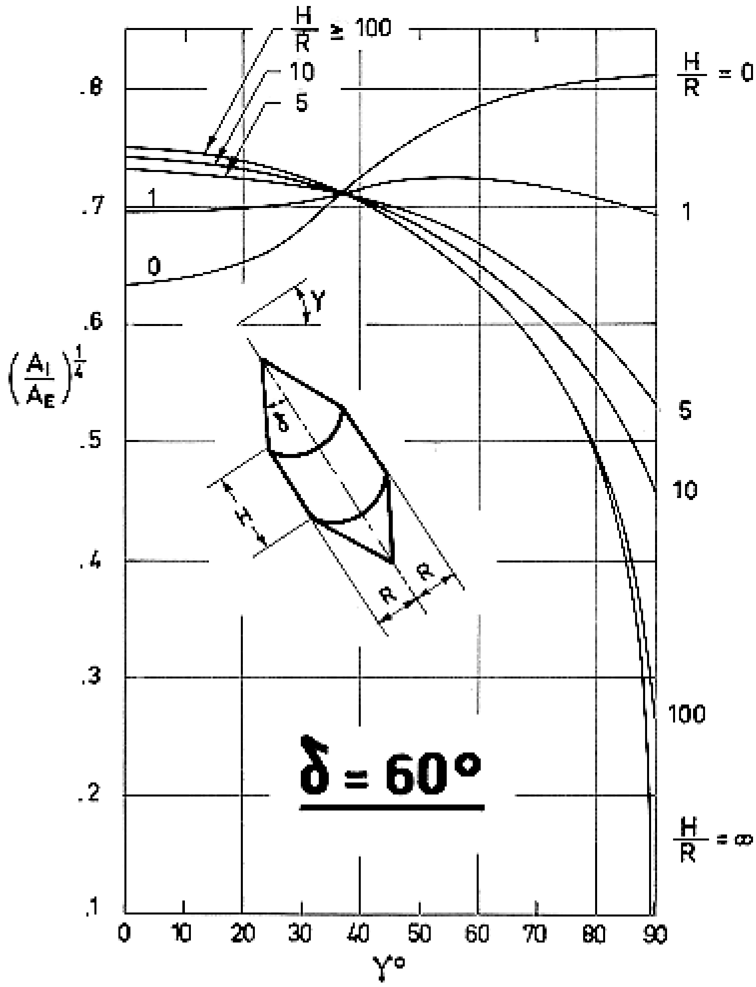

Note: non-si units are used in this figure

Figure 4-24: Ratio (A_I/A_E)$^{1/4}$ as a function of γ and H/R, in the case of a cone-cylinder-cone. Calculated by the compiler.

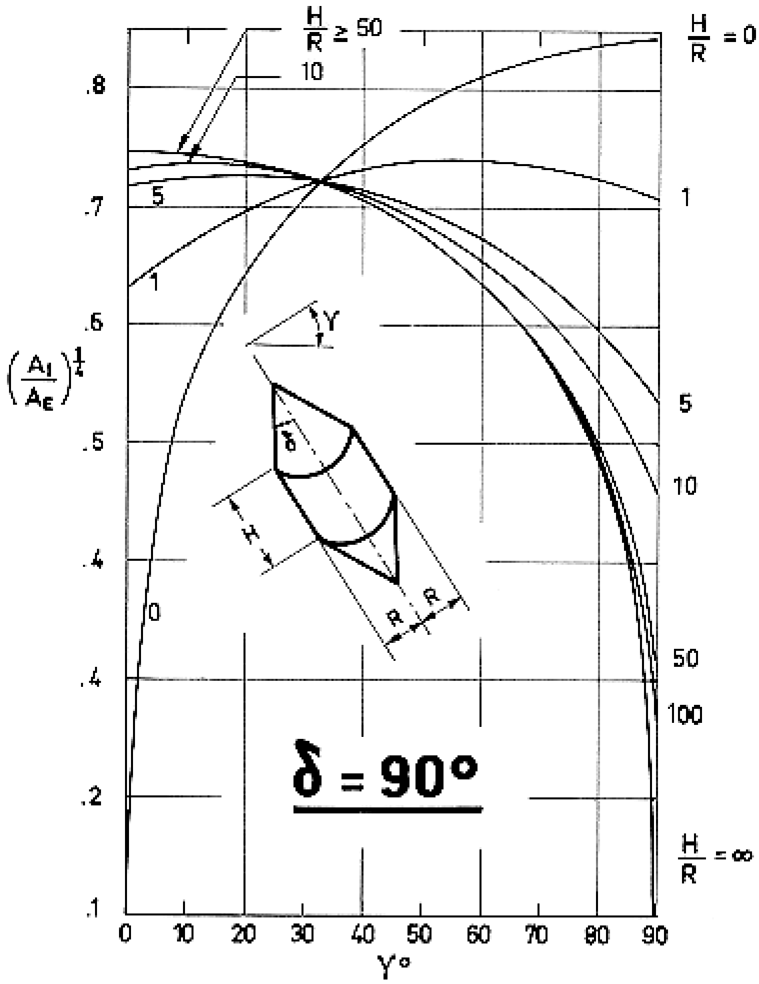

Note: non-si units are used in this figure

Figure 4-25: Ratio $(A_I/A_E)^{1/4}$ as a function of γ and H/R, in the case of a cone-cylinder-cone. Calculated by the compiler.

4.7 Infinitely conductive prismatic surfaces

4.7.1 Prism with an n-sided regular polygonal section

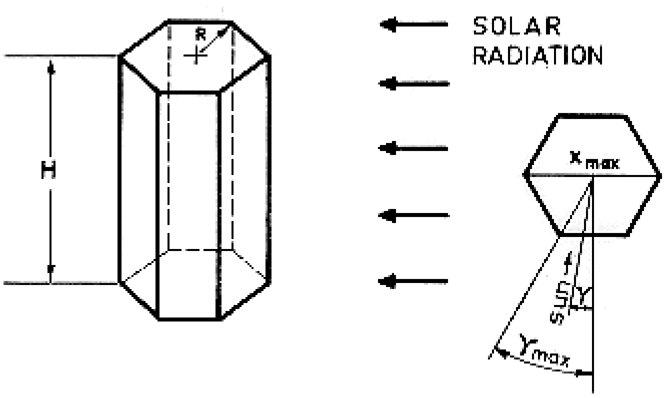

Area Projected from the Sun, A_I:

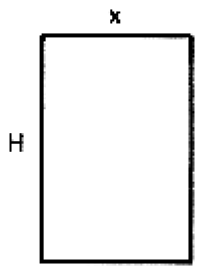

$X/R = 2\cos\gamma$, for n even ,

$X/R = 2\cos(\pi/2n)\cos\gamma$, for n odd.

Formula:

$$\frac{A_I}{A_E} = \frac{\frac{H}{R}\frac{X}{R}}{n\left(\sin\frac{2\pi}{n} + 2\frac{H}{R}\sin\frac{\pi}{n}\right)} \qquad [4\text{-}8]$$

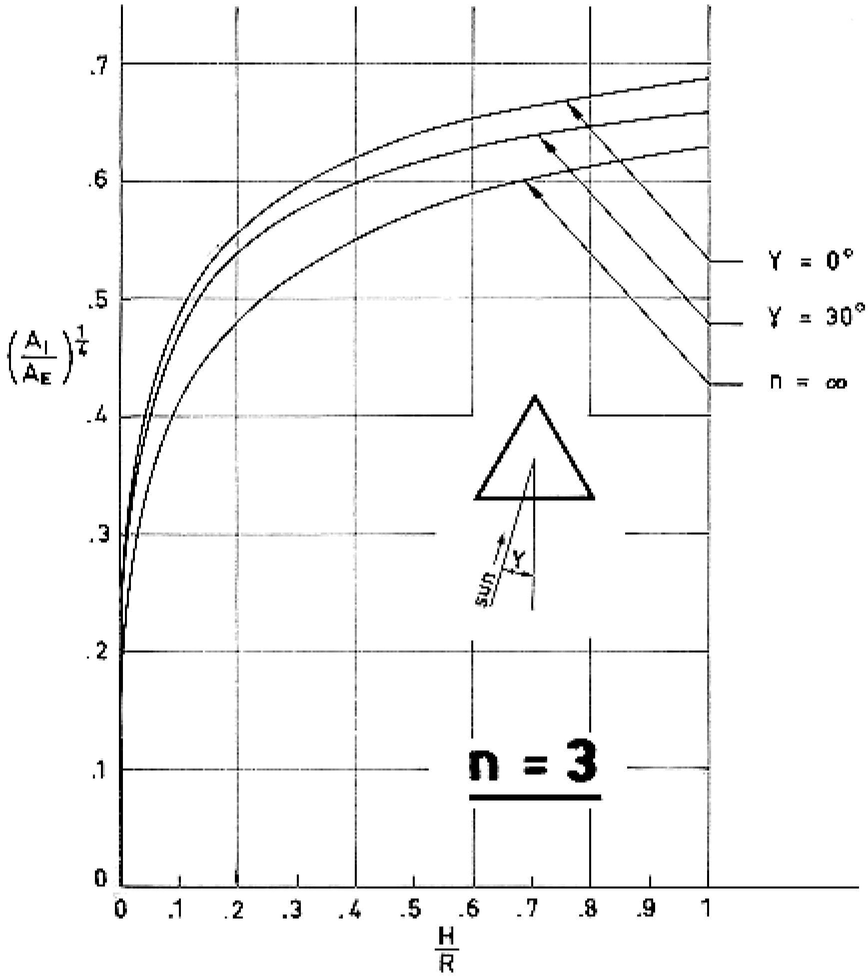

Note: non-si units are used in this figure

Figure 4-26: Ratio (A_I/A_E)$^{1/4}$ as a function of H/R, in the case of a prism. The curves plotted are those corresponding to the largest and smallest areas projected from the Sun. Circular cylinder, $n = \infty$. Calculated by the compiler.

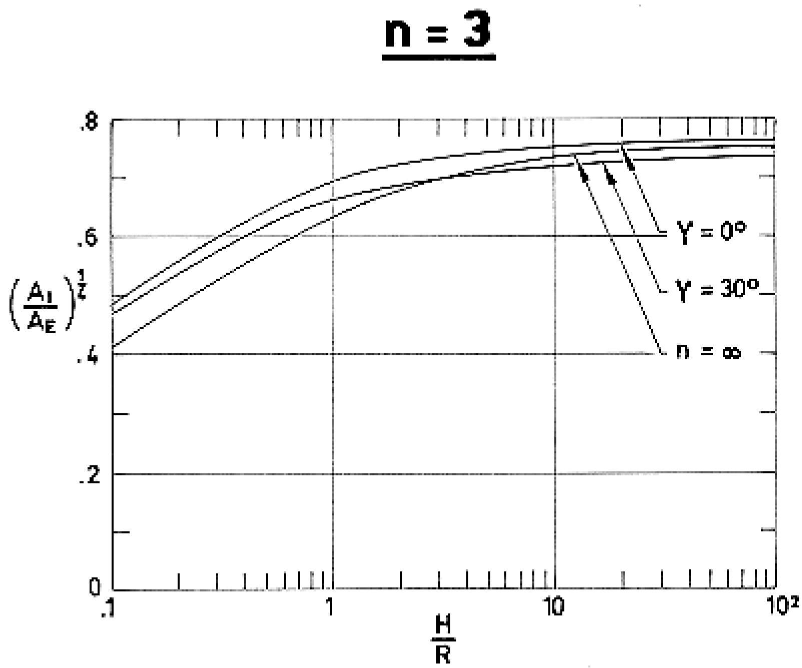

Note: non-si units are used in this figure

Figure 4-27: Ratio $(A_I/A_E)^{1/4}$ as a function of H/R, in the case of a prism. The curves plotted are those corresponding to the largest and smallest areas projected from the Sun. The values corresponding to $H/R \leq 1$ are also plotted in the previous figure. Circular cylinder, $n = \infty$. Calculated by the compiler.

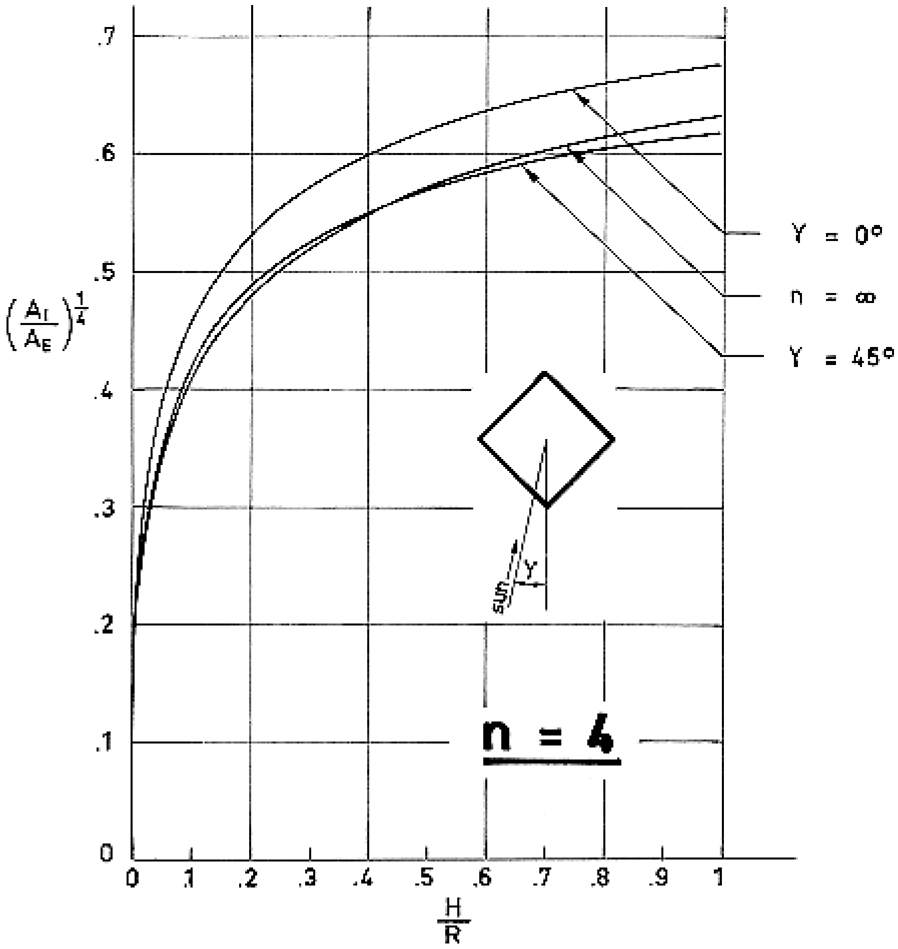

Note: non-si units are used in this figure

Figure 4-28: Ratio $(A_I/A_E)^{1/4}$ as a function of H/R, in the case of a prism. The curves plotted are those corresponding to the largest and smallest areas projected from the Sun. Circular cylinder, $n = \infty$. Calculated by the compiler.

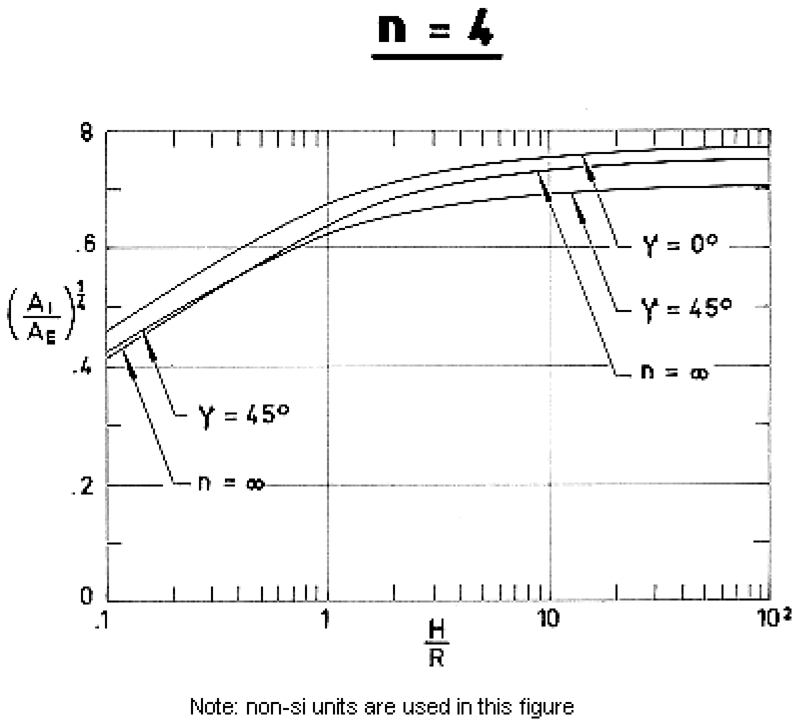

Figure 4-29: Ratio $(A_I/A_E)^{1/4}$ as a function of *H*/*R*, in the case of a prism. The curves plotted are those corresponding to the largest and smallest areas projected from the Sun. The values corresponding to *H*/*R* ≤1 are also plotted in the previous figure. Circular cylinder, $n = \infty$. Calculated by the compiler.

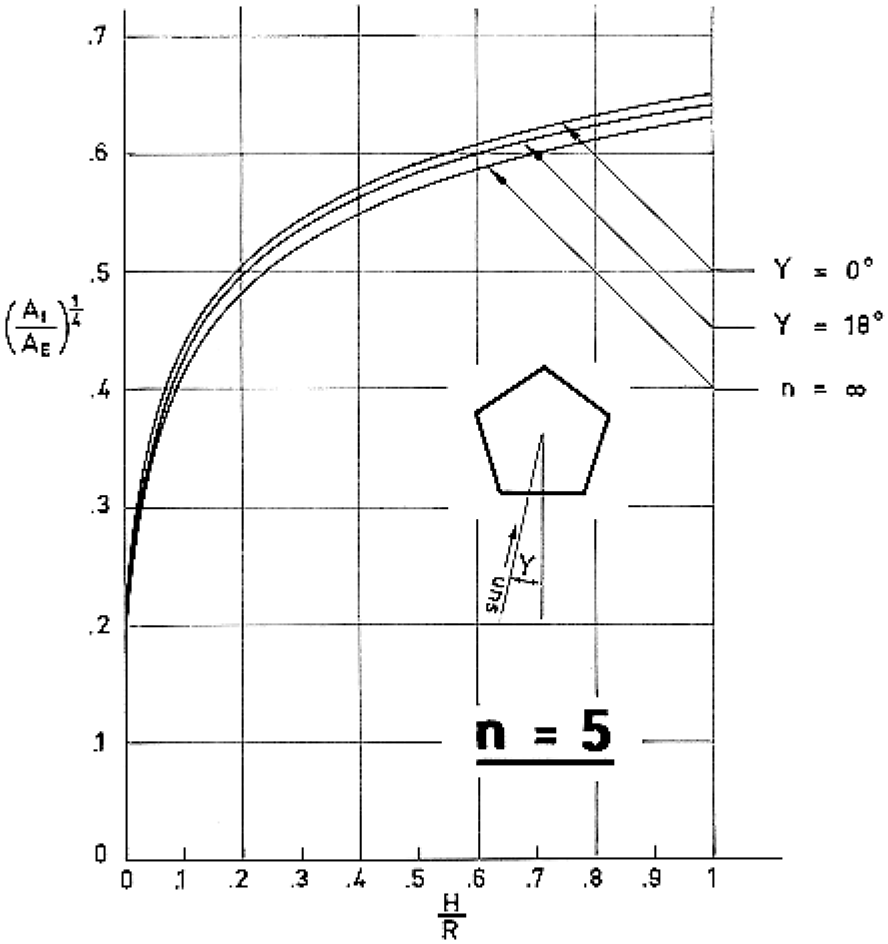

Note: non-si units are used in this figure

Figure 4-30: Ratio $(A_I/A_E)^{1/4}$ as a function of H/R, in the case of a prism. The curves plotted are those corresponding to the largest and smallest areas projected from the Sun. Circular cylinder, $n = \infty$. Calculated by the compiler.

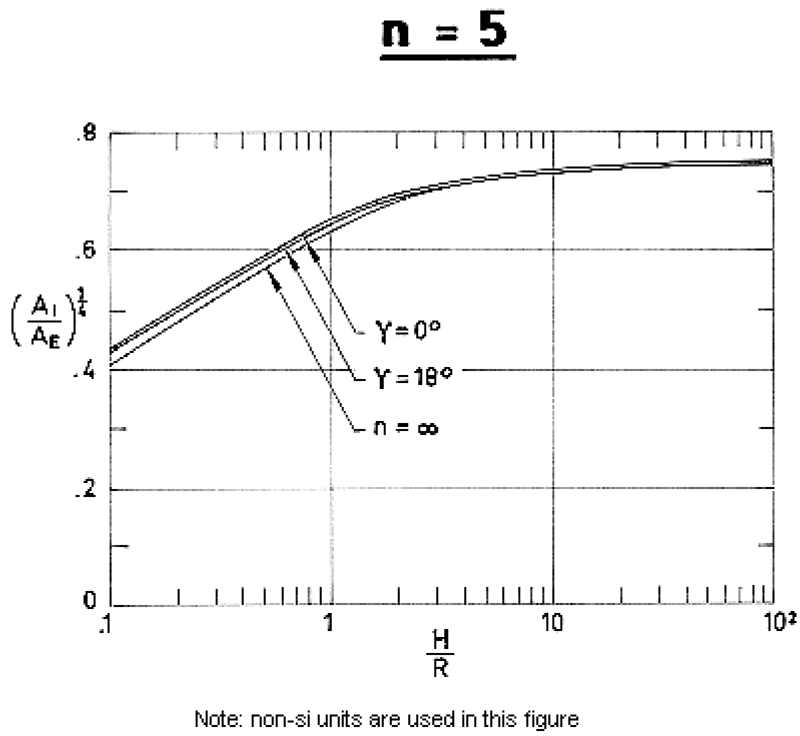

Figure 4-31: Ratio $(A_I/A_E)^{1/4}$ as a function of H/R, in the case of a prism. The curves plotted are those corresponding to the largest and smallest areas projected from the Sun. The values corresponding to $H/R \leq 1$ are also plotted in the previous figure. Circular cylinder, $n = \infty$. Calculated by the compiler.

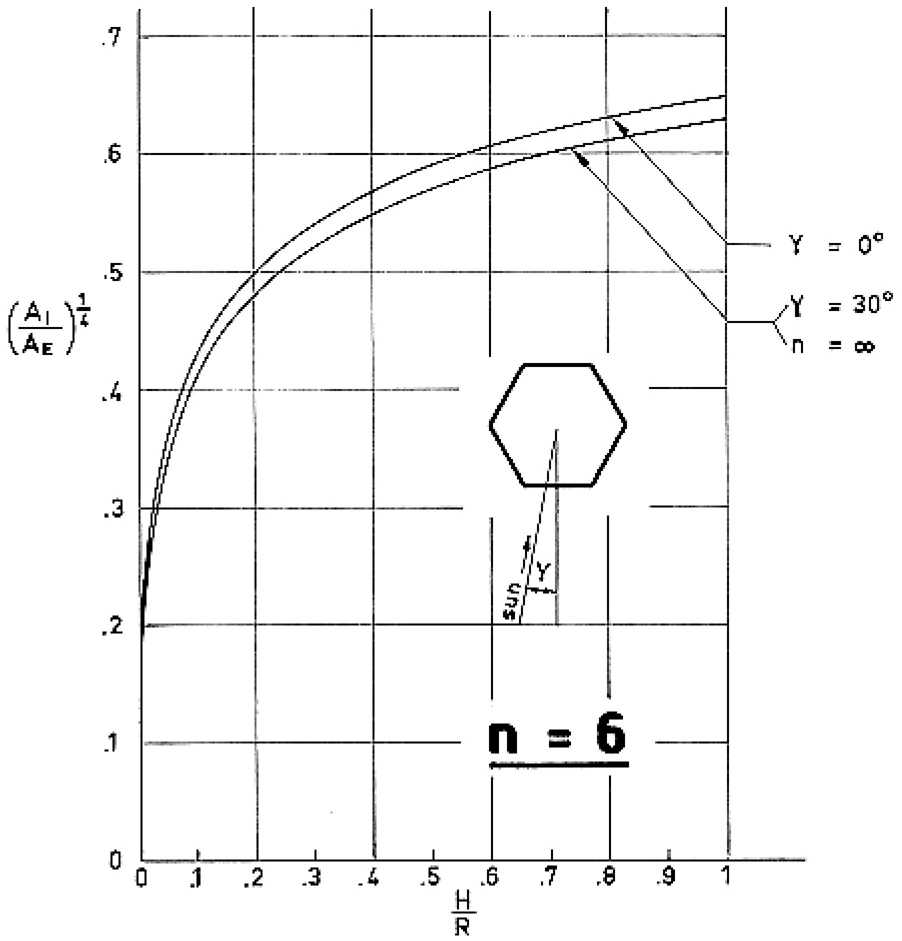

Note: non-si units are used in this figure

Figure 4-32: Ratio $(A_I/A_E)^{1/4}$ as a function of *H*/*R*, in the case of a prism. The curves plotted are those corresponding to the largest and smallest areas projected from the Sun. Circular cylinder, $n = \infty$. Calculated by the compiler.

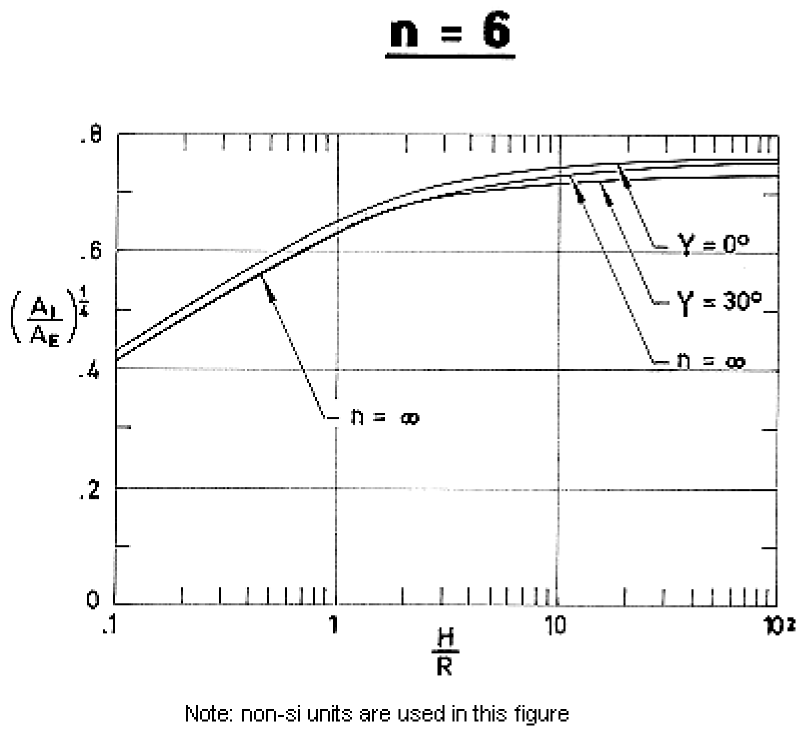

Figure 4-33: Ratio $(A_I/A_E)^{1/4}$ as a function of H/R, in the case of a prism. The curves plotted are those corresponding to the largest and smallest areas projected from the Sun. The values corresponding to $H/R \leq 1$ are also plotted in the previous figure. Circular cylinder, $n = \infty$. Calculated by the compiler.

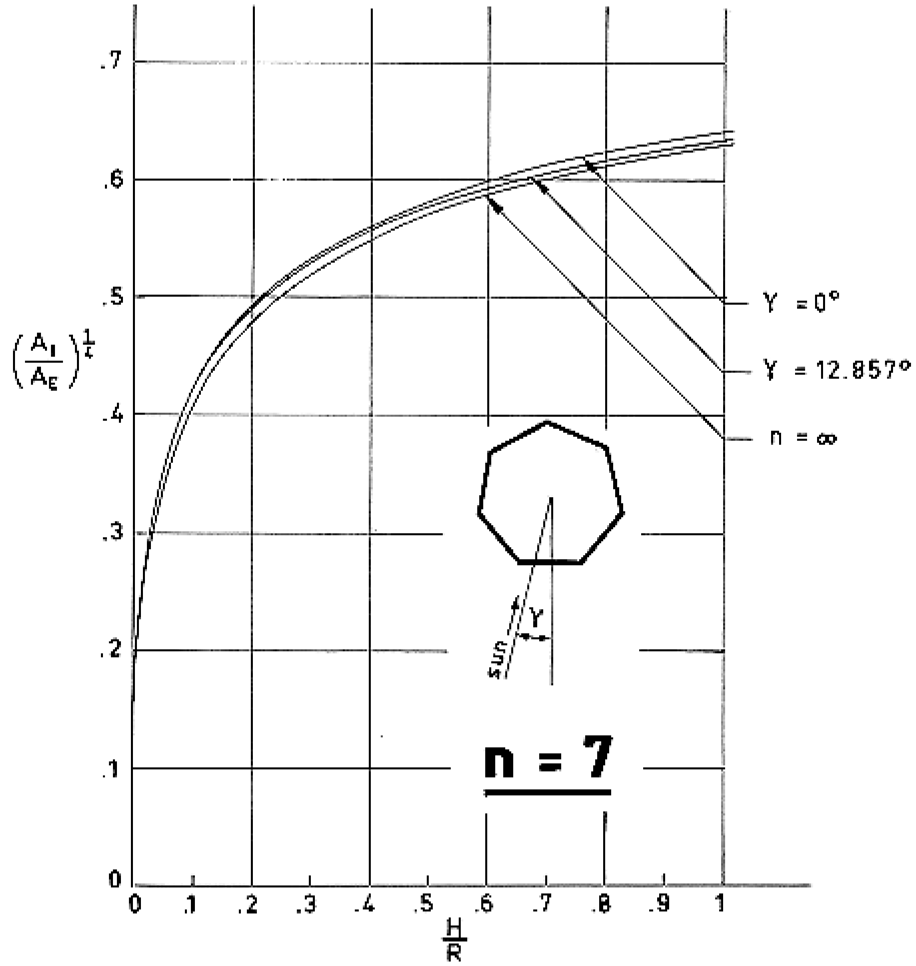

Note: non-si units are used in this figure

Figure 4-34: Ratio $(A_I/A_E)^{1/4}$ as a function of H/R, in the case of a prism. The curves plotted are those corresponding to the largest and smallest areas projected from the Sun. Circular cylinder, $n = \infty$. Calculated by the compiler.

n = 7

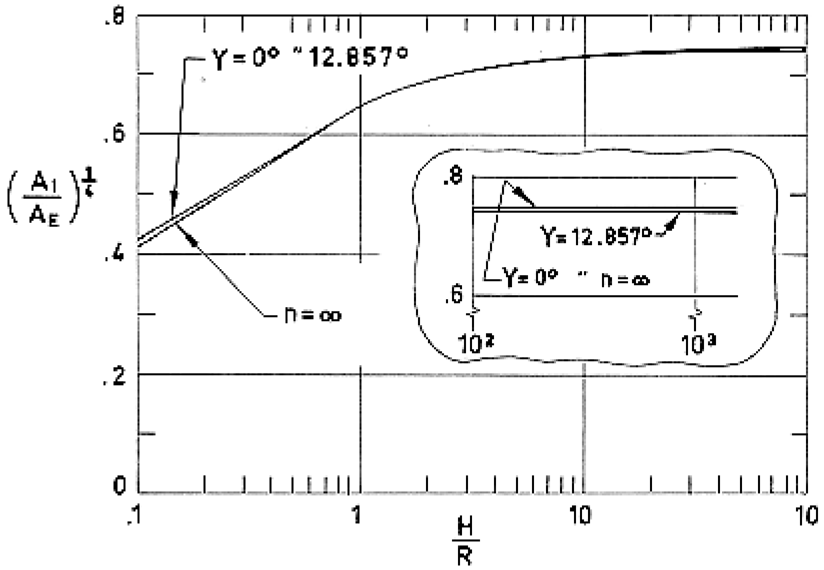

Note: non-si units are used in this figure

Figure 4-35: Ratio (A_I/A_E)$^{1/4}$ as a function of *H*/*R*, in the case of a prism. The curves plotted are those corresponding to the largest and smallest areas projected from the Sun. The values corresponding to *H*/*R* ≤ 1 are also plotted in the previous figure. Circular cylinder, *n* = ∞. Calculated by the compiler.

4.8 Infinitely conductive pyramidal surfaces

4.8.1 Pyramid with an n-sided regular polygonal section

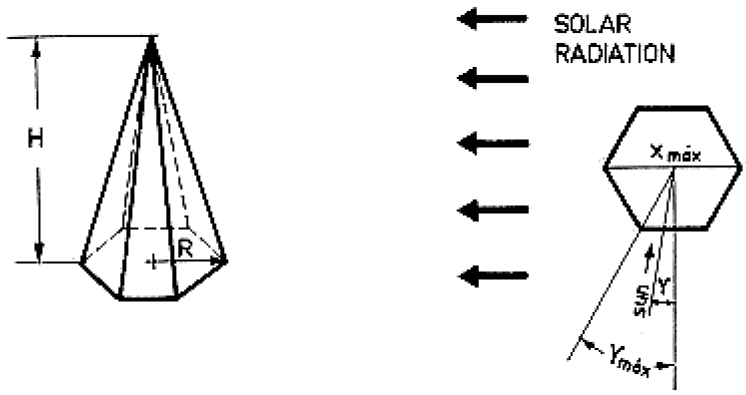

Area Projected from the Sun, A_I:

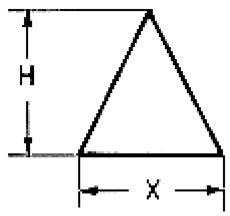

$X/R = 2\cos\gamma$, for n even ,

$X/R = 2\cos(\pi/2n)\cos\gamma$, for n odd.

Formula:

$$\frac{A_I}{A_E} = \frac{\frac{H}{R}\frac{X}{R}}{n\sin\frac{2\pi}{n}\left[1+\sqrt{1+\left(\frac{H/R}{\cos(\pi/n)}\right)^2}\right]} \qquad [4\text{-}9]$$

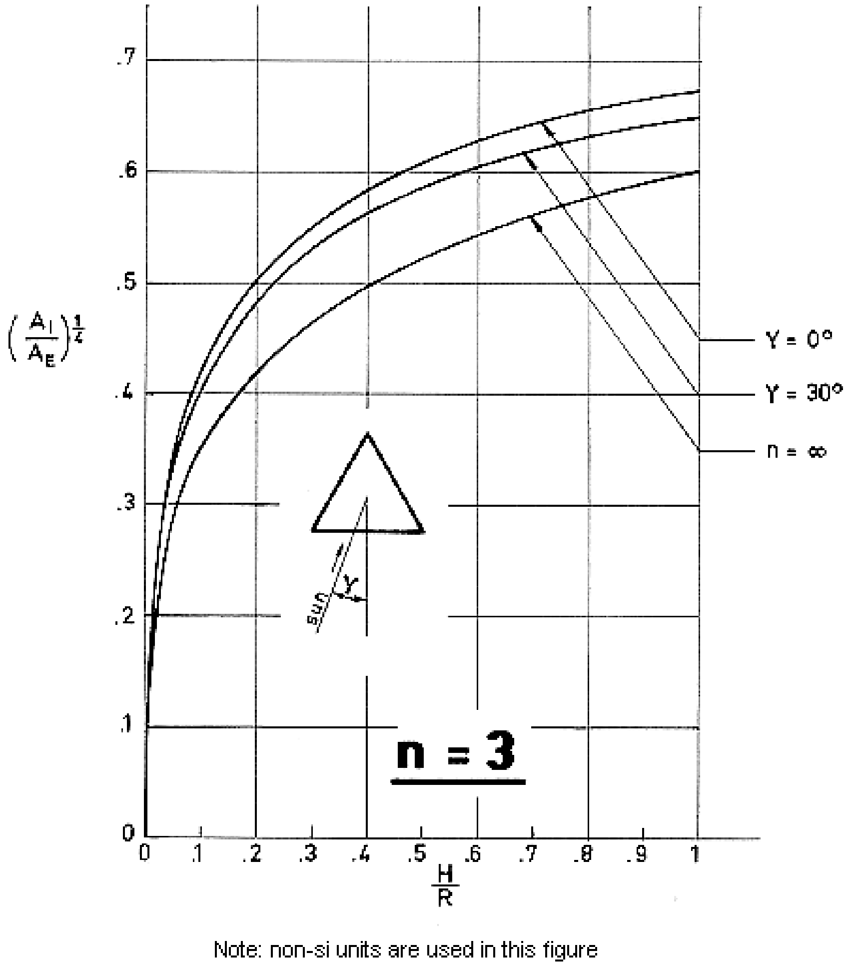

Figure 4-36: Ratio $(A_I/A_E)^{1/4}$ as a function of H/R, in the case of a pyramid. The curves plotted are those corresponding to the largest and smallest areas projected from the Sun. Circular cone, $n = \infty$. Calculated by the compiler.

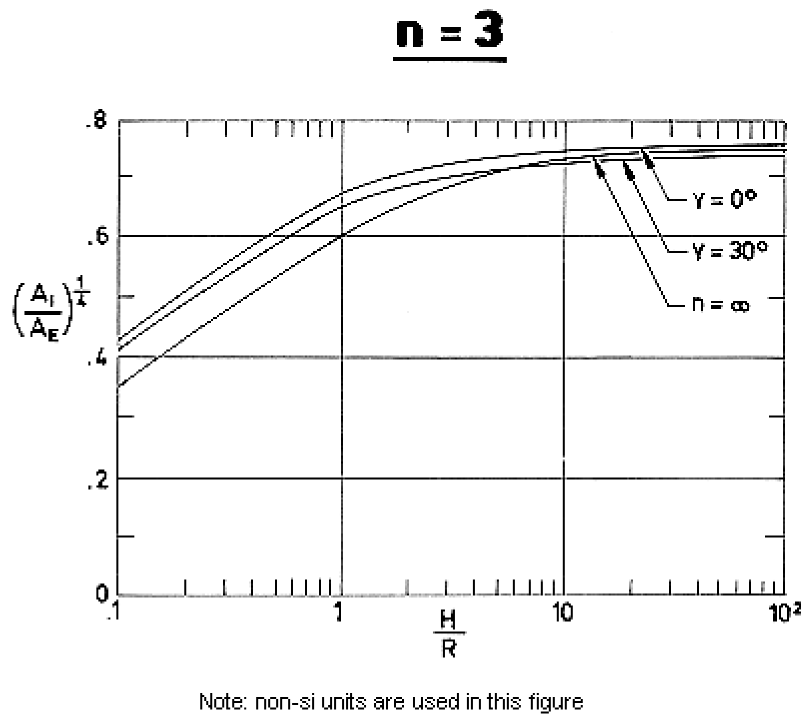

Figure 4-37: Ratio $(A_I/A_E)^{1/4}$ as a function of H/R, in the case of a pyramid. The curves plotted are those corresponding to the largest and smallest areas projected from the Sun. The values corresponding to $H/R \leq 1$ are also plotted in the previous figure. Circular cone, $n = \infty$. Calculated by the compiler.

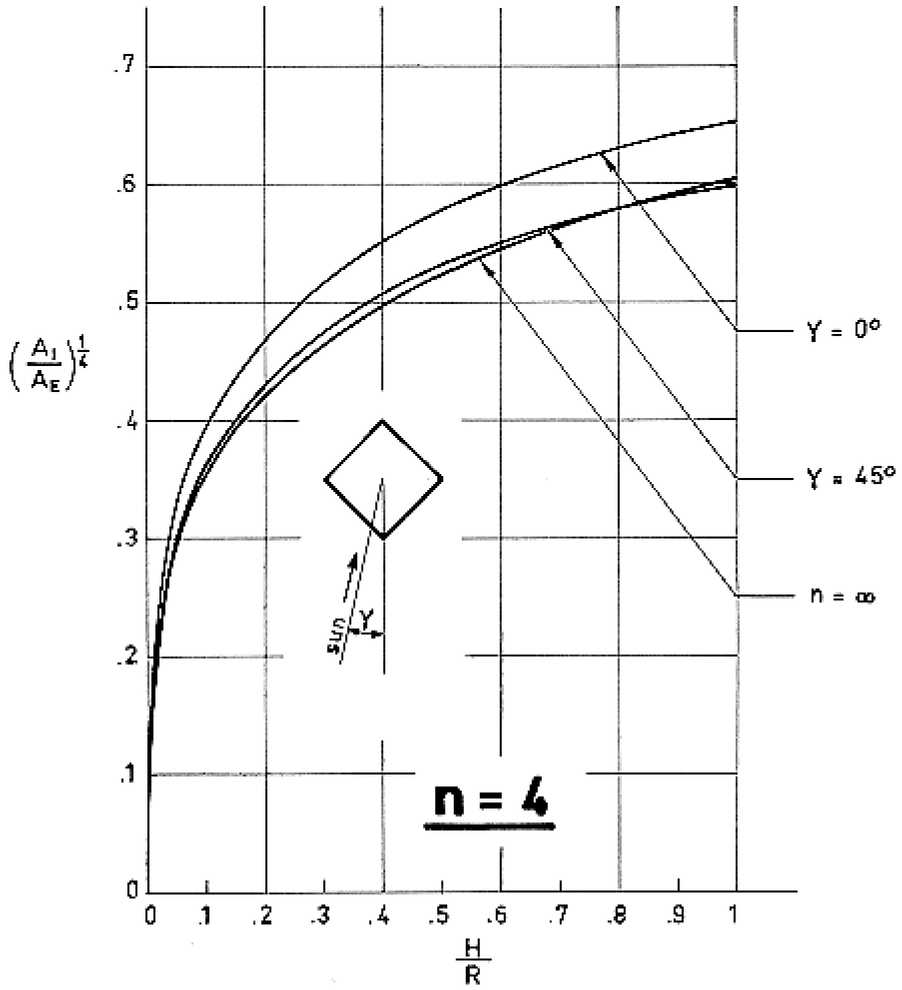

Note: non-si units are used in this figure

Figure 4-38: Ratio $(A_I/A_E)^{1/4}$ as a function of H/R, in the case of a pyramid. The curves plotted are those corresponding to the largest and smallest areas projected from the Sun. Circular cone, $n = \infty$. Calculated by the compiler.

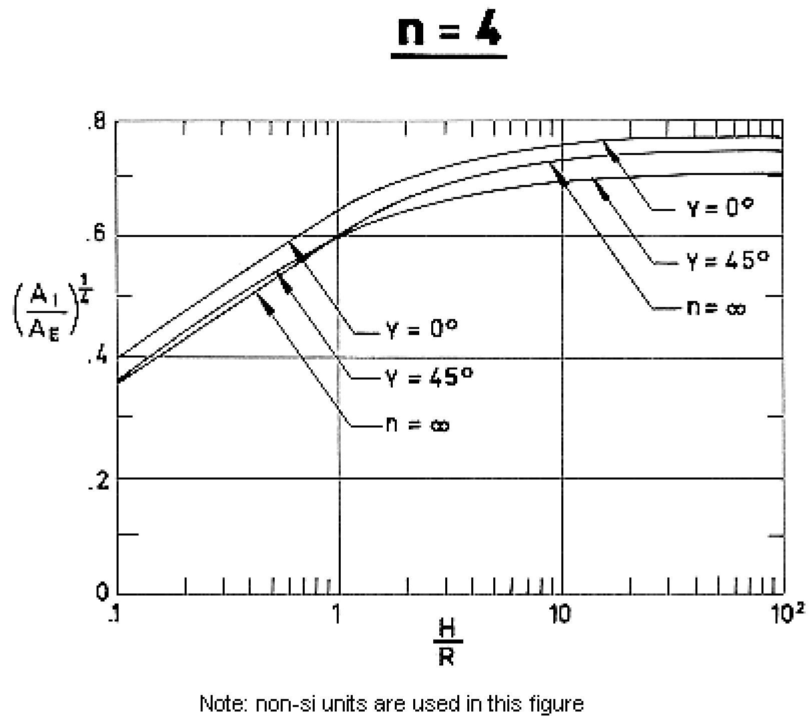

Figure 4-39: Ratio $(A_I/A_E)^{1/4}$ as a function of H/R, in the case of a pyramid. The curves plotted are those corresponding to the largest and smallest areas projected from the Sun. The values corresponding to $H/R \leq 1$ are also plotted in the previous figure. Circular cone, $n = \infty$. Calculated by the compiler.

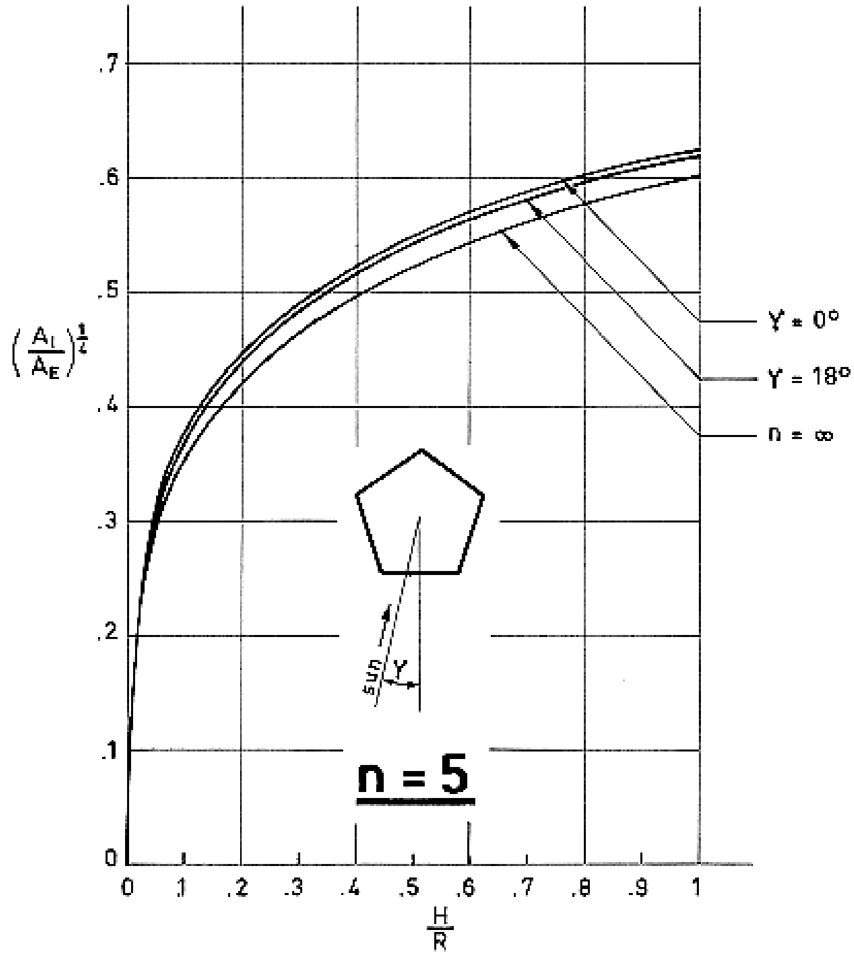

Note: non-si units are used in this figure

Figure 4-40: Ratio $(A_I/A_E)^{1/4}$ as a function of H/R, in the case of a pyramid. The curves plotted are those corresponding to the largest and smallest areas projected from the Sun. Circular cone, $n = \infty$. Calculated by the compiler.

n = 5

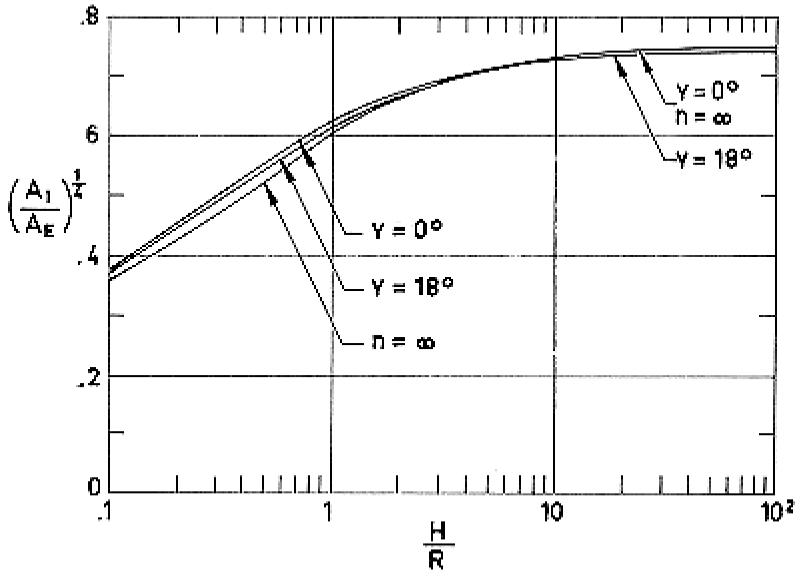

Note: non-si units are used in this figure

Figure 4-41: Ratio $(A_I/A_E)^{1/4}$ as a function of H/R, in the case of a pyramid. The curves plotted are those corresponding to the largest and smallest areas projected from the Sun. The values corresponding to $H/R \leq 1$ are also plotted in the previous figure. Circular cone, $n = \infty$. Calculated by the compiler.

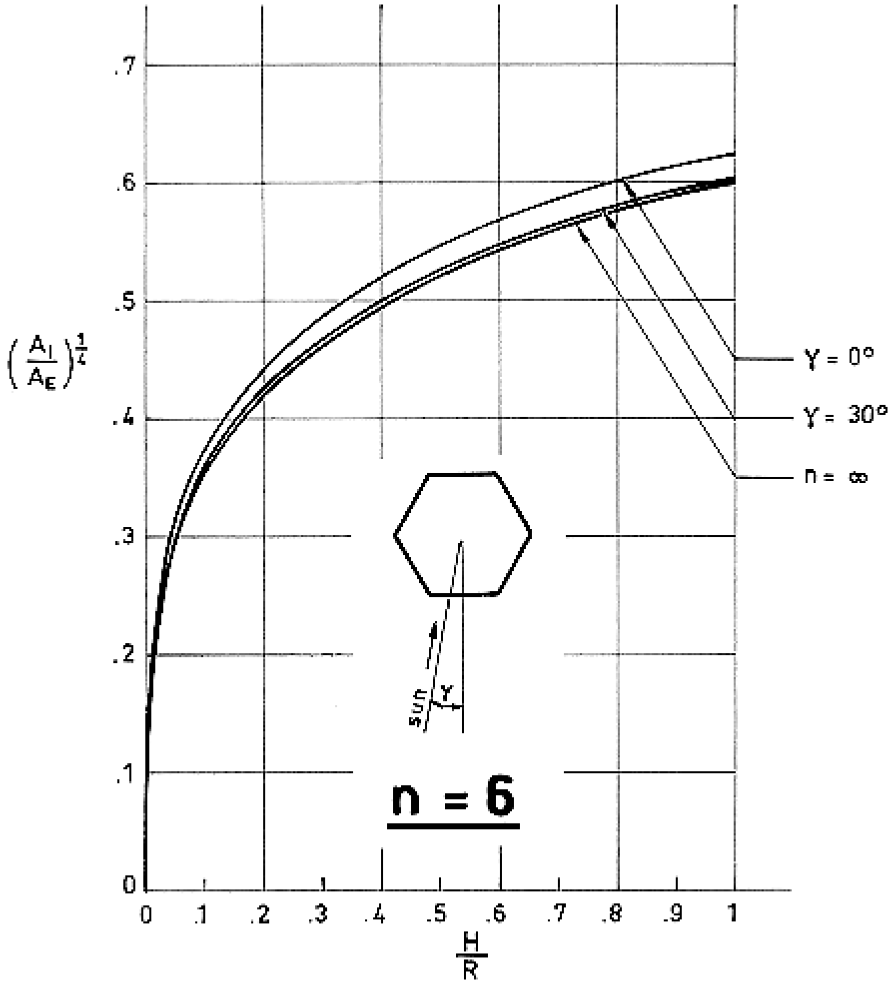

Note: non-si units are used in this figure

Figure 4-42: Ratio $(A_I/A_E)^{1/4}$ as a function of H/R, in the case of a pyramid. The curves plotted are those corresponding to the largest and smallest areas projected from the Sun. Circular cone, $n = \infty$. Calculated by the compiler.

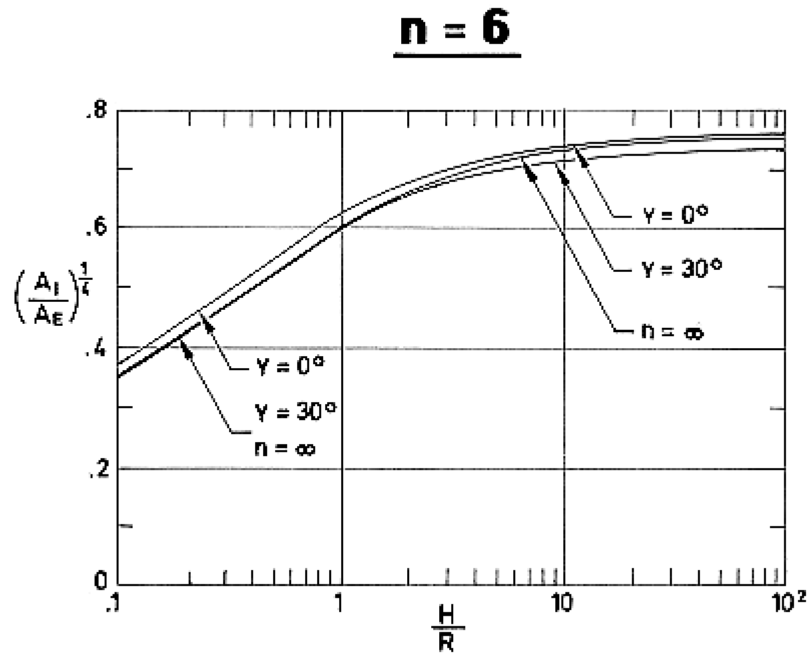

Note: non-si units are used in this figure

Figure 4-43: Ratio $(A_I/A_E)^{1/4}$ as a function of H/R, in the case of a pyramid. The curves plotted are those corresponding to the largest and smallest areas projected from the Sun. The values corresponding to $H/R \leq 1$ are also plotted in the previous figure. Circular cone, $n = \infty$. Calculated by the compiler.

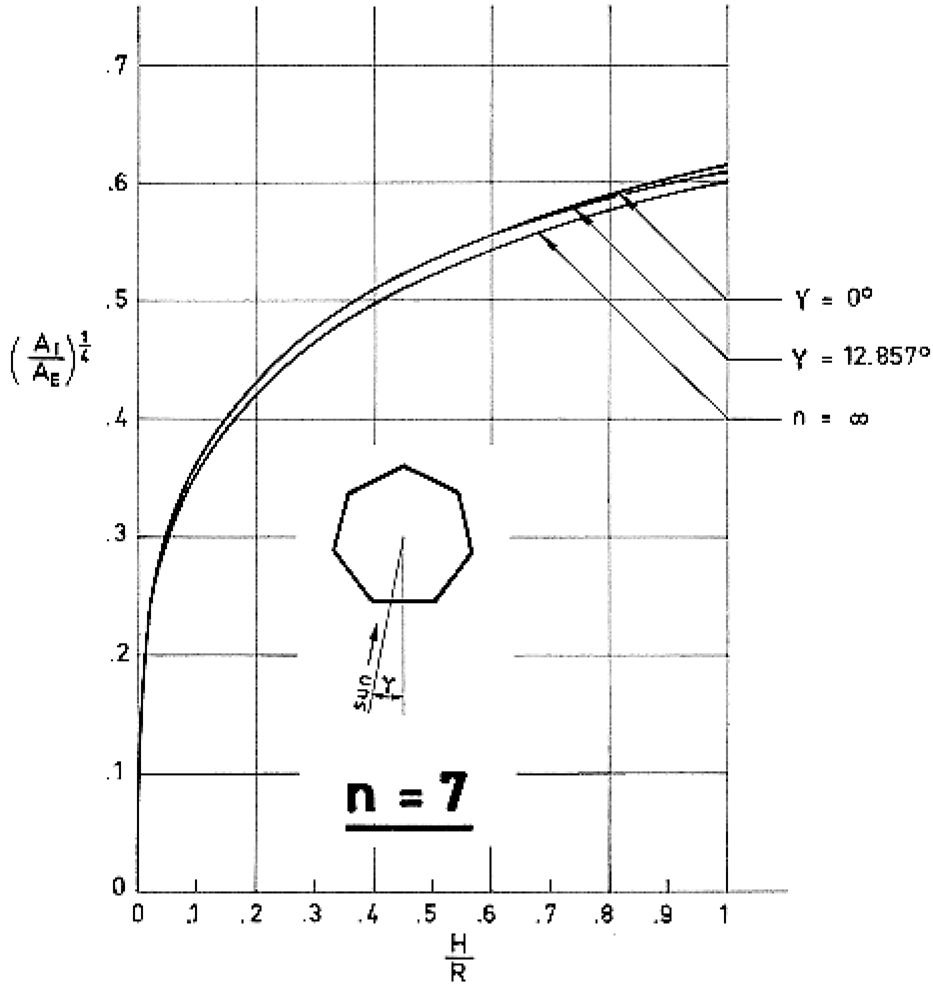

Note: non-si units are used in this figure

Figure 4-44: Ratio $(A_I/A_E)^{1/4}$ as a function of H/R, in the case of a pyramid. The curves plotted are those corresponding to the largest and smallest areas projected from the Sun. Circular cone, $n = \infty$. Calculated by the compiler.

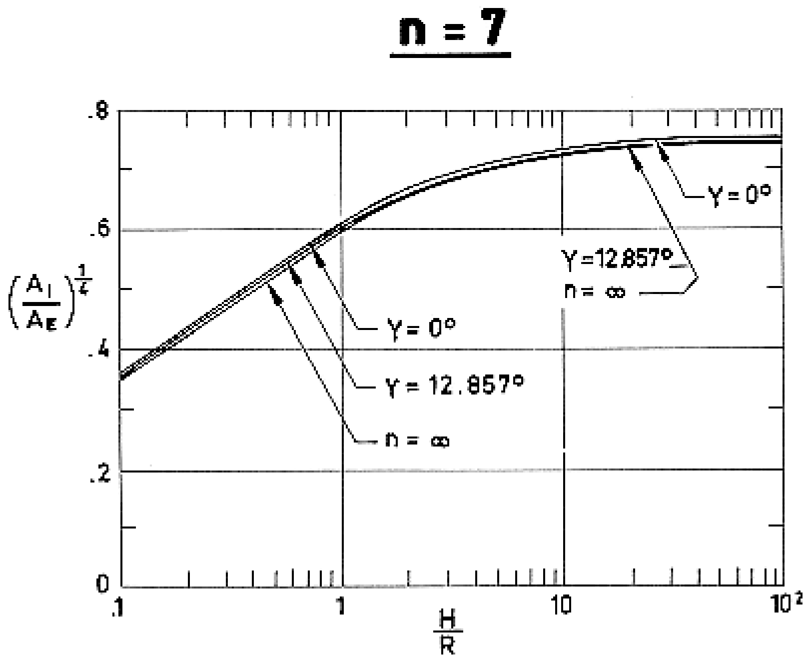

Note: non-si units are used in this figure

Figure 4-45: Ratio $(A_I/A_E)^{1/4}$ as a function of H/R, in the case of a pyramid. The curves plotted are those corresponding to the largest and smallest areas projected from the Sun. The values corresponding to $H/R \leq 1$ are also plotted in the previous figure. Circular cone, $n = \infty$. Calculated by the compiler.

4.9 Infinitely conductive prismatic-pyramidal surfaces

4.9.1.1 Pyramid-prism-pyramid with an n-sided regular polygonal section

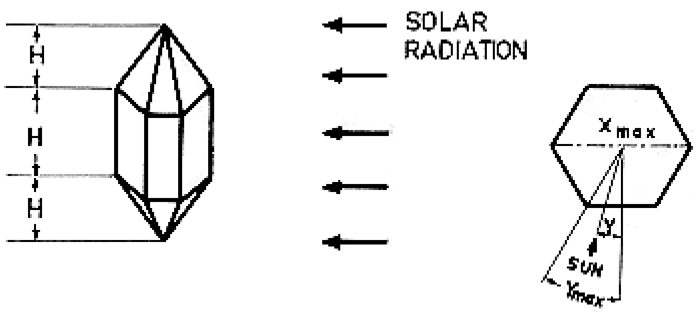

Area Projected from the Sun, A_I:

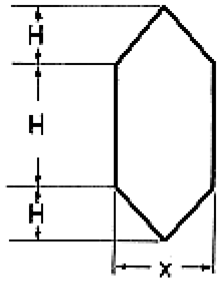

$X/R = 2\cos\gamma$, for n even ,

$X/R = 2\cos(\pi/2n)\cos\gamma$, for n odd.

Formula:

$$\frac{A_I}{A_E} = \frac{\frac{X}{R}}{n\sin\frac{\pi}{n}\left[1+\sqrt{1+\left(\frac{\cos(\pi/n)}{H/R}\right)^2}\right]} \qquad [4\text{-}10]$$

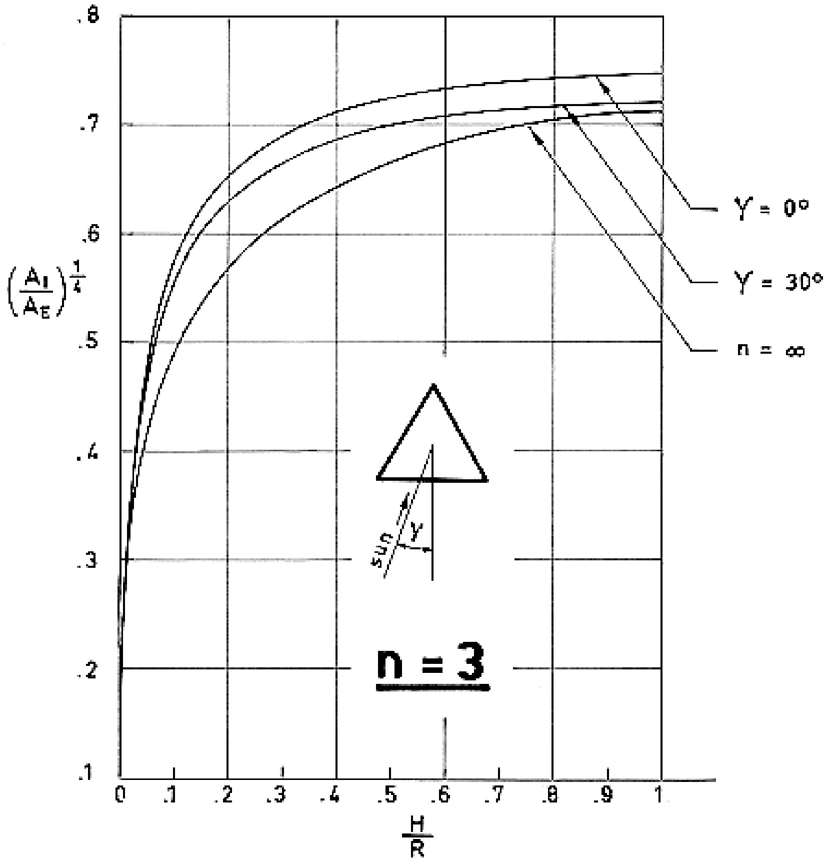

Note: non-si units are used in this figure

Figure 4-46: Ratio $(A_I/A_E)^{1/4}$ as a function of H/R, in the case of a pyramid - prism - pyramid. The curves plotted are those corresponding to the largest and smallest areas projected from the Sun. Cone - cylinder - cone, $n = \infty$. Calculated by the compiler.

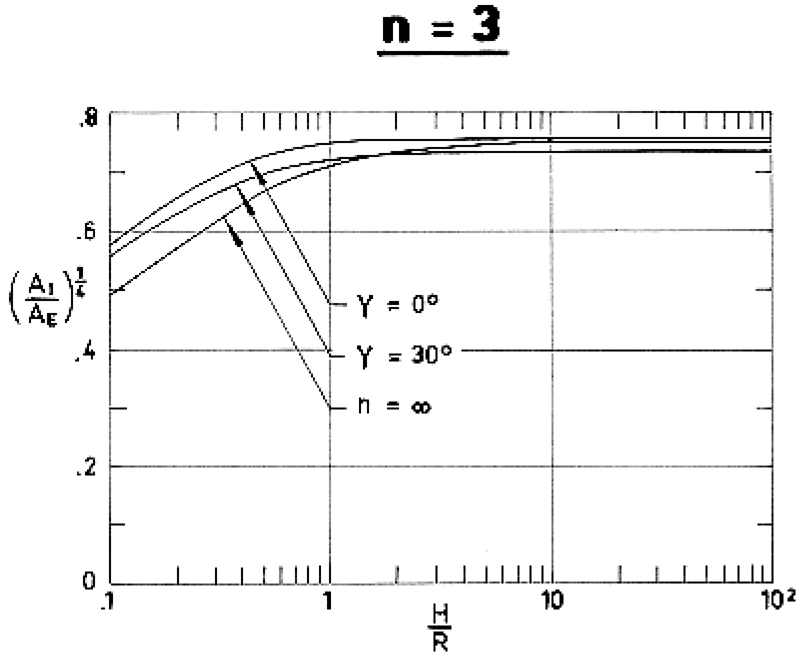

Note: non-si units are used in this figure

Figure 4-47: Ratio $(A_I/A_E)^{1/4}$ as a function of *H*/*R*, in the case of a pyramid - prism - pyramid. The curves plotted are those corresponding to the largest and smallest areas projected from the Sun. The values corresponding to *H*/*R* ≤ 1 are also plotted in the previous figure. Cone - cylinder - cone, *n* = ∞. Calculated by the compiler.

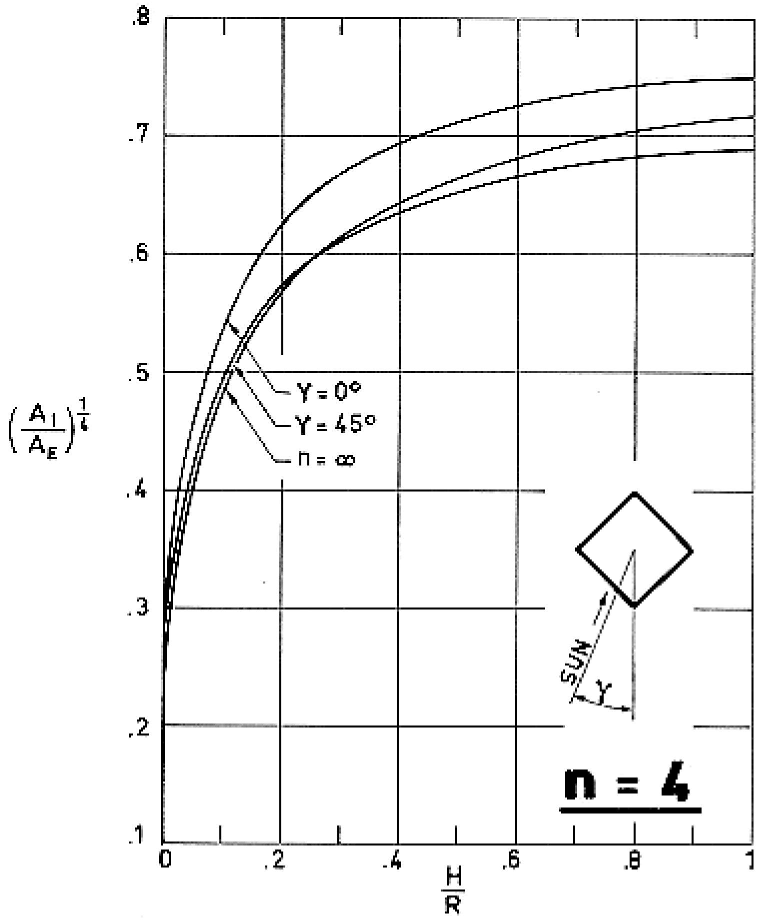

Note: non-si units are used in this figure

Figure 4-48: Ratio $(A_I/A_E)^{1/4}$ as a function of H/R, in the case of a pyramid - prism - pyramid. The curves plotted are those corresponding to the largest and smallest areas projected from the Sun. Cone - cylinder - cone, $n = \infty$. Calculated by the compiler.

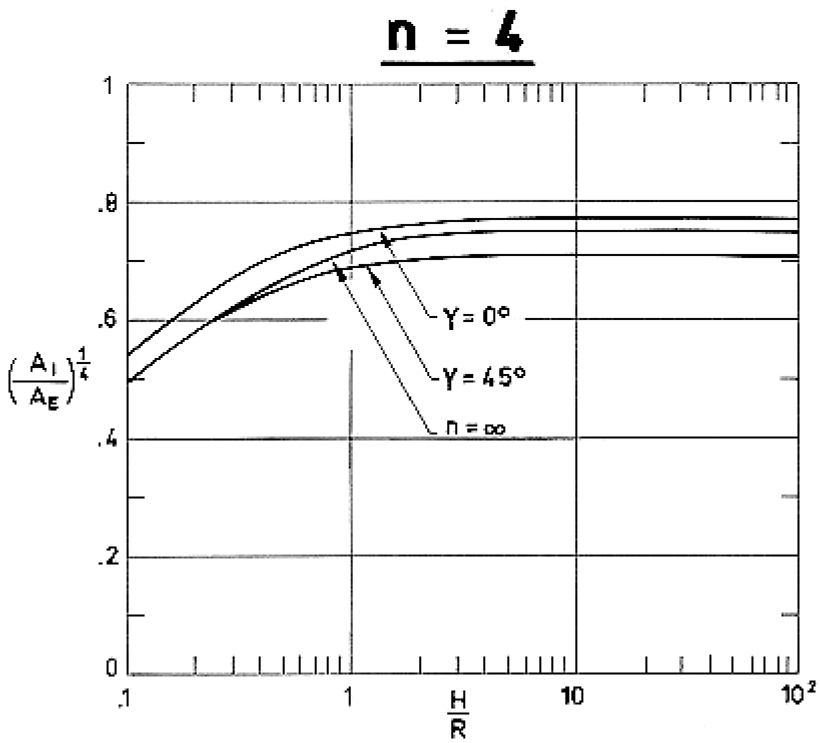

Note: non-si units are used in this figure

Figure 4-49: Ratio $(A_I/A_E)^{1/4}$ as a function of *H*/*R*, in the case of a pyramid - prism - pyramid. The curves plotted are those corresponding to the largest and smallest areas projected from the Sun. The values corresponding to *H*/*R* ≤ 1 are also plotted in the previous figure. Cone - cylinder - cone, *n* = ∞. Calculated by the compiler.

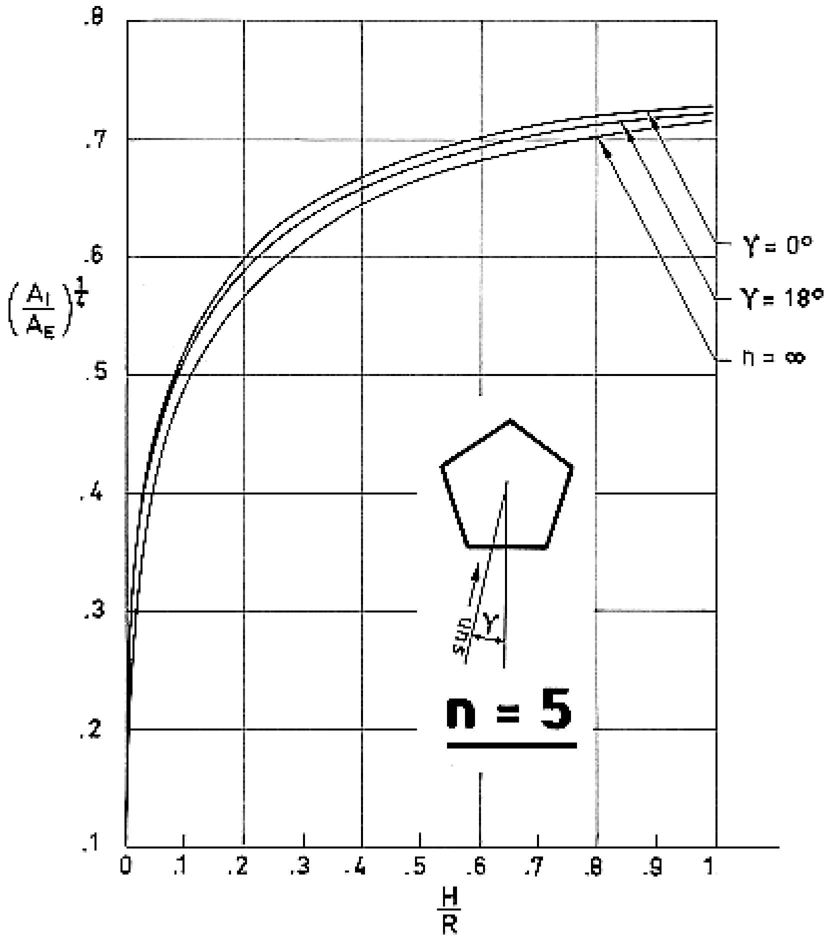

Note: non-si units are used in this figure

Figure 4-50: Ratio $(A_I/A_E)^{1/4}$ as a function of H/R, in the case of a pyramid - prism - pyramid. The curves plotted are those corresponding to the largest and smallest areas projected from the Sun. Cone - cylinder - cone, $n = \infty$. Calculated by the compiler.

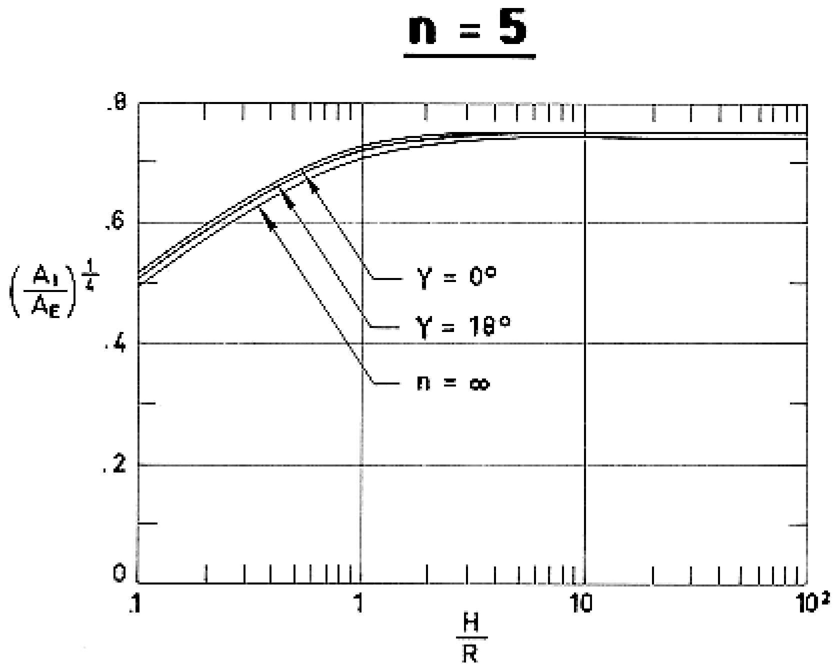

Note: non-si units are used in this figure

Figure 4-51: Ratio $(A_I/A_E)^{1/4}$ as a function of H/R, in the case of a pyramid - prism - pyramid. The curves plotted are those corresponding to the largest and smallest areas projected from the Sun. The values corresponding to $H/R \leq 1$ are also plotted in the previous figure. Cone - cylinder - cone, $n = \infty$. Calculated by the compiler.

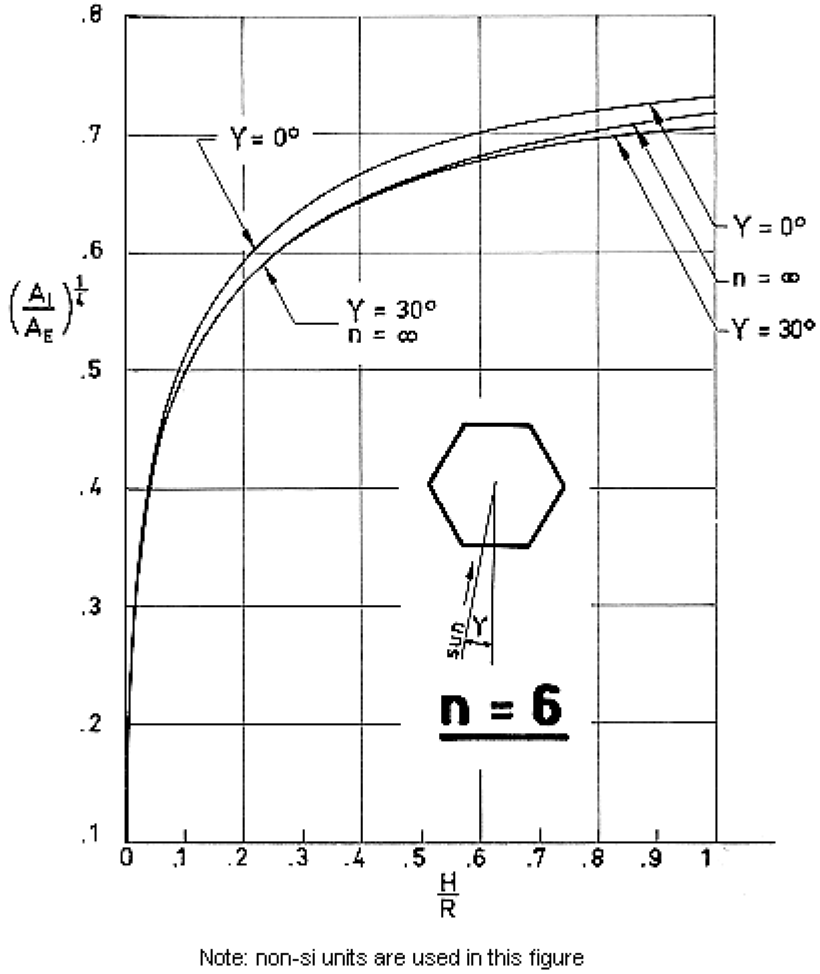

Figure 4-52: Ratio $(A_I/A_E)^{1/4}$ as a function of H/R, in the case of a pyramid - prism - pyramid. The curves plotted are those corresponding to the largest and smallest areas projected from the Sun. Cone - cylinder - cone, $n = \infty$. Calculated by the compiler.

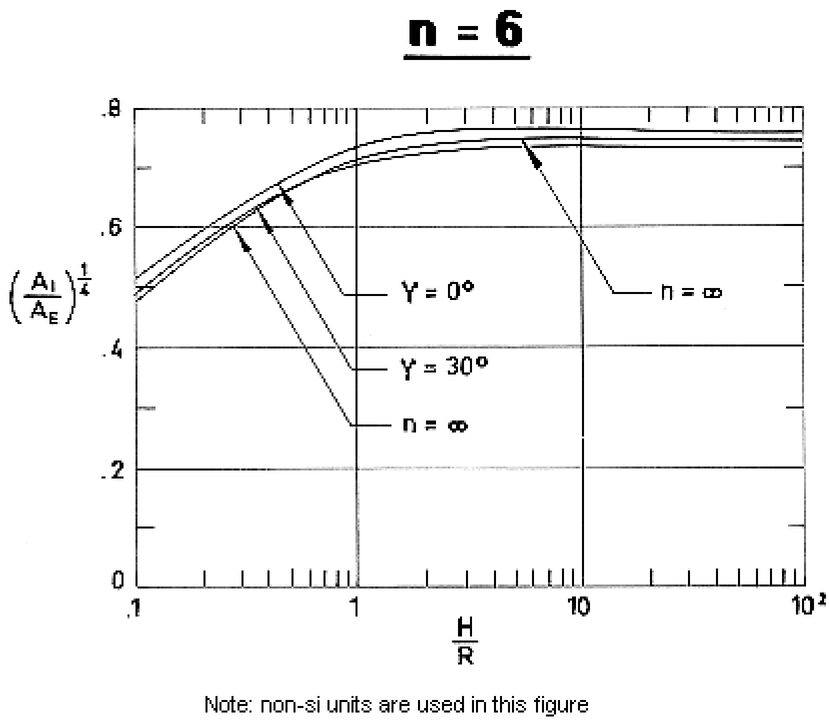

Figure 4-53: Ratio $(A_I/A_E)^{1/4}$ as a function of H/R, in the case of a pyramid - prism - pyramid. The curves plotted are those corresponding to the largest and smallest areas projected from the Sun. The values corresponding to $H/R \leq 1$ are also plotted in the previous figure. Cone - cylinder - cone, $n = \infty$. Calculated by the compiler.

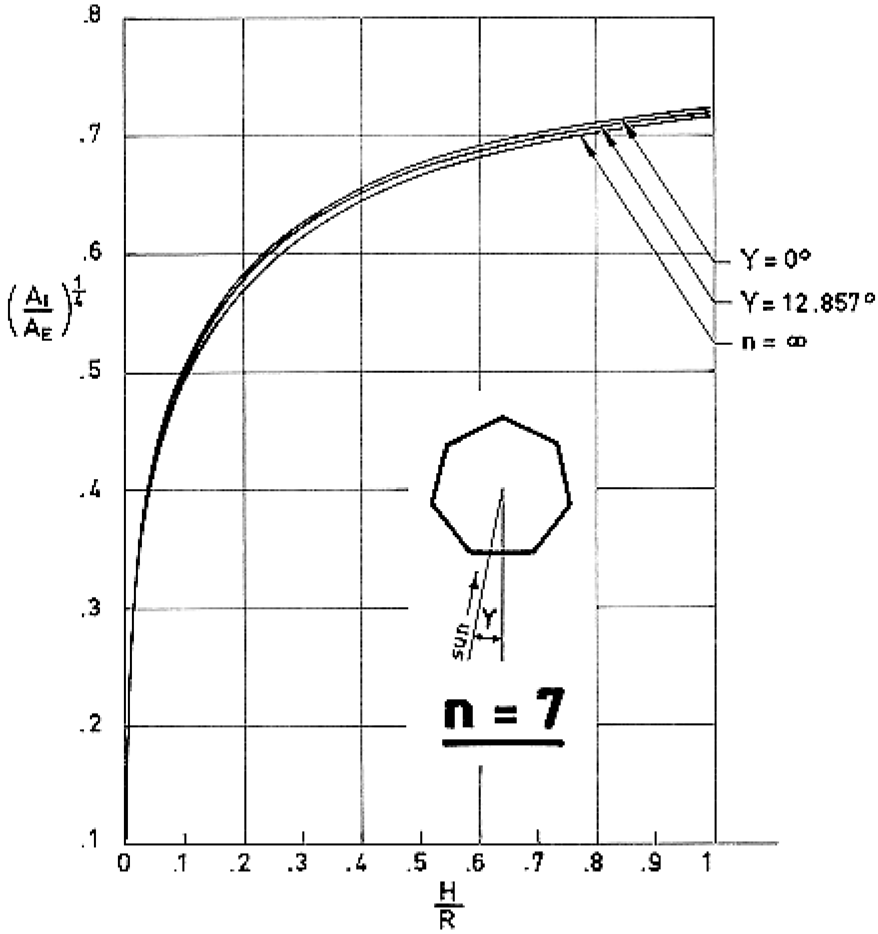

Note: non-si units are used in this figure

Figure 4-54: Ratio $(A_I/A_E)^{1/4}$ as a function of *H*/*R*, in the case of a pyramid - prism - pyramid. The curves plotted are those corresponding to the largest and smallest areas projected from the Sun. Cone - cylinder - cone, $n = \infty$. Calculated by the compiler.

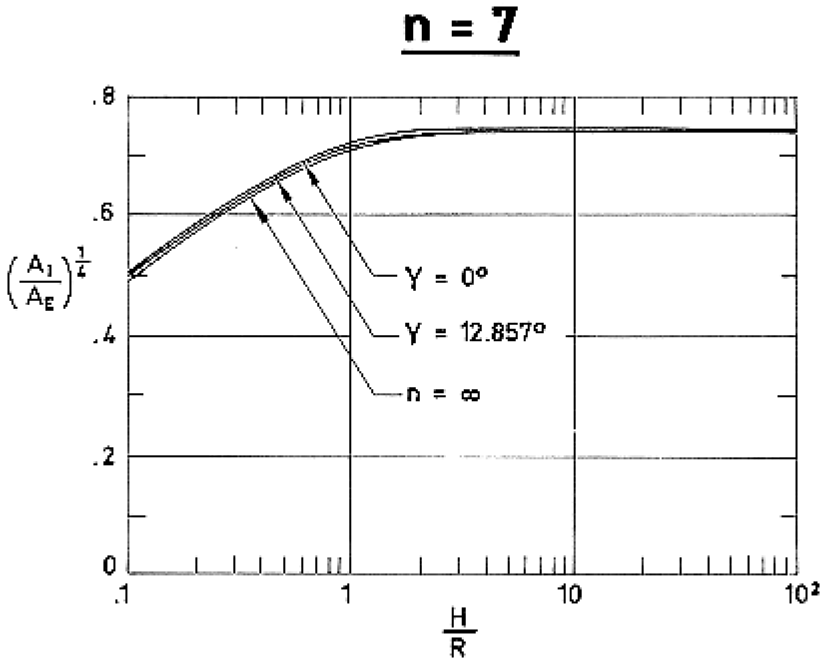

Note: non-si units are used in this figure

Figure 4-55: Ratio $(A_I/A_E)^{1/4}$ as a function of H/R, in the case of a pyramid - prism - pyramid. The curves plotted are those corresponding to the largest and smallest areas projected from the Sun. Cone - cylinder - cone, $n = \infty$. Calculated by the compiler.

4.10 Thin-walled spherical bodies. Finite conductivity

4.10.1 Non-spinning sphere

Sketch:

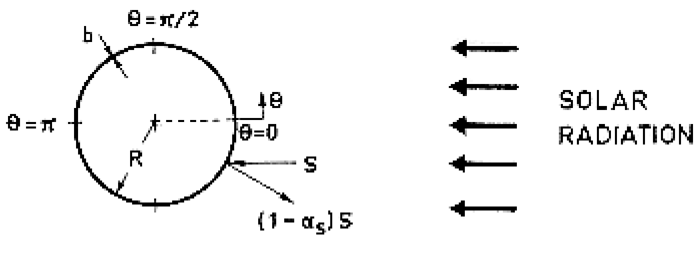

Dimensionless Parameters:

$\tau(\theta) = T(\theta)/T_R$, $\mu = kb/\varepsilon\sigma T_R^3 R^2$

Differential Equations:

$$\frac{\mu}{\sin\theta}\frac{d}{d\theta}\left(\sin\theta\frac{d\tau}{d\theta}\right) = \begin{cases} \tau^4 - 4\cos\theta \quad , & when\, 0 \le \theta \le \pi/2 \\ \tau^4 \quad , & when\, \pi/2 \le \theta \le \pi \end{cases} \qquad [4\text{-}11]$$

Boundary Conditions:

$$\left.\frac{d\tau}{d\theta}\right|_{\theta=0} = \left.\frac{d\tau}{d\theta}\right|_{\theta=\pi} = 0 \quad , \quad \tau\Big|_{\theta=\pi/2} \; and \; \left.\frac{d\tau}{d\theta}\right|_{\theta=\pi/2} \; continuous \qquad [4\text{-}12]$$

Comments: The results obtained by numerically solving this problem are given in the following.

Reference: Nichols (1961) [11].

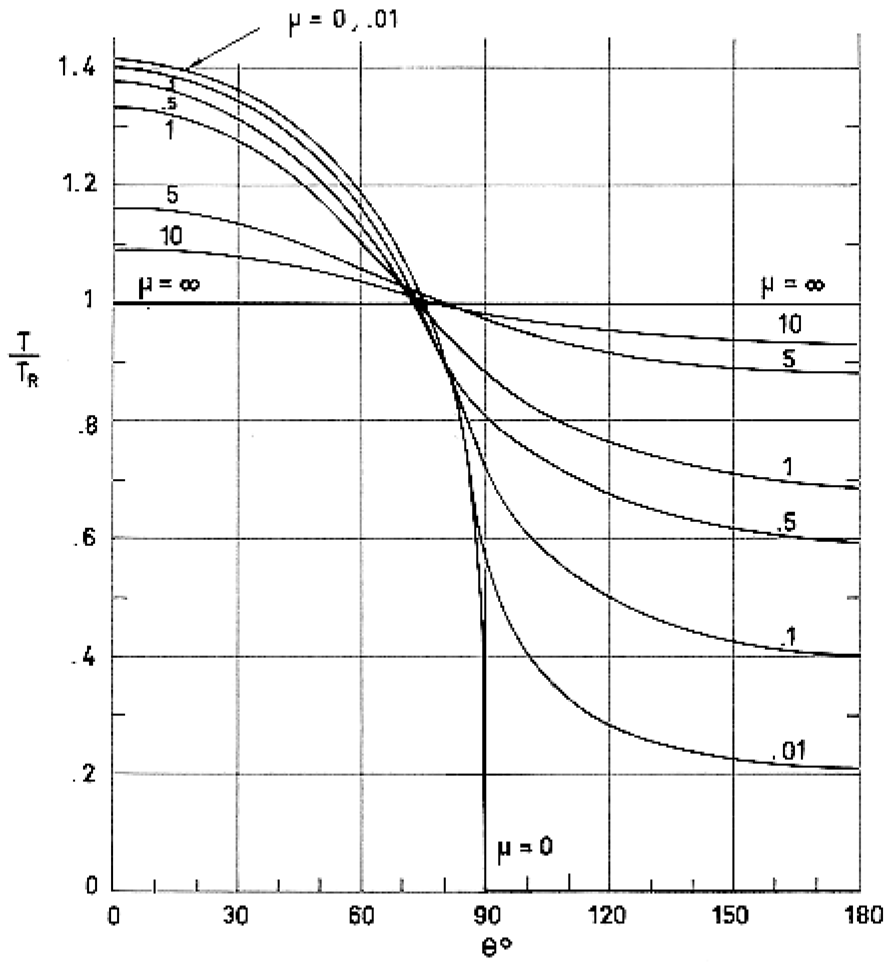

Note: non-si units are used in this figure

Figure 4-56: Temperature distribution on sphere. No spin. No internal radiation. Calculated by the compiler.

4.10.2 Non-spinning sphere. Including internal radiation

Sketch:

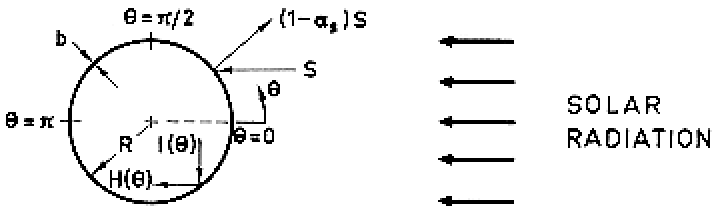

H(θ), Radiation Flux Density Leaving Inside the Sphere.

I(θ), Radiation Flux Density Impinging on Inside the Sphere.

Dimensionless Parameters:

$\tau(\theta) = T(\theta)/T_R$, $\mu = kb/\varepsilon\sigma T_R^3 R^2$

Differential Equations:

$$\frac{\mu}{\sin\theta}\frac{d}{d\theta}\left(\sin\theta\frac{d\tau}{d\theta}\right) = \begin{cases} 2\tau^4 - 4\cos\theta - 1 \quad , & when\ 0 \le \theta \le \pi/2 \\ 2\tau^4 - 1 \quad , & when\ \pi/2 \le \theta \le \pi \end{cases} \qquad [4\text{-}13]$$

Note: non-si units are used in this figure

Boundary Conditions:

$$\left.\frac{d\tau}{d\theta}\right|_{\theta=0} = \left.\frac{d\tau}{d\theta}\right|_{\theta=\pi} = 0 \quad , \quad \tau\big|_{\theta=\pi/2}\ and\ \left.\frac{d\tau}{d\theta}\right|_{\theta=\pi/2}\ continuous \qquad [4\text{-}14]$$

Note: non-si units are used in this figure

Comments: The results obtained by numerically solving this problem are given in the following.

Reference: Nichols (1961) [11].

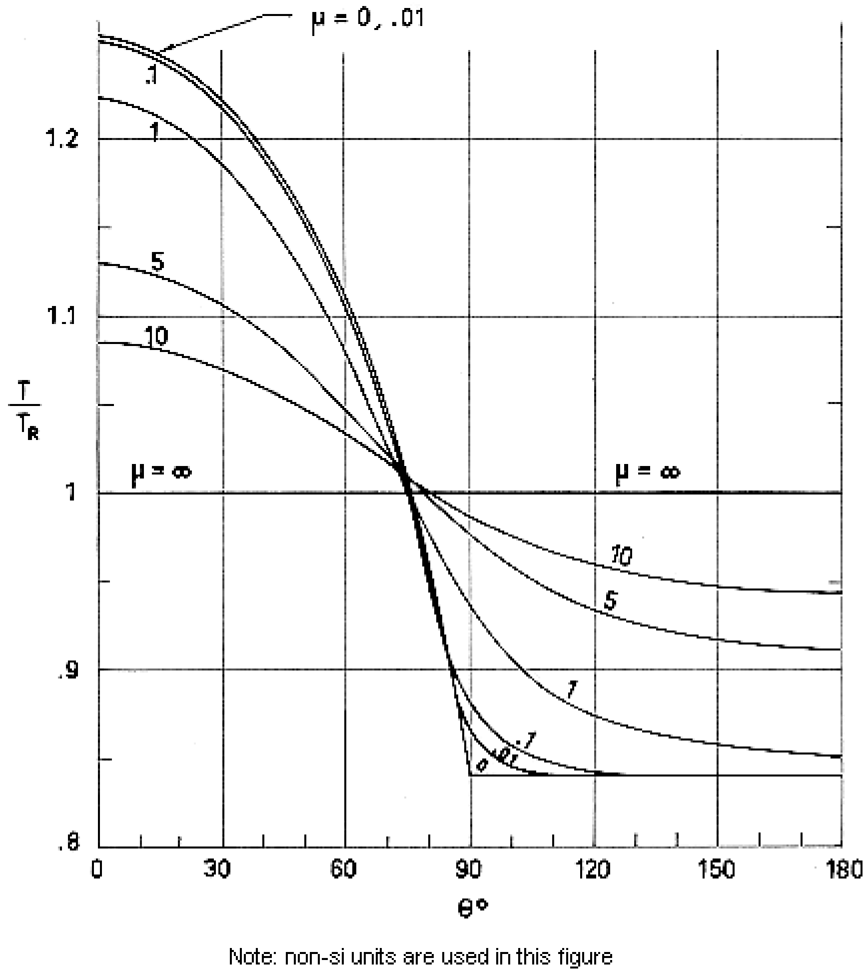

Figure 4-57: Temperature distribution on sphere including internal radiation. No spin. Calculated by the compiler.

4.11 Thin-walled cylindrical bodies. Finite conductivity.

4.11.1 Non-spinning two-dimensional circular cylinder

Sketch:

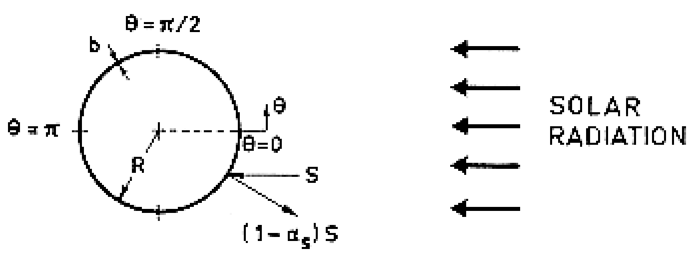

Dimensionless Parameters:

$\tau(\theta) = T(\theta)/T_R$, $\mu = kb/\varepsilon\sigma T_R^3 R^2$

Differential Equations:

$$\mu\frac{d^2\tau}{d\theta^2}=\begin{cases}\tau^4-\pi\cos\theta & , \quad when\ 0\le\theta\le\pi/2\\ \tau^4 & , \quad when\ \pi/2\le\theta\le\pi\end{cases} \qquad [4\text{-}15]$$

Note: non-si units are used in this figure

Boundary Conditions:

$$\left.\frac{d\tau}{d\theta}\right|_{\theta=0}=\left.\frac{d\tau}{d\theta}\right|_{\theta=\pi}=0 \quad , \quad \left.\tau\right|_{\theta=\pi/2}\ and\ \left.\frac{d\tau}{d\theta}\right|_{\theta=\pi/2}\ continuous \qquad [4\text{-}16]$$

Note: non-si units are used in this figure

Comments: Assumption concerning axial-symmetry is, obviously, not applicable in this case.

The results presented in the following involve a linearization of the radiative transfer term.

Reference: Charners & Raynor (1960) [4].

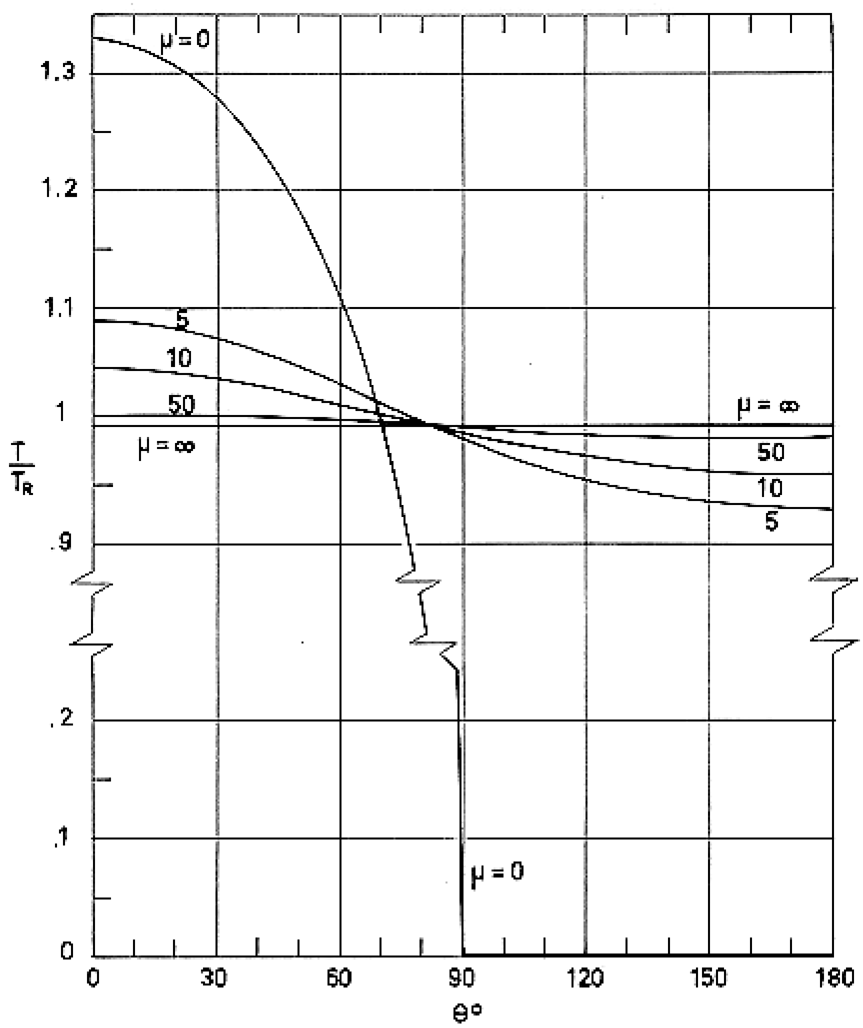

Note: non-si units are used in this figure

Figure 4-58: Temperature distribution on a two-dimensional cylinder. No spin. No internal radiation. Calculated by the compiler.

4.11.2 Spinning two-dimensional circular cylinder

Sketch:

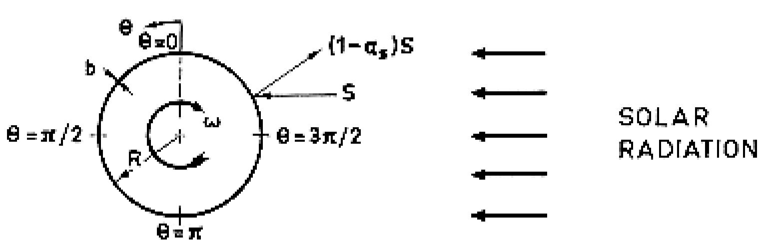

Dimensionless Parameters:

$\tau(\theta) = T(\theta)/T_R$, $\mu = kb/\varepsilon\sigma T_R^3 R^2$, $\gamma = \rho bc\omega/\varepsilon\sigma T_R^3$

where:

ω, Angular Velocity. [sec^{-1}].

c, Specific Heat of the Material. [$J.kg^{-1}.K^{-1}$].

ρ, Density of the Material. [$kg.m^{-3}$]

Differential Equations:

$$\mu \frac{d^2\tau}{d\theta^2} + \gamma \frac{d\tau}{d\theta} = \begin{cases} \tau^4 \quad , & when\ 0 \le \theta \le \pi \\ \tau^4 + \pi \sin\theta \quad , & when \pi \le \theta \le 2\pi \end{cases} \qquad [4\text{-}17]$$

Note: non-si units are used in this figure

Boundary Conditions:

$$\left.\frac{d\tau}{d\theta}\right|_{\theta=0} = \left.\frac{d\tau}{d\theta}\right|_{\theta=2\pi} \quad , \quad \tau|_{\theta=\pi}\ and\ \left.\frac{d\tau}{d\theta}\right|_{\theta=\pi}\ continuous \qquad [4\text{-}18]$$

Note: non-si units are used in this figure

Comments: The results presented have been obtained linearizing the equations, either assuming $\mu/\gamma << 2\pi$, Figure 4-59 or $|\tau-1| << 1$, Figure 4-60. In the last case terms of order $(\tau-1)^2$ have been neglected, so that $\tau^4 = 1+4(\tau-1)$. This approximation is valid when $\mu/\gamma \sim 1$.

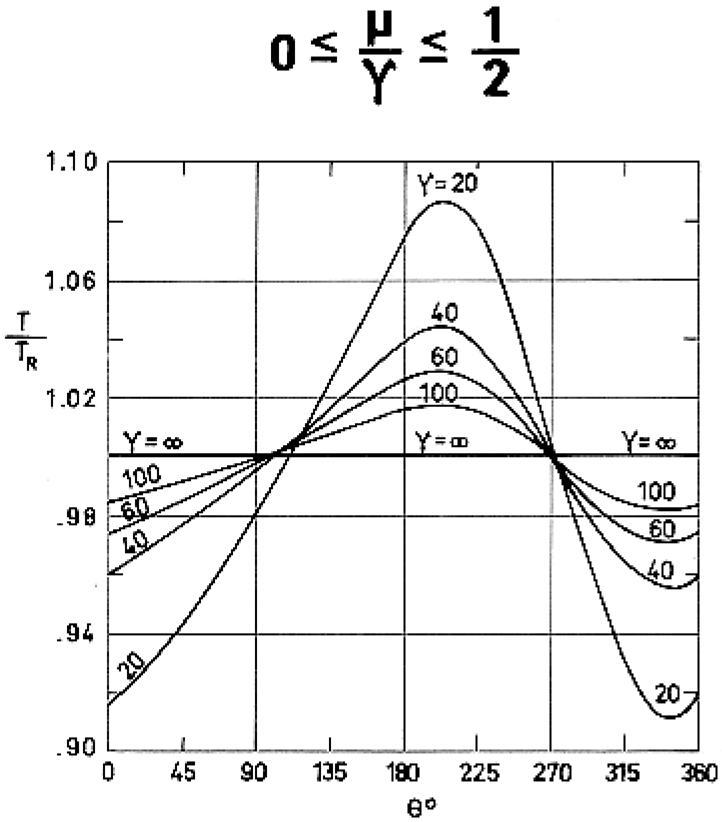

Note: non-si units are used in this figure

Figure 4-59: Temperature distribution on a two - dimensional spinning cylinder for several μ an γ values. No internal radiation. Calculated by the compiler.

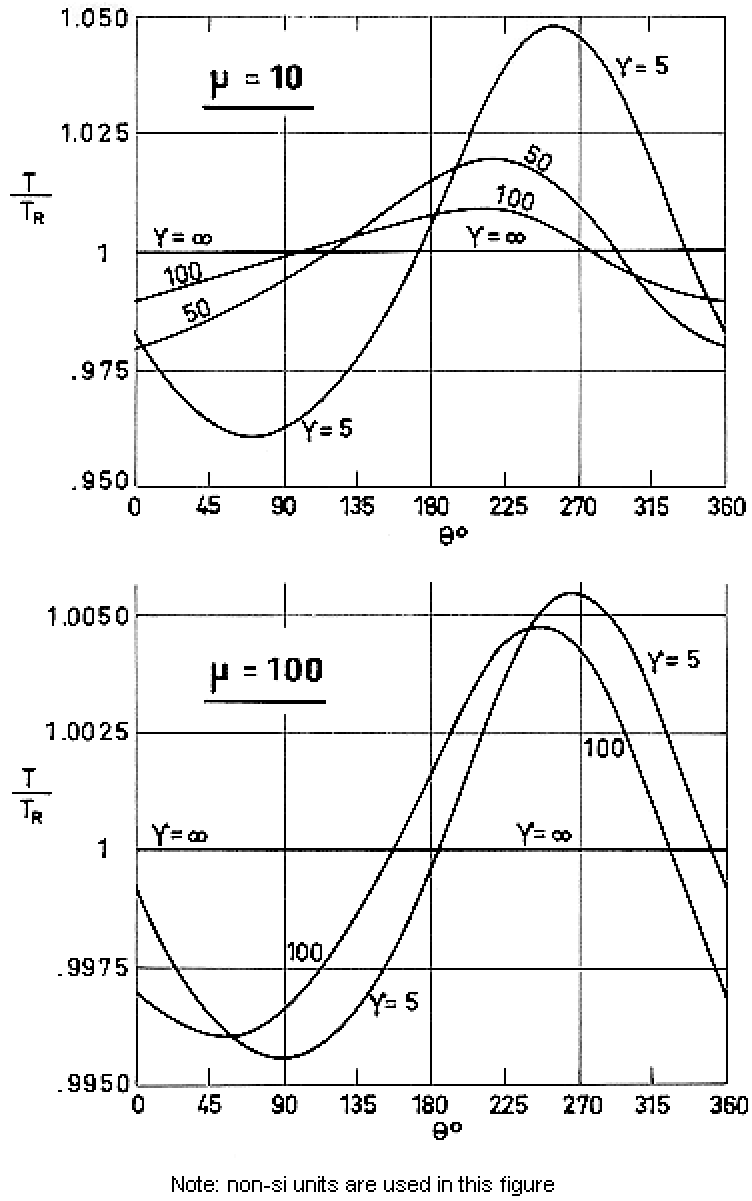

Figure 4-60: Temperature distribution on a two - dimensional spinning cylinder for several μ an γ values. No internal radiation. Calculated by the compiler.

4.11.3 Circular cylinder. solar radiation parallel to axis of symmetry

Sketch:

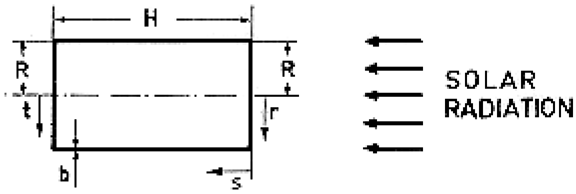

Dimensionless Parameters:

$x = r/R$, for $0 \le x \le 1$; $x = 1+s/H$, for $1 \le x \le 2$; $x = 3 - t/R$, for $2 \le x \le 3$; $\tau = T/T_R$; $\lambda = H/R$; $\mu = kb/\varepsilon\sigma T_R^3 R^2$.

Differential Equations:

$$\frac{\mu}{x}\frac{d}{dx}\left(x\frac{d\tau_1}{dx}\right) = \tau_1^4 - 2(\lambda+1) \quad , \quad when\ 0 \le x \le 1$$

$$\frac{\mu}{\lambda^2}\frac{d^2\tau_2}{dx^2} = \tau_2^4 \quad , \quad when\ 1 \le x \le 2 \qquad [4\text{-}19]$$

$$\frac{\mu}{3-x}\frac{d}{dx}\left[(3-x)\frac{d\tau_3}{dx}\right] = \tau_3^4 \quad , \quad when\ 2 \le x \le 3$$

Note: non-si units are used in this figure

Boundary Conditions:

$$\left.\frac{d\tau_1}{dx}\right|_{x=0} = \left.\frac{d\tau_3}{dx}\right|_{x=3} = 0 \quad , \quad \tau_1\big|_{x=1} = \tau_2\big|_{x=1} \quad , \quad \tau_2\big|_{x=2} = \tau_3\big|_{x=2}$$

$$\lambda\left.\frac{d\tau_1}{dx}\right|_{x=1} = \left.\frac{d\tau_2}{dx}\right|_{x=1} \quad , \quad \left.\frac{d\tau_2}{dx}\right|_{x=2} = \lambda\left.\frac{d\tau_3}{dx}\right|_{x=2}$$

$$\left.\frac{d\tau_1}{dx}\right|_{x=0} = \left.\frac{d\tau_3}{dx}\right|_{x=3} = 0 \quad , \quad \tau_1\big|_{x=1} = \tau_2\big|_{x=1} \quad , \quad \tau_2\big|_{x=2} = \tau_3\big|_{x=2} \qquad [4\text{-}20]$$

$$\lambda\left.\frac{d\tau_1}{dx}\right|_{x=1} = \left.\frac{d\tau_2}{dx}\right|_{x=1} \quad , \quad \left.\frac{d\tau_2}{dx}\right|_{x=2} = \lambda\left.\frac{d\tau_3}{dx}\right|_{x=2}$$

Note: non-si units are used in this figure

Comments: To obtain the results presented in the following, the 4th power temperature terms, which appear in the above equations, have been linearized according to the expression $\tau^4 = 4\tau\text{-}3$. Note that this linearization will give results with increased accuracy as the parameter μ gets larger.

Reference: Nichols (1961) [11].

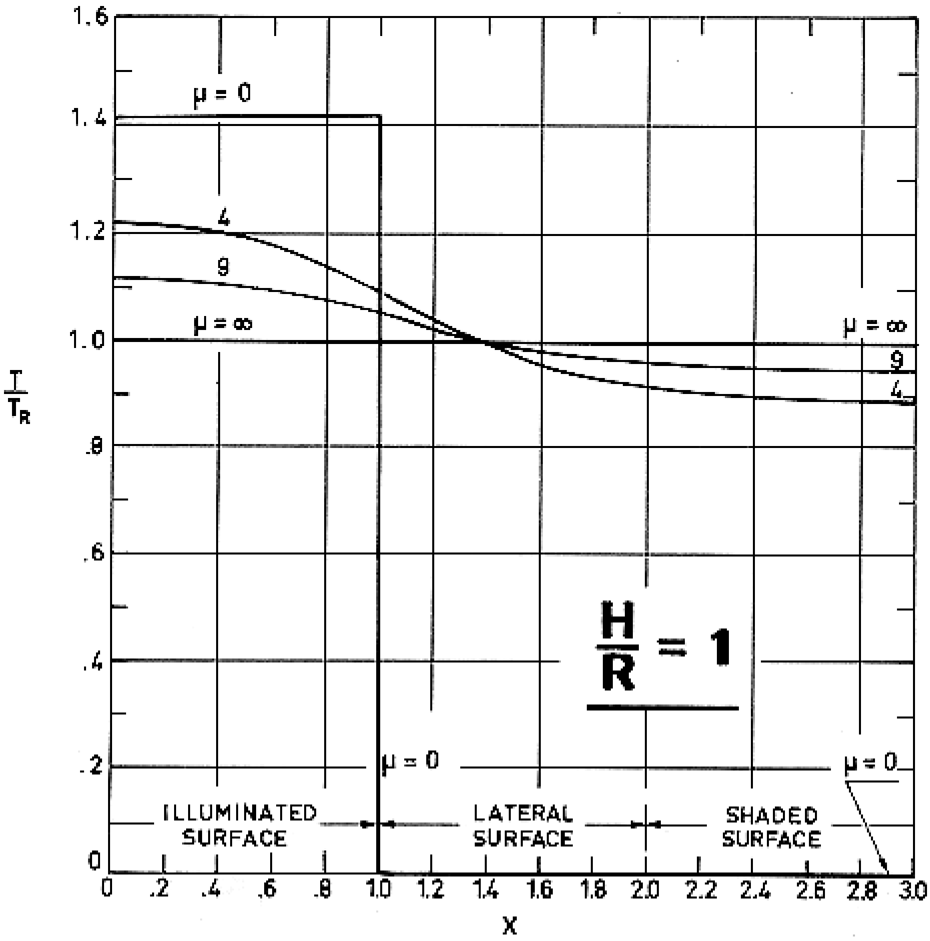

Note: non-si units are used in this figure

Figure 4-61: Temperature distribution on cylinder. No spin. No internal radiation. From Nichols (1961) [11].

4.11.4 Cylindrical surface of rectangular cross section. Solar radiation normal to face

Sketch:

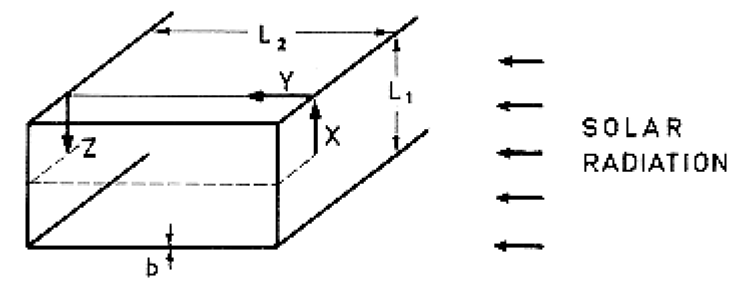

Dimensionless Parameters:

$x = 2X/L_1$, for $0 \leq x \leq 1$; $x = 1+2Y/L_1$, for $1 \leq x \leq 1+2\lambda$; $x = 1+2\lambda + 2Z/L_1$, for $1+2\lambda \leq x \leq 2(1+\lambda)$; $\tau = T/T_R$; $\lambda = L_2/L_1$; $\mu = 4kb/\varepsilon\sigma T_R^3 L_1^2$.

Differential Equations:

$$\mu \frac{d^2\tau_1}{dx^2} = \tau_1^4 - 4 \quad , \quad when\; 0 \le x \le 1$$
$$\mu \frac{d^2\tau_2}{dx^2} = \tau_2^4 \quad , \quad when\; 1 \le x \le 2(1+\lambda) \qquad [4\text{-}21]$$

Note: non-si units are used in this figure

Boundary Conditions:

$$\left.\frac{d\tau_1}{dx}\right|_{x=0} = \left.\frac{d\tau_2}{dx}\right|_{x=2(1+\lambda)} = 0 \quad , \quad \tau_1\big|_{x=1} = \tau_2\big|_{x=1} \quad , \quad \left.\frac{d\tau_1}{dx}\right|_{x=1} = \left.\frac{d\tau_2}{dx}\right|_{x=1} \qquad [4\text{-}22]$$

Note: non-si units are used in this figure

Comments: The results obtained by numerically solving this problem are given in the following.

Reference: Compiler.

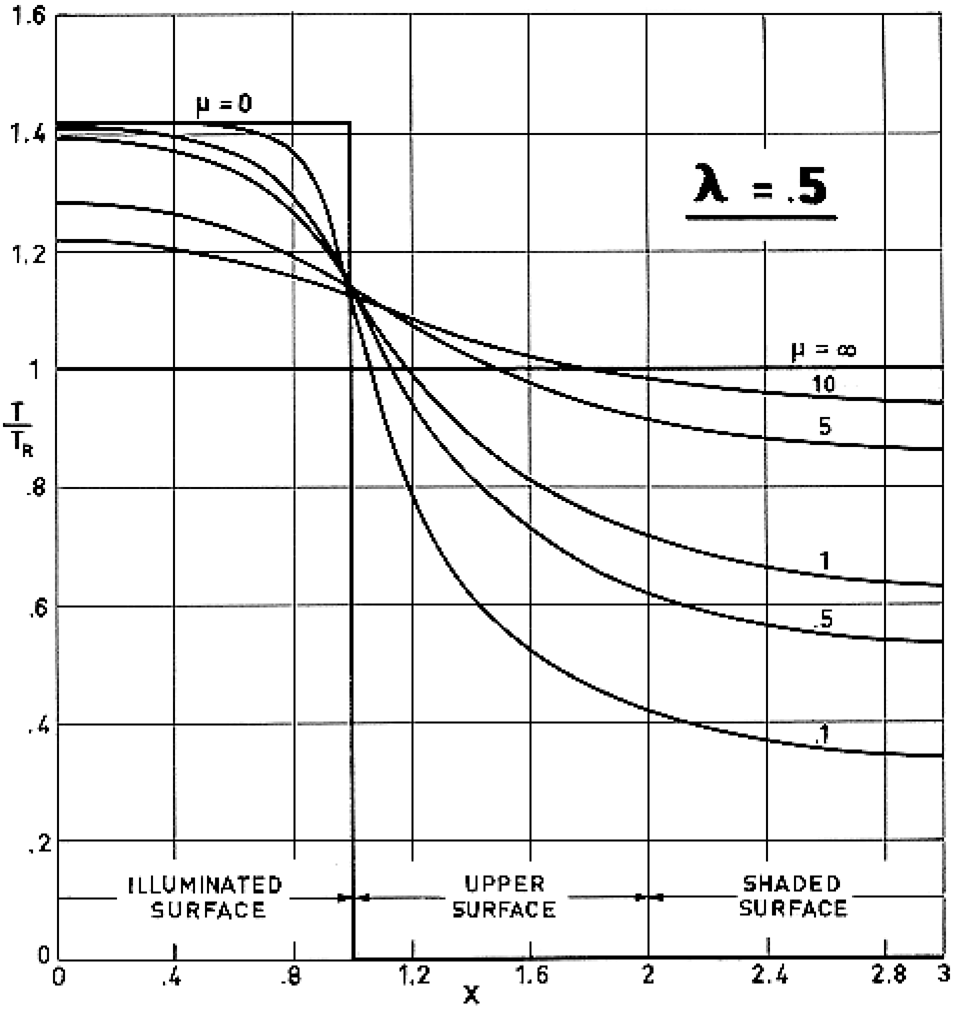

Note: non-si units are used in this figure

Figure 4-62: Temperature distribution on a cylindrical surface whose cross section is a rectangle of aspect - ratio $\lambda = 0{,}5$. No internal radiation. Calculated by the compiler.

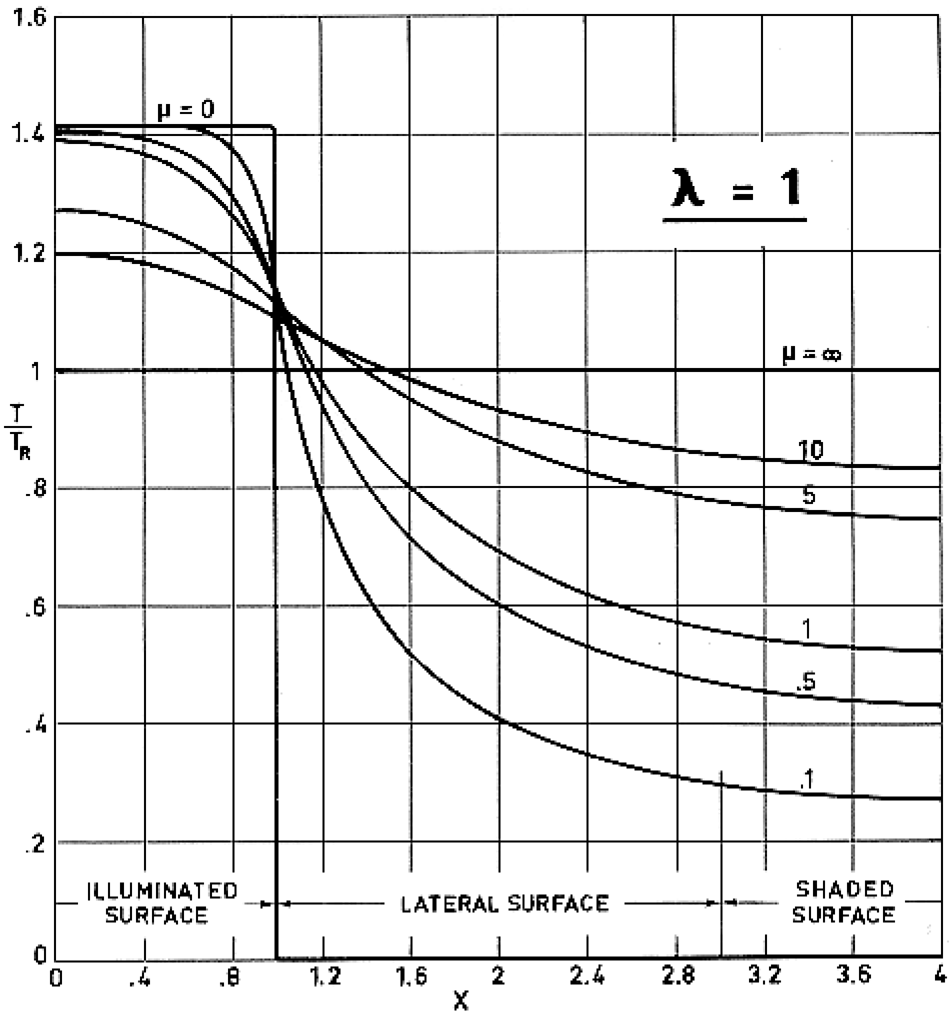

Figure 4-63: Temperature distribution on a cylindrical surface whose cross section is a rectangle on aspect - ration $\lambda = 1$. No internal radiation. Calculated by the compiler.

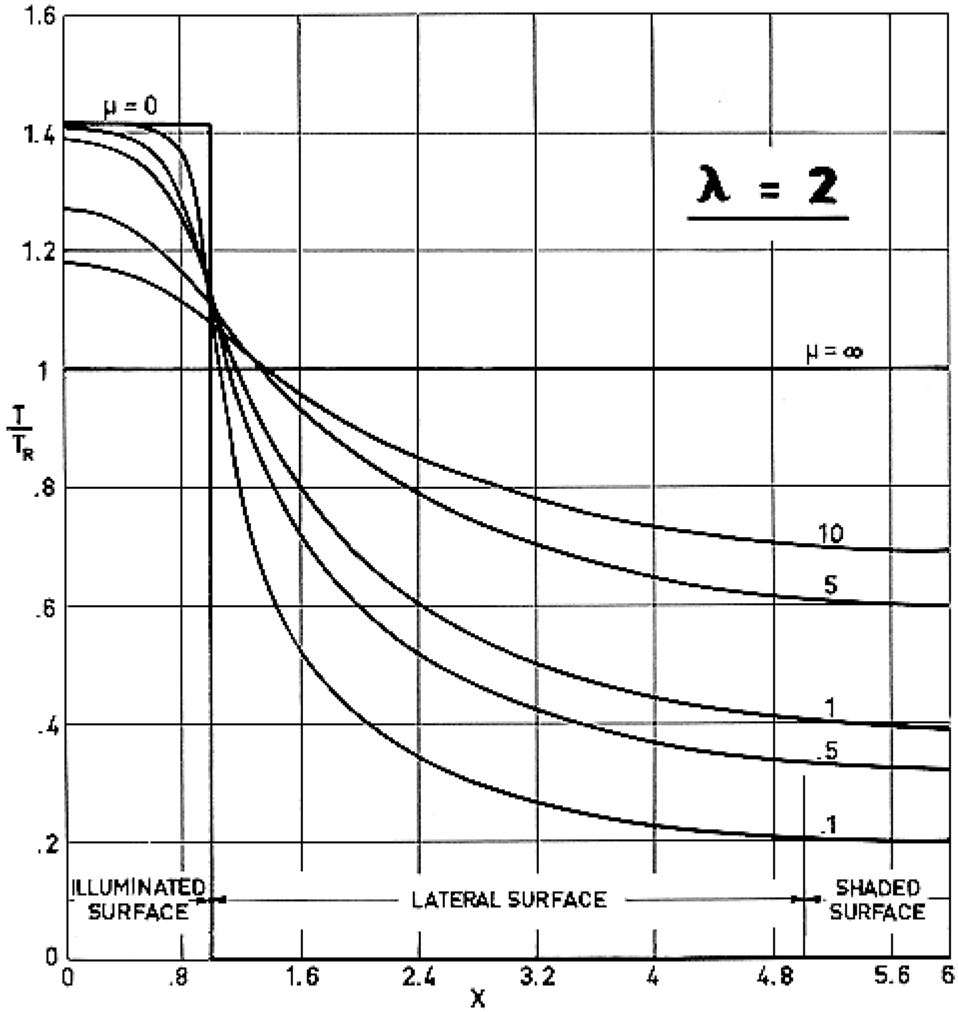

Note: non-si units are used in this figure

Figure 4-64: Temperature distribution on a cylindrical surface whose cross section is a rectangle on aspect - ration $\lambda = 2$. No internal radiation. Calculated by the compiler.

4.12 Thin-walled conical bodies. Conductivity

4.12.1 Non-spinning cone

Sketch:

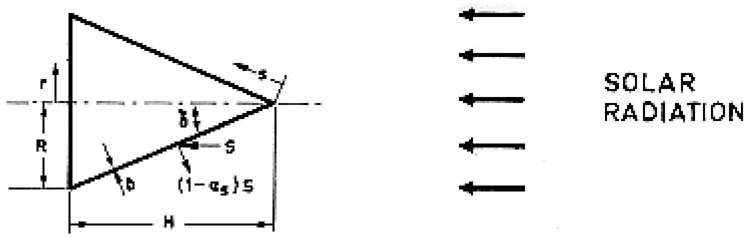

Dimensionless Parameters:

$$x = \frac{s}{\sqrt{R^2 + H^2}} \quad , \quad when\ 0 \le x \le 1$$
$$x = 2 - \frac{r}{R} \quad , \quad when\ 1 \le x \le 2 \qquad [4\text{-}23]$$

$\tau(x) = T(x)/T_R$; $\mu = kb/\varepsilon\sigma T_R^3 R^2$.

Differential Equations:

$$\frac{\mu \sin^2\delta}{x}\frac{d}{dx}\left(x\frac{d\tau_1}{dx}\right) = \tau_1^4 - (1+\sin\delta) \quad , \quad when\ 0 \le x \le 1$$
$$\frac{\mu}{2-\mu}\frac{d}{dx}\left[(2-x)\frac{d\tau_2}{dx}\right] = \tau_2^4 \quad , \quad when\ 1 \le x \le 2 \qquad [4\text{-}24]$$

Note: non-si units are used in this figure

Boundary *conditions*:

$$\left.\frac{d\tau_1}{dx}\right|_{x=0} = \left.\frac{d\tau_2}{dx}\right|_{x=2} = 0 \quad , \quad \tau_1|_{x=1} = \tau_2|_{x=1} \quad , \quad \sin\delta\left.\frac{d\tau_1}{dx}\right|_{x=1} = \left.\frac{d\tau_2}{dx}\right|_{x=1} \qquad [4\text{-}25]$$

Note: non-si units are used in this figure

Comments: The results obtained by numerically solving this problem are given in the following.

Reference: Nichols (1961) [11].

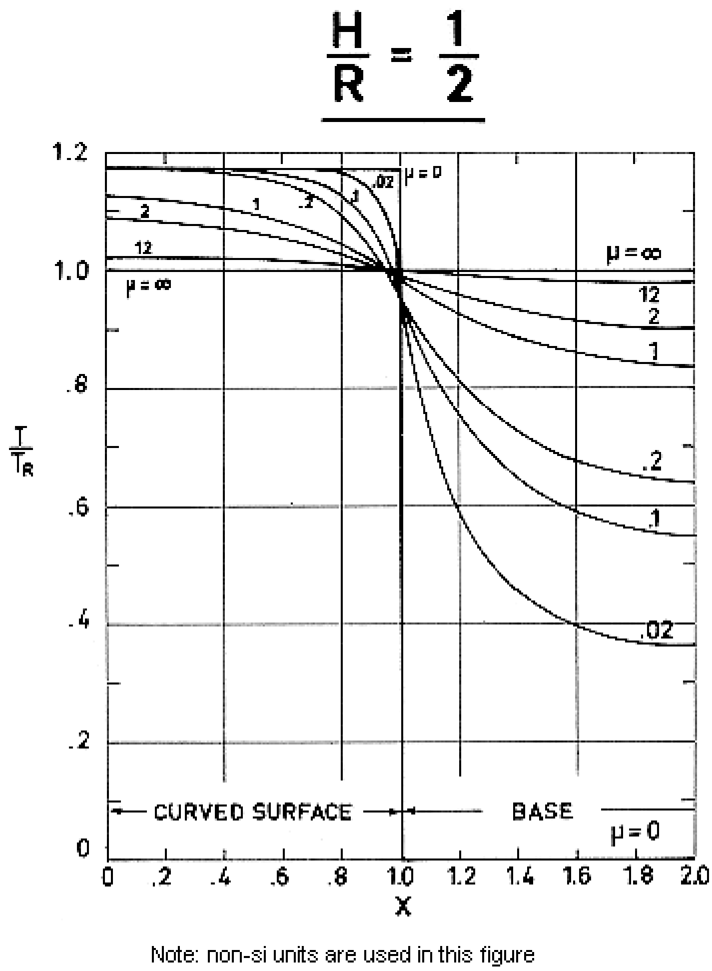

Figure 4-65: Temperature distribution on cone. No spin. No internal radiation. From Nichols (1961) [11].

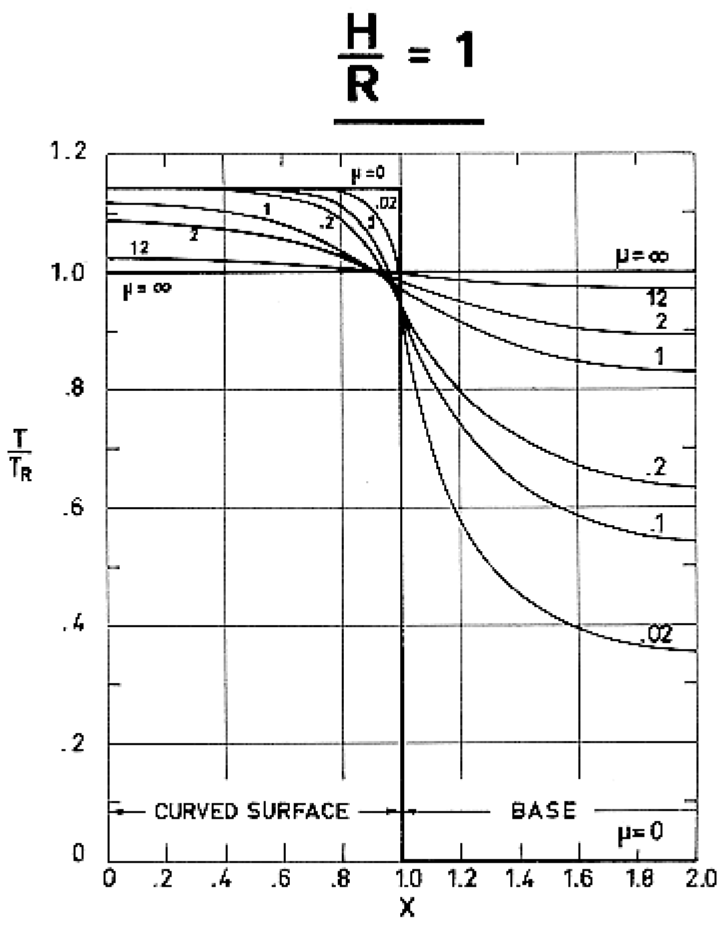

Note: non-si units are used in this figure

Figure 4-66: Temperature distribution on cone. No spin. No internal radiation. From Nichols (1961) [11].

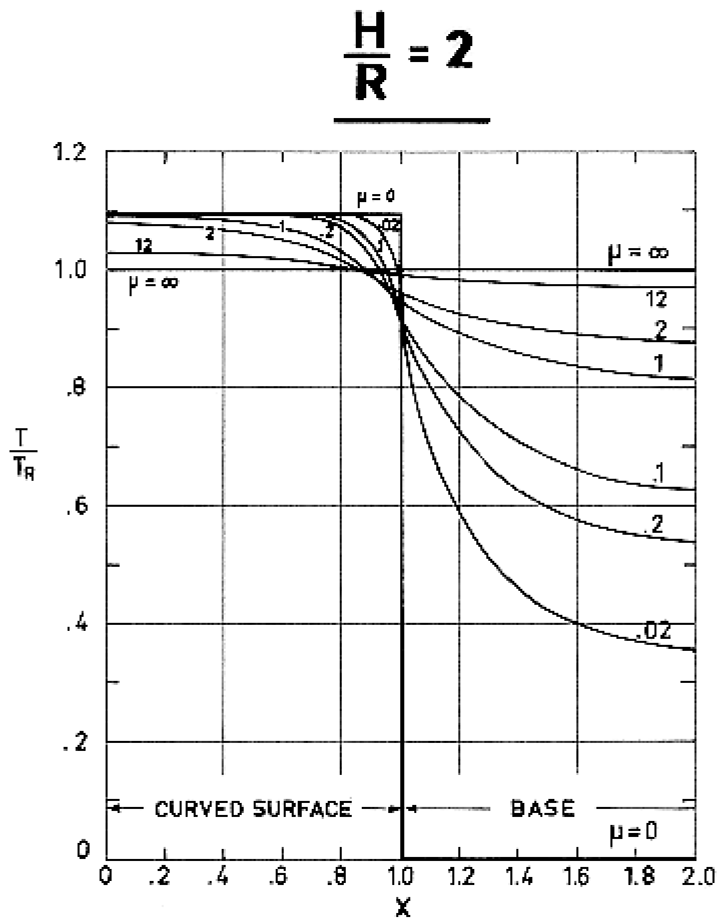

Note: non-si units are used in this figure

Figure 4-67: Temperature distribution on cone. No spin. No internal radiation. From Nichols (1961) [11].

5 Planetary radiation

5.1 General

Data on the equilibrium temperature of a satellite, heated by radiation from a planet, and cooled by radiation to the outer space, are presented in this Clause. Only satellites of very simple geometrical configurations are considered.

The data presented have been calculated on the basis of the following assumptions:

(a) The satellite is constituted by a homogeneous solid body, exhibiting infinitely large thermal conductivity.

(b) The characteristic length of the satellite is small compared with the mean radius of the planet.

(c) The emission from the planet is assumed to follow Lambert's law.

(d) The Equivalent Surrounding Temperature, T_s, is assumed to be zero.

(e) Emittance and infrared absorptance of the satellite surface are independent of both temperature and wavelength.

The Spacecraft Planetary Radiation Equilibrium Temperature, T_{RP}, is given by:

$T_{RP} = [(\alpha/\varepsilon)F_{SP}T_P^4 + T_s^4]^{1/4}$

Once T_s has been assumed to be zero, the above expression gives the ratio T_{RP}/T_P as a function of the optical characteristics of the satellite surface (through α/ε) for arbitrary values of the view factor from spacecraft to planet, F_{SP}. The results are given in Figure 5-1.

These results can be also used to estimate the radiation from a satellite to a sub satellite or appendage provided that the above assumption hold.

Values of T_{RP} as a function of T_{RP}/T_P for radiation from several planets are given in Figure 5-2. Radiation from the Earth is considered in Figure 5-3.

The remaining data are values of F_{SP} for simple geometries. From cylindrical and conical configurations F_{SP} is calculated by expansion in powers of sin λ and (or) cos λ, λ being the angle defining the orientation of the spacecraft. The coefficients of these power expansions depends on the parameter B_i. The five first parameter B_i are given below, as calculated by Clark & Anderson (1965) [5].

$$B_0 = \frac{2}{7\pi}\left[\frac{577}{105} - 7\cos\alpha_L + \frac{4}{3}\cos^3\alpha_L - \frac{2}{5}\cos^5\alpha_L + \frac{4}{7}\cos^7\alpha_L\right] \quad [5\text{-}1]$$

$$B_1 = \frac{1}{2}\sin^2 a_L \quad [5\text{-}2]$$

$$B_2 = \frac{8}{7\pi}\left[\cos\alpha_L - 2\cos^3\alpha_L + 4\cos^5\alpha_L - 3\cos^7\alpha_L\right] \qquad [5\text{-}3]$$

$$B_3 = \frac{4}{7\pi}\left[-\cos\alpha_L + \frac{40}{3}\cos^3\alpha_L - \frac{91}{3}\cos^5\alpha_L + 18\cos^7\alpha_L\right] \qquad [5\text{-}4]$$

$$B_4 = \frac{8}{35\pi}\left[5\cos\alpha_L - 35\cos^3\alpha_L + 63\cos^5\alpha_L - 33\cos^7\alpha_L\right] \qquad [5\text{-}5]$$

where:

$$\alpha_L = \sin^{-1}\frac{R_P}{h + R_P} \qquad [5\text{-}6]$$

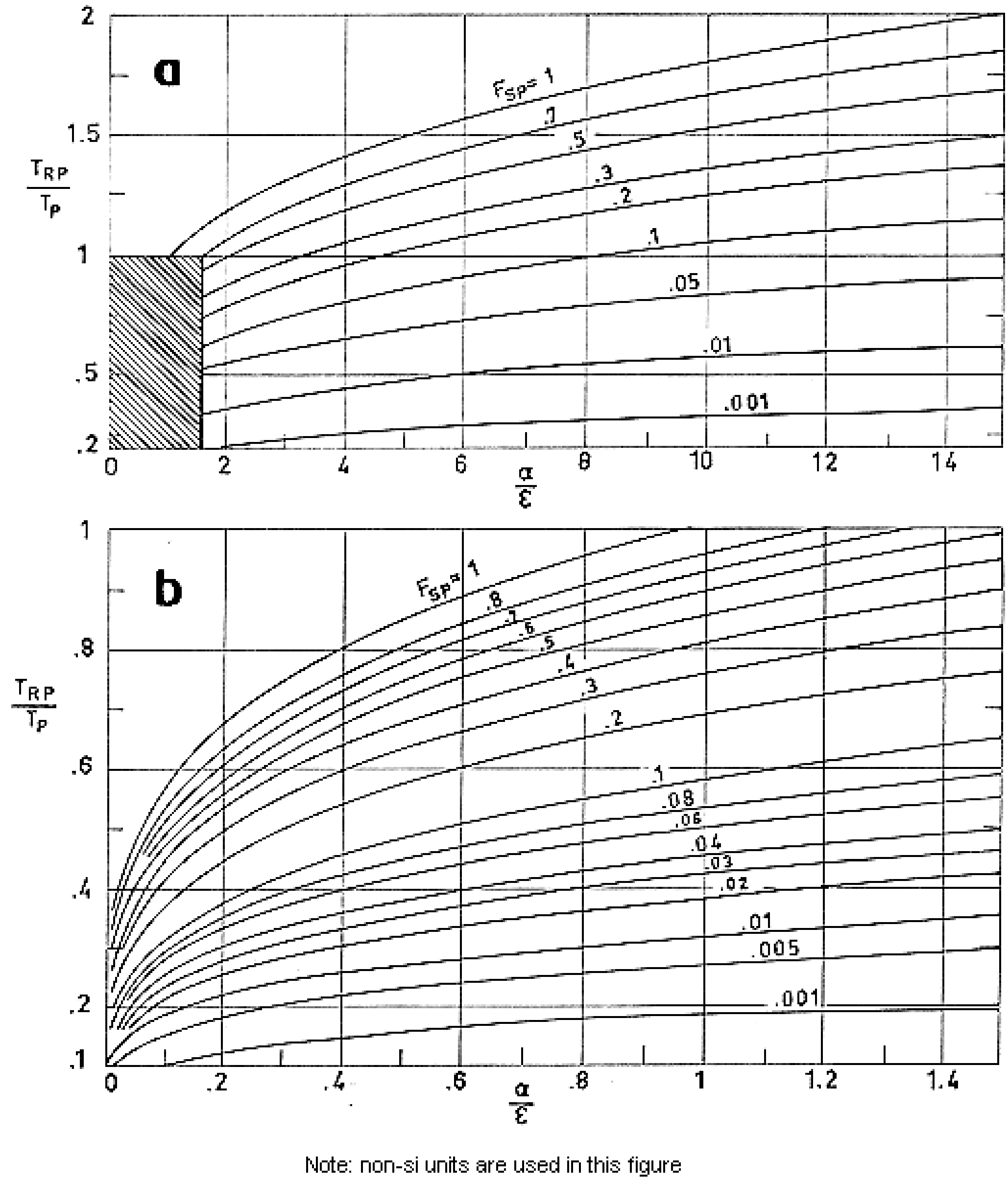

Figure 5-1: The ratio T_{RP}/T_P vs. the optical characteristics of the surface for different values of F_{SP}. Shaded zone of *a* is enlarged in *b*. Calculated by the compiler.

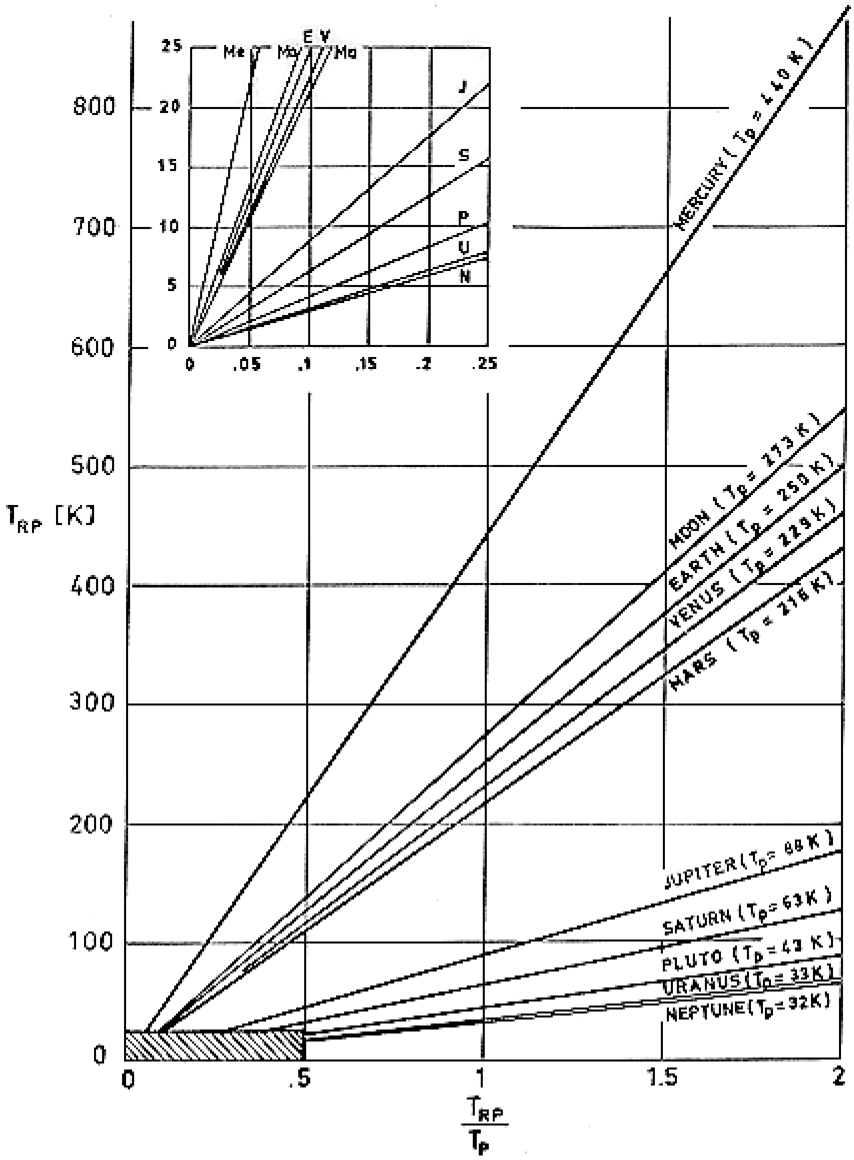

Note: non-si units are used in this figure

Figure 5-2: Radiation equilibrium temperature T_{RP} vs. ratio T_{RP}/T_P. Incoming radiation from different planets. After NASA - SP - 3051 (1965).

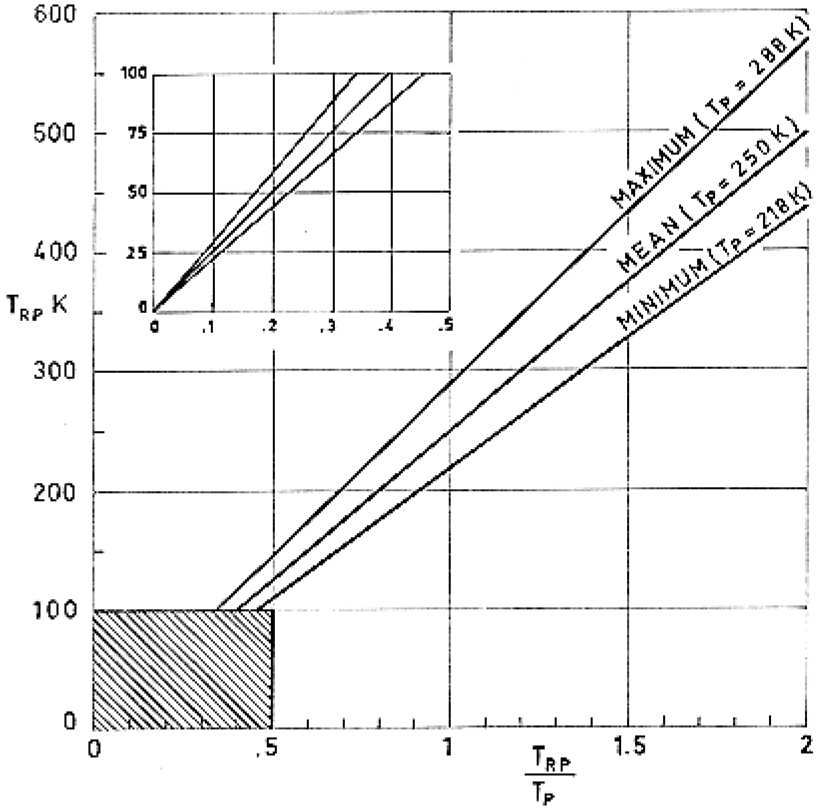

Note: non-si units are used in this figure

Figure 5-3: Different estimates of radiation equilibrium temperature T_{RP} vs. T_{RP}/T_P, for radiation from the Earth. Plotted from data by Johnson (1965) [9].

Table 5-1: Relevant data on the Planets and the Moon.

	Distance to the sun $x10^{-9}$ [m]	Distance to the sun in AU	Radius of the planet $x10^{-3}$ [m]	Planet to earth radius ratio	Solar constant [$W.m^{-2}$]	Equivalent temperature of the planet [K]
MERCURY	57,9	0,387	2330	0,3659	9034	440
VENUS	108,1	0,723	6100	0,9580	2588	229
EARTH	149,5	1,0	6367,5	1,0	1353	250
MARS	227,4	1,521	3415	0,5363	585	216
JUPITER	773,3	5,173	71375	11,2093	51	88
SATURN	1425,7	9,536	60500	9,5014	15	63
URANUS	2880,7	19,269	24850	3,9026	3,6	33
NEPTUNE	4490,1	30,034	25000	3,9262	1,5	32
PLUTO	5841,9	39,076	2930	0,4600	0,89	43
MOON	149,5	1,0	1738	0,2729	1353	273

NOTE 1 References: Kreith (1962) [10], Wolverton (1963) [13], Anderson (1969) [1].

5.2 Infinitely conductive planar surfaces

5.2.1 Flat plate absorbing and emitting on one side

Sketch:

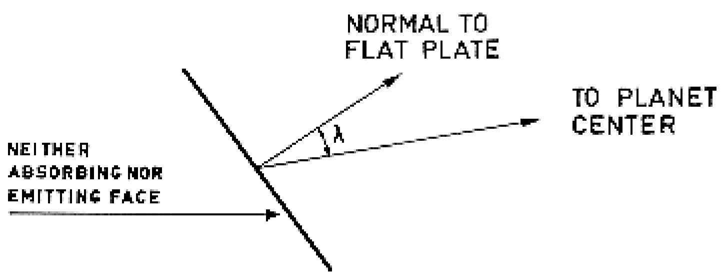

Formula:

$F_{SP} = B_0 + B_1 \cos\lambda + B_2 \cos^2\lambda + B_3 \cos^4\lambda + B_4 \cos^6\lambda$

Where the parameters B_i ($i = 0,1,\ldots,4$) are defined in clause 5.1.

Reference: Clark & Anderson (1965) [5].

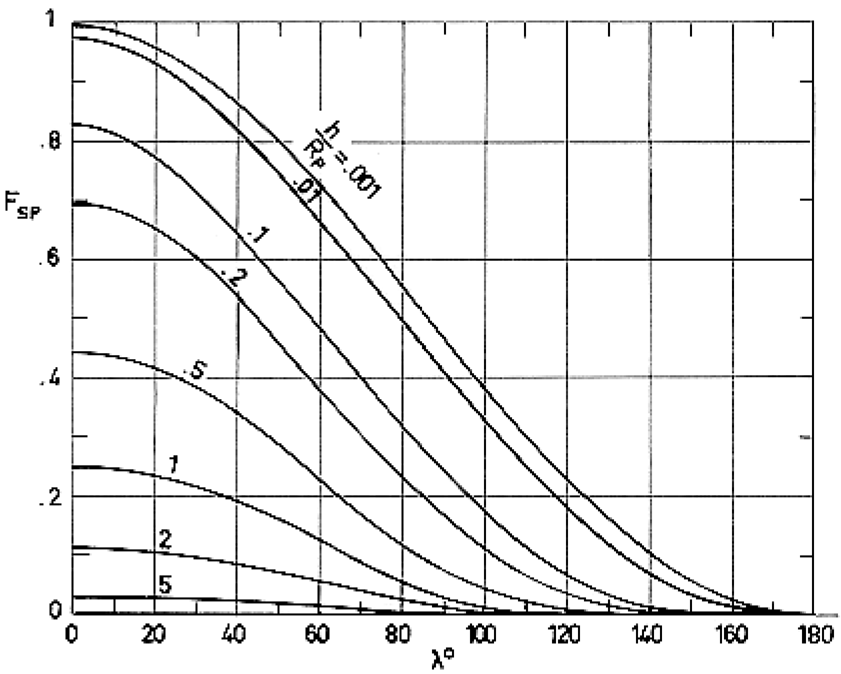

Figure 5-4: F_{SP} as a function of λ and h / R_P in the case of a flat plate absorbing and emitting on one side. Calculated by the compiler.

5.3 Infinitely conductive spherical surfaces

5.3.1 Sphere

Sketch:

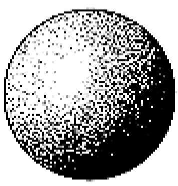

Formula:

$$F_{SP} = \frac{1}{2}\left[1 - \frac{\sqrt{\left(\frac{h}{R_P}\right)^2 + 2\frac{h}{R_P}}}{1 + \frac{h}{R_P}}\right] \qquad [5\text{-}7]$$

Reference: Clark & Anderson (1965) [5], Watts (1965) [12].

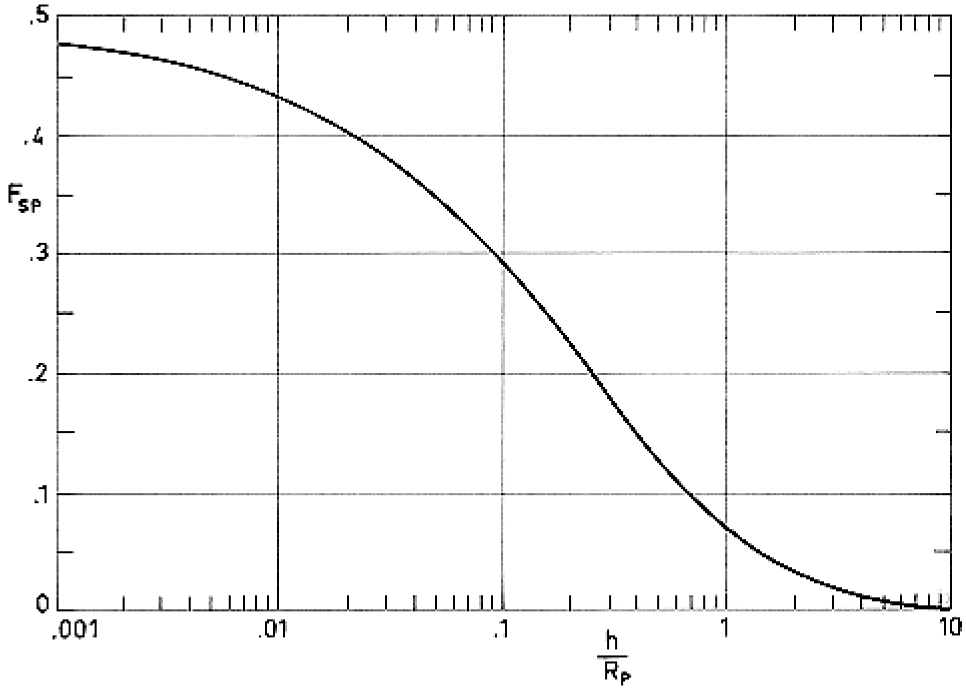

Figure 5-5: F_{SP} as a function of h / R_P in the case of a sphere. Calculated by the compiler.

5.3.2 Hemispherical surface absorbing and emitting on outer face

Sketch:

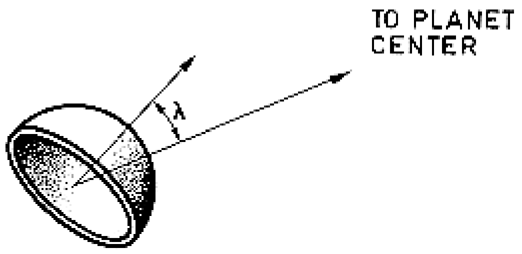

Formula:

$$F_{SP} = \frac{1}{2}\left[1 - \frac{\sqrt{\left(\frac{h}{R_P}\right)^2 + 2\frac{h}{R_P}}}{1+\frac{h}{R_P}} + \frac{1}{1+\frac{h}{r_P}}\frac{\cos\lambda}{2}\right] \quad [5\text{-}8]$$

Reference: Watts (1965) [12].

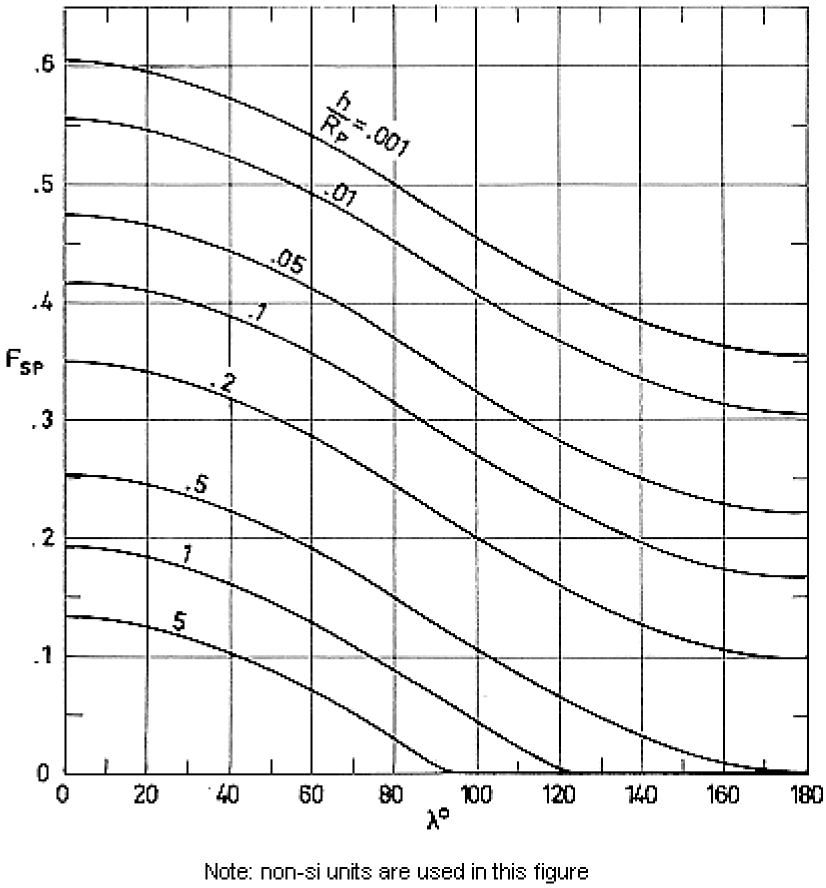

Figure 5-6: F_{SP} as a function of λ and h / R_P in the case of a hemispherical surface absorbing and emitting on outer face. Calculated by the compiler.

5.4 Infinitely conductive cylindrical surfaces

5.4.1 Circular cylinder with insulated bases

Sketch:

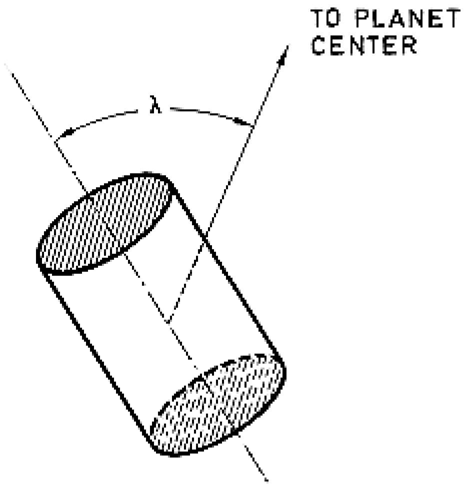

Formula:

$$F_{SP} = B_0 + \frac{B_2}{2}\sin^2\lambda + \frac{3B_3}{8}\sin^4\lambda + \frac{5B_4}{16}\sin^6\lambda \qquad [5\text{-}9]$$

where the parameters B_i (i = 0,1,...,4) are defined in clause 5.1.

Reference: Clark & Anderson (1965) [5], Watts (1965) [12].

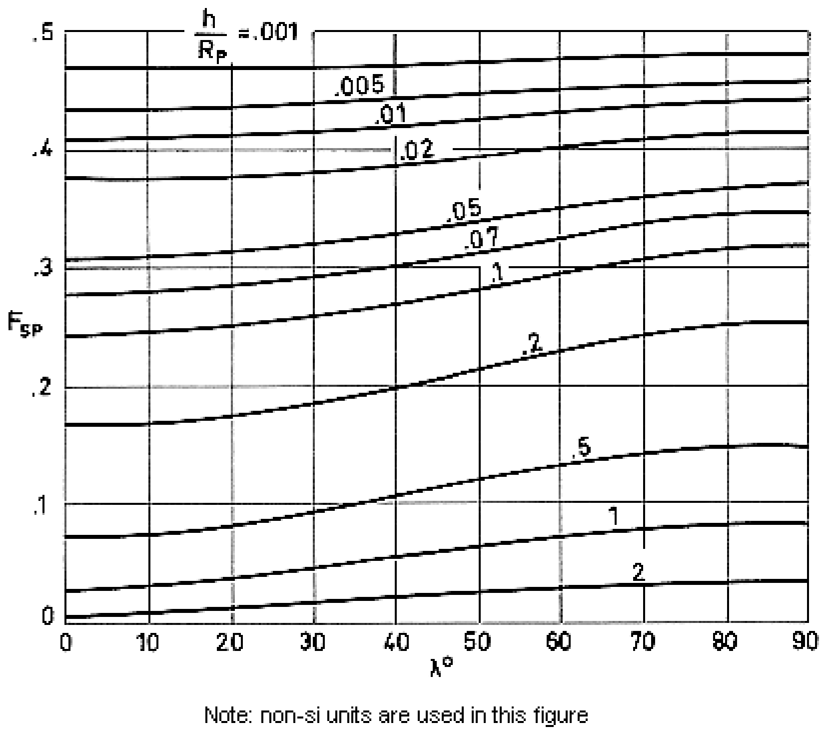

Figure 5-7: F_{SP} as a function of λ and h / R_P in the case of a circular cylinder with insulated bases. Calculated by the compiler.

5.4.2 Finite height circular cylinder

Sketch:

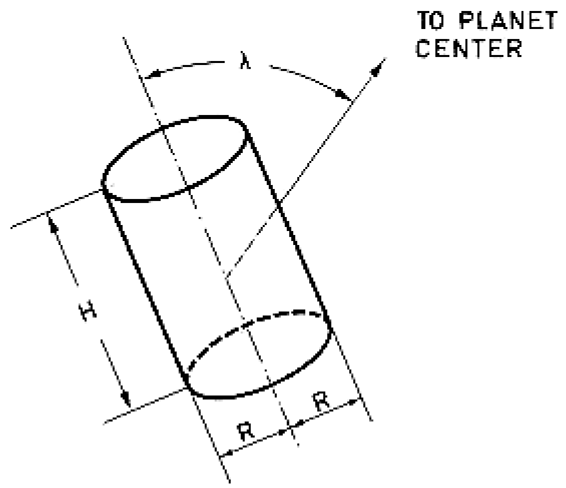

Formula:

$$F_{SP} = \frac{1}{1+\frac{H}{R}} \left[\begin{array}{l} B_0 + B_2\cos^2\lambda + B_3\cos^4\lambda + B_4\cos^6\lambda + \\ +\frac{H}{R}\left(B_0 + \frac{B_2}{2}\sin^2\lambda + \frac{3B_3}{8}\sin^4\lambda + \frac{5B_4}{16}\sin^6\lambda \right) \end{array} \right] \quad [5\text{-}10]$$

where the parameters B_i (i = 0,1,...,4) are defined in clause 5.1.

Reference: Clark & Anderson (1965) [5].

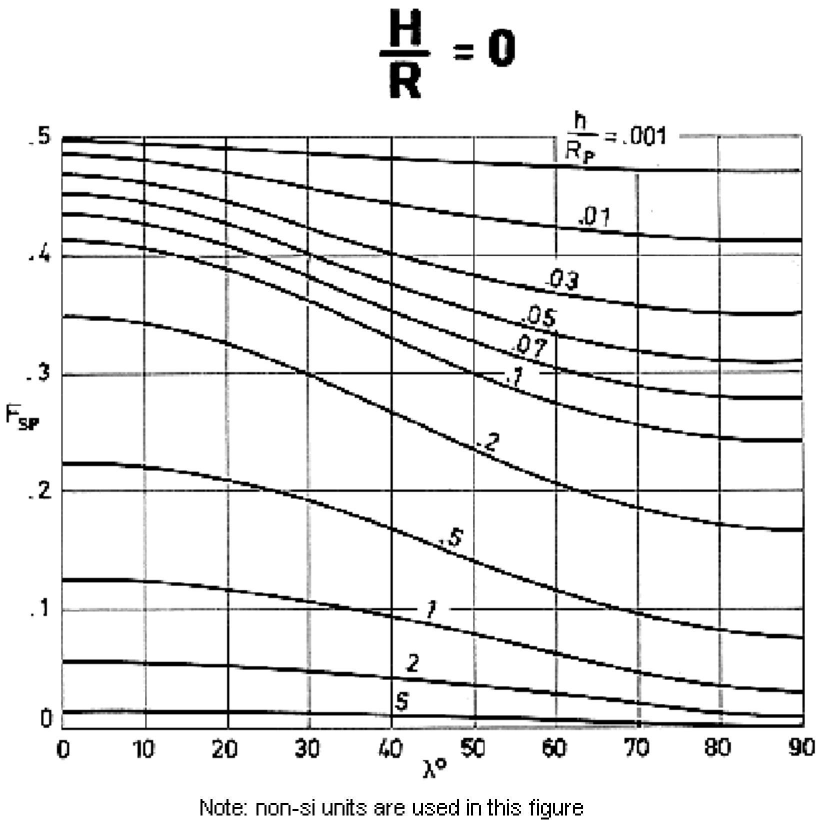

Figure 5-8: F_{SP} as a function of λ and h / R_P in the case of a finite height circular cylinder. Calculated by the compiler.

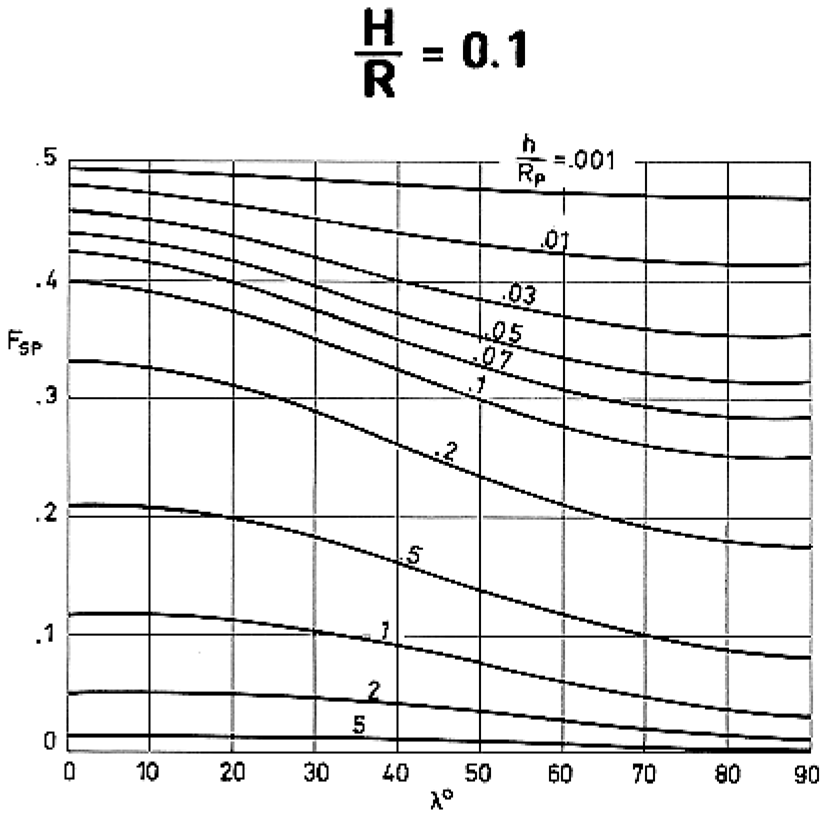

Note: non-si units are used in this figure

Figure 5-9: F_{SP} as a function of λ and h / R_P in the case of a finite height circular cylinder. Calculated by the compiler.

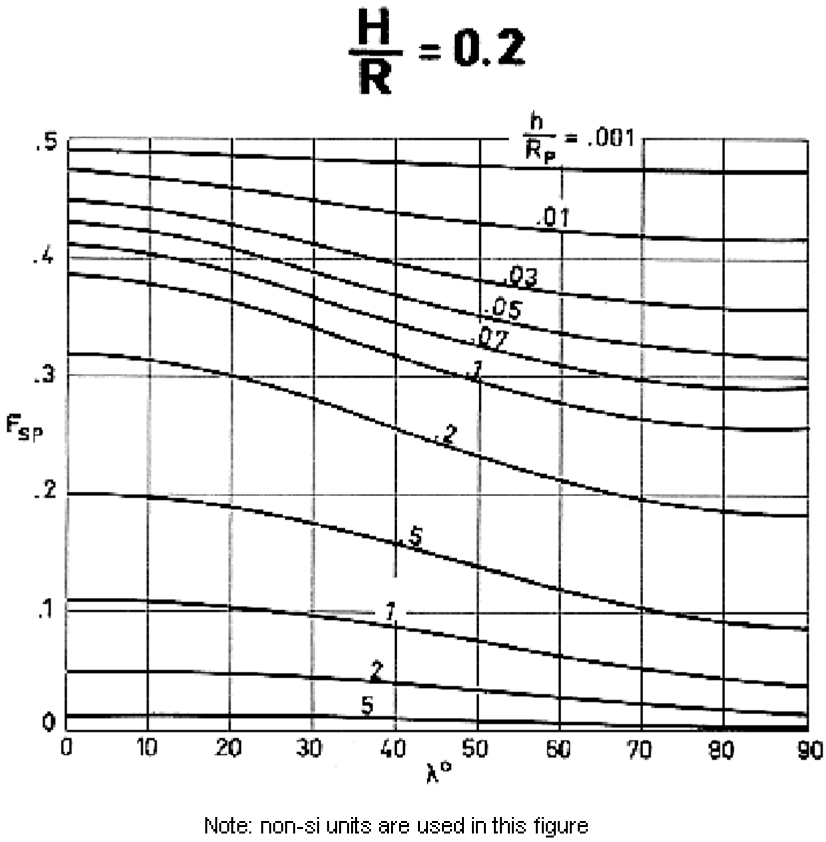

Figure 5-10: F_{SP} as a function of λ and h / R_P in the case of a finite height circular cylinder. Calculated by the compiler.

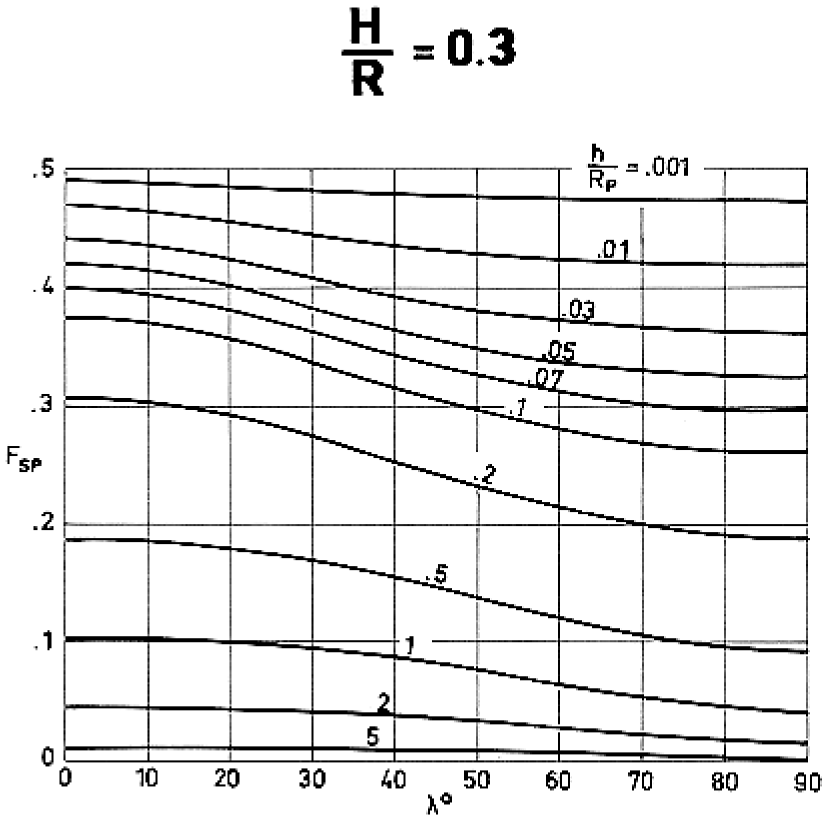

Note: non-si units are used in this figure

Figure 5-11: F_{SP} as a function of λ and h / R_P in the case of a finite height circular cylinder. Calculated by the compiler.

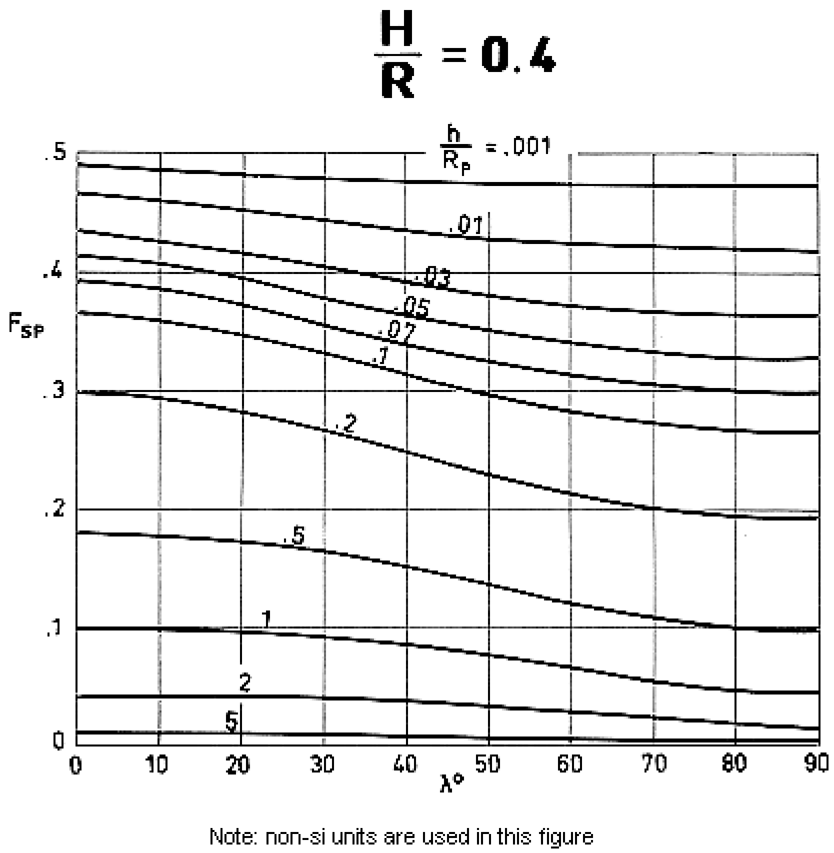

Figure 5-12: F_{SP} as a function of λ and h / R_P in the case of a finite height circular cylinder. Calculated by the compiler.

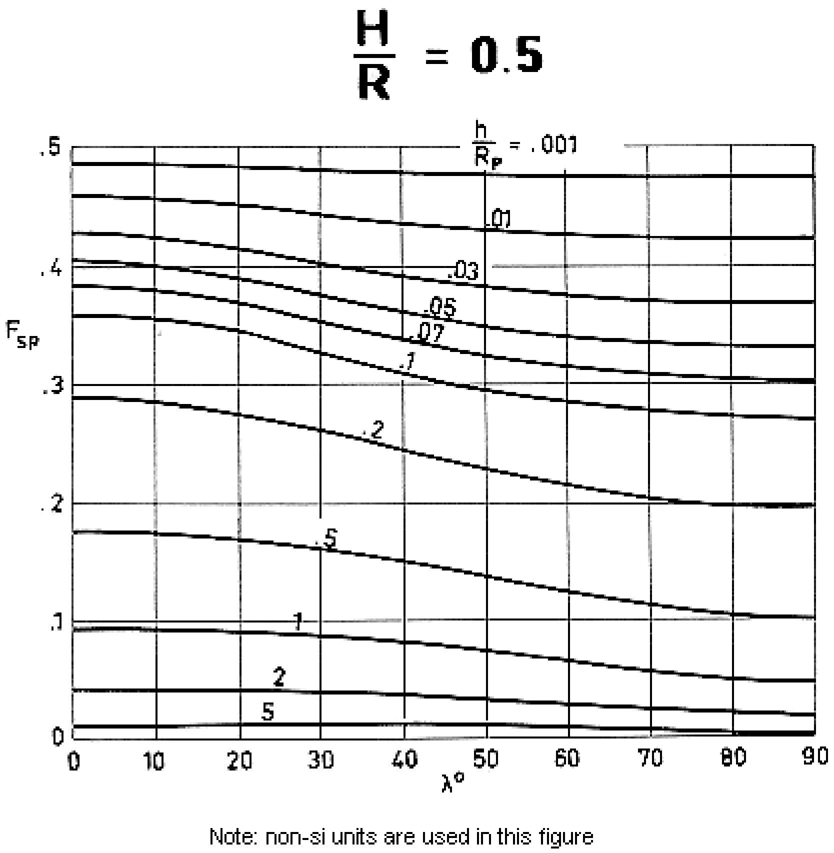

Figure 5-13: F_{SP} as a function of λ and h / R_P in the case of a finite height circular cylinder. Calculated by the compiler.

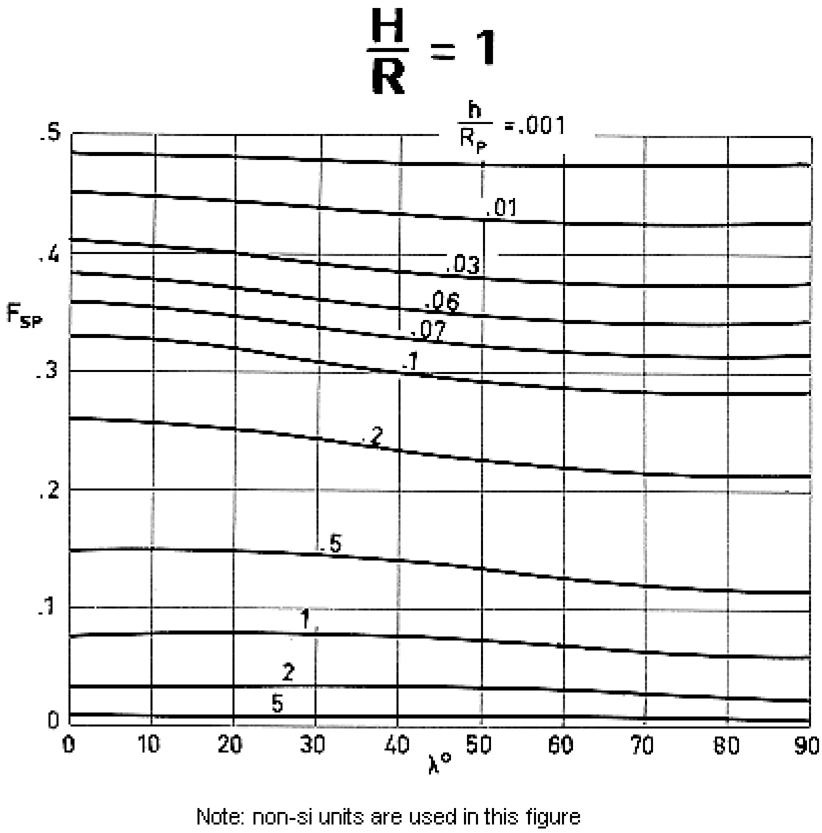

Figure 5-14: F_{SP} as a function of λ and h / R_P in the case of a finite height circular cylinder. Calculated by the compiler.

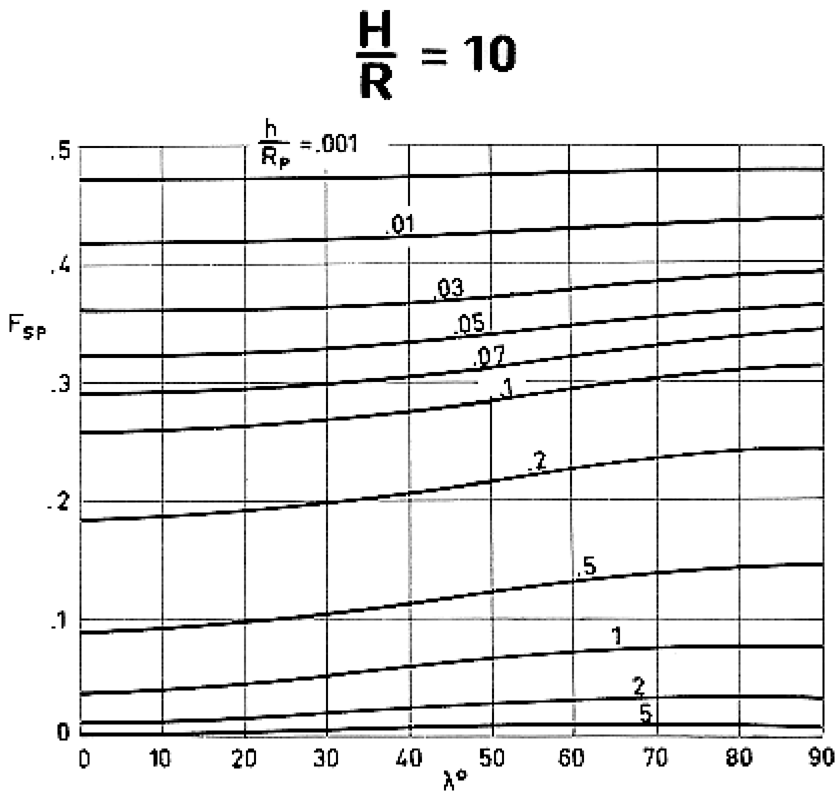

Note: non-si units are used in this figure

Figure 5-15: F_{SP} as a function of λ and h / R_P in the case of a finite height circular cylinder. Calculated by the compiler.

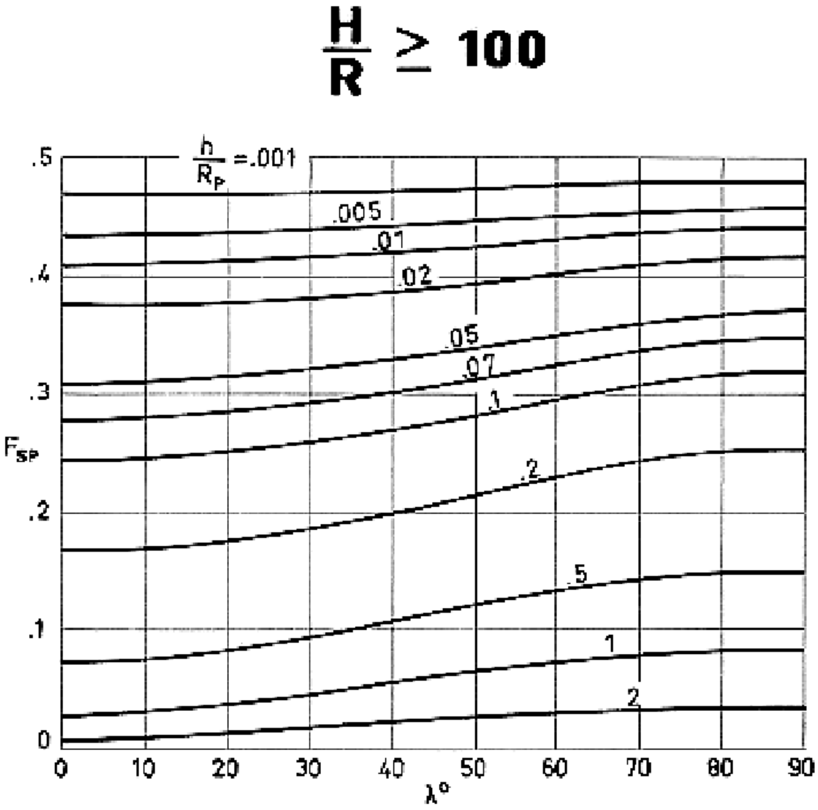

Note: non-si units are used in this figure

Figure 5-16: F_{SP} as a function of λ and h / R_P in the case of a finite height circular cylinder. Calculated by the compiler.

5.5 Infinitely conductive conical surfaces

5.5.1 Circular cone with insulated base

Sketch:

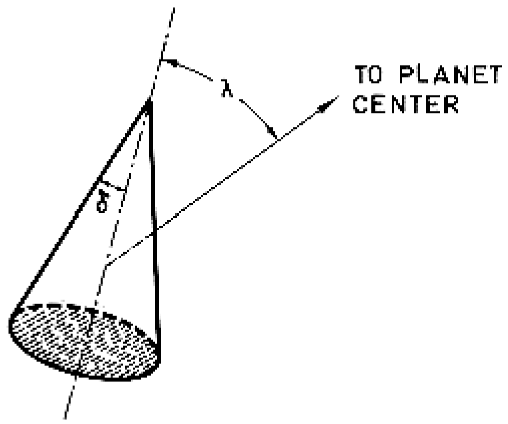

Formula:

$$F_{SP} = B_0 + B_1 C + B_2\left(C^2 + \frac{D^2}{2}\right) + B_3\left(C^4 + 3C^2D^2 + \frac{3}{8}D^4\right) + B_4\left(C^6 + \frac{15}{2}C^4D^2 + \frac{45}{8}C^2D^4 + \frac{5}{16}D^6\right) \quad [5\text{-}11]$$

where the parameters B_i ($i = 0,1,...,4$) are defined in clause 5.1.

In addition:

$C = \sin\delta\cos\lambda$

$D = \cos\delta\sin\lambda$

Reference: Clark & Anderson (1965) [5].

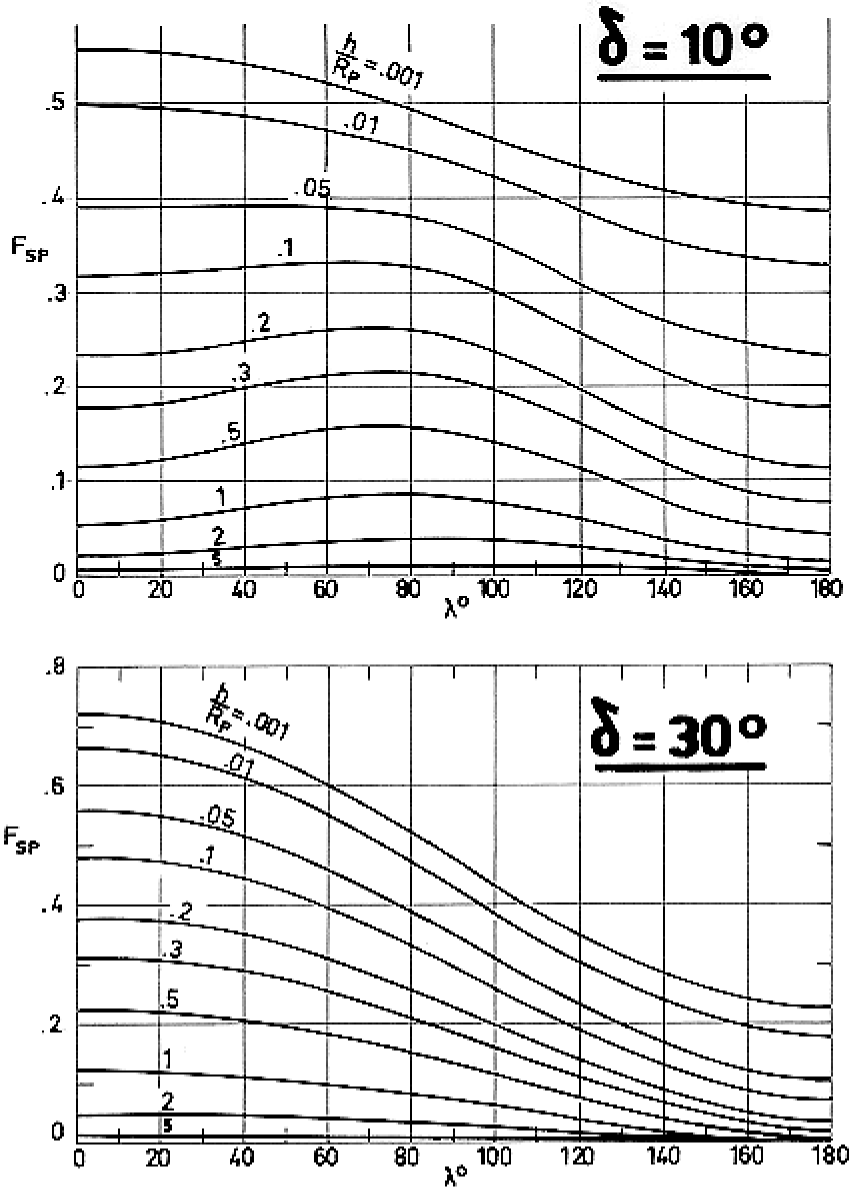

Note: non-si units are used in this figure

Figure 5-17: F_{SP} as a function of λ and h / R_P in the case of a circular cone with insulated base. Calculated by the compiler.

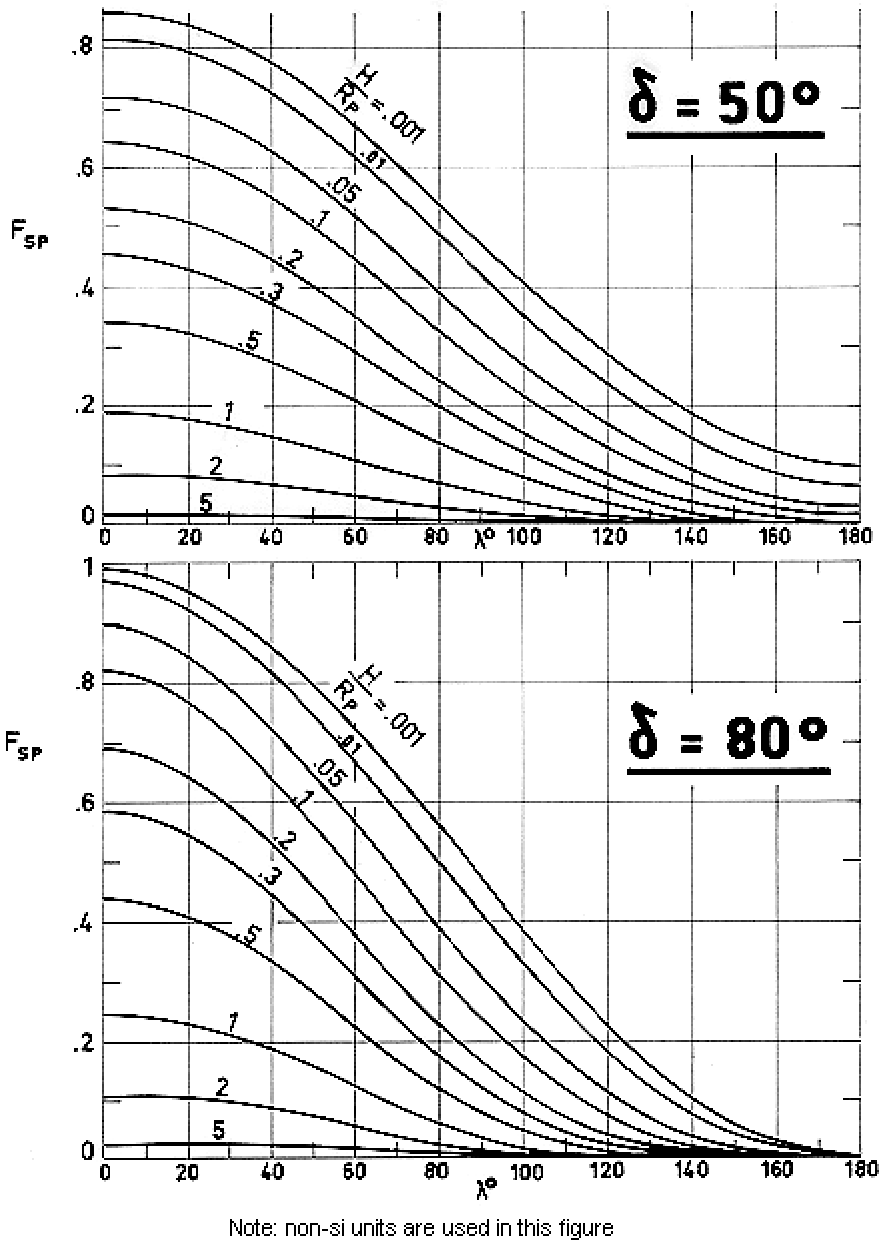

Figure 5-18: F_{SP} as a function of λ and h / R_P in the case of a circular cone with insulated base. Calculated by the compiler.

5.5.2 Finite height circular cone

Sketch:

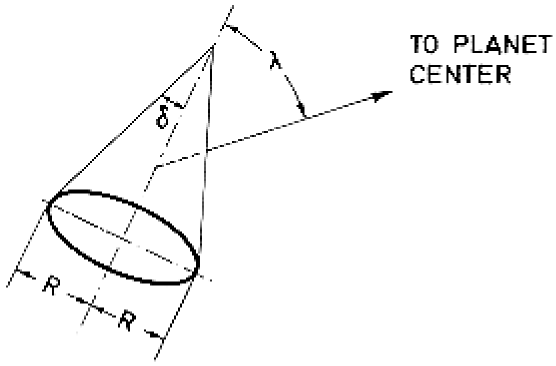

Formula:

$$F_{SP} = \frac{1}{1+\sin\delta}\left[\begin{array}{l} \sin\delta\left(B_0 - B_1\cos\lambda + B_2\cos^2\lambda + B_3\cos^4\lambda + B_4\cos^6\lambda\right) + \\ + B_0 + B_1 C + B_2\left(C^2 + \frac{D^2}{2}\right) + B_3\left(C^4 + 3C^2D^2 + \frac{3}{8}D^4\right) + \\ + B_4\left(C^6 + \frac{15}{2}C^4D^2 + \frac{45}{8}C^2D^4 + \frac{5}{16}D^6\right) \end{array}\right] \quad [5\text{-}12]$$

where the parameters B_i ($i = 0,1,\ldots,4$) are defined in clause 5.1.

In addition:

$C = \sin\delta\cos\lambda$

$D = \cos\delta\sin\lambda$

Reference: Clark & Anderson (1965) [5].

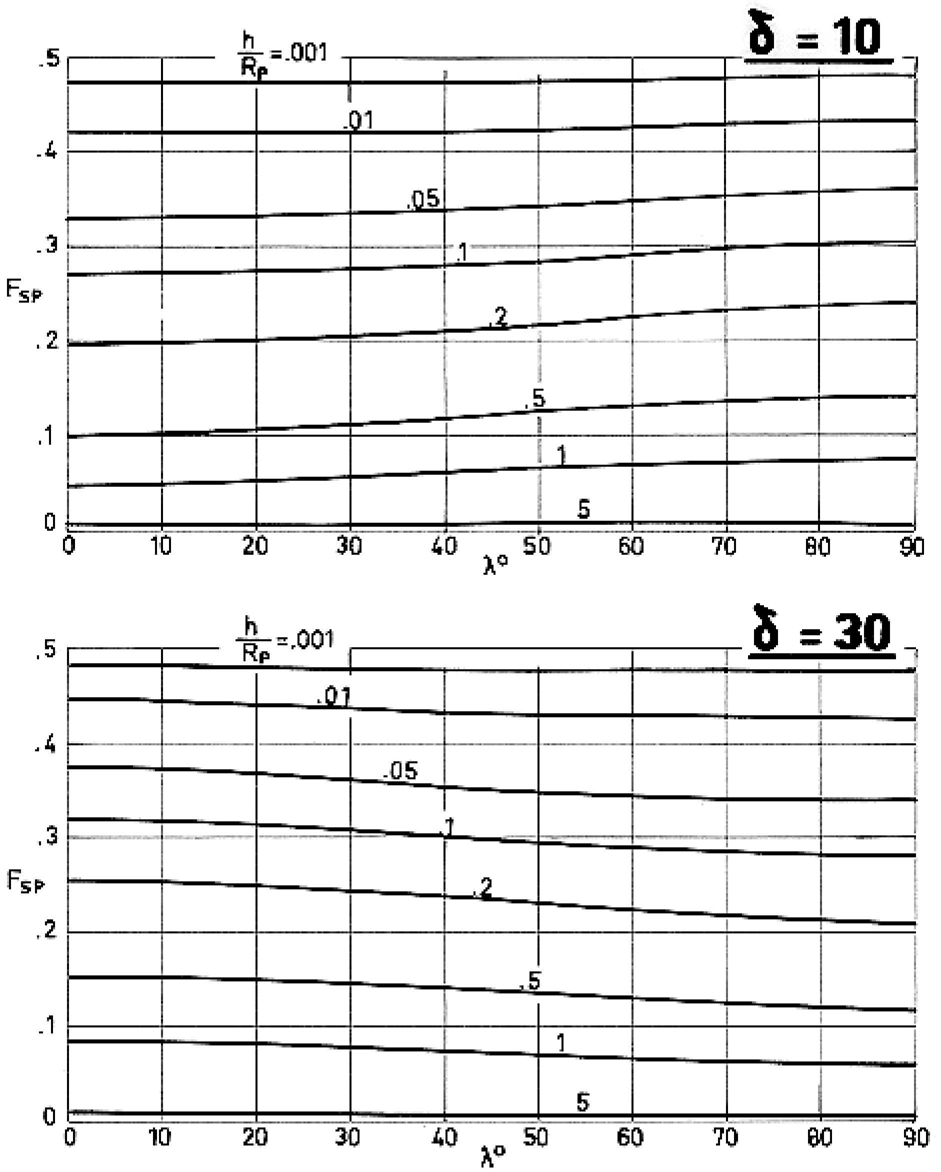

Note: non-si units are used in this figure

Figure 5-19: F_{SP} as a function of λ in the case of a finite height circular cone. Calculated by the compiler.

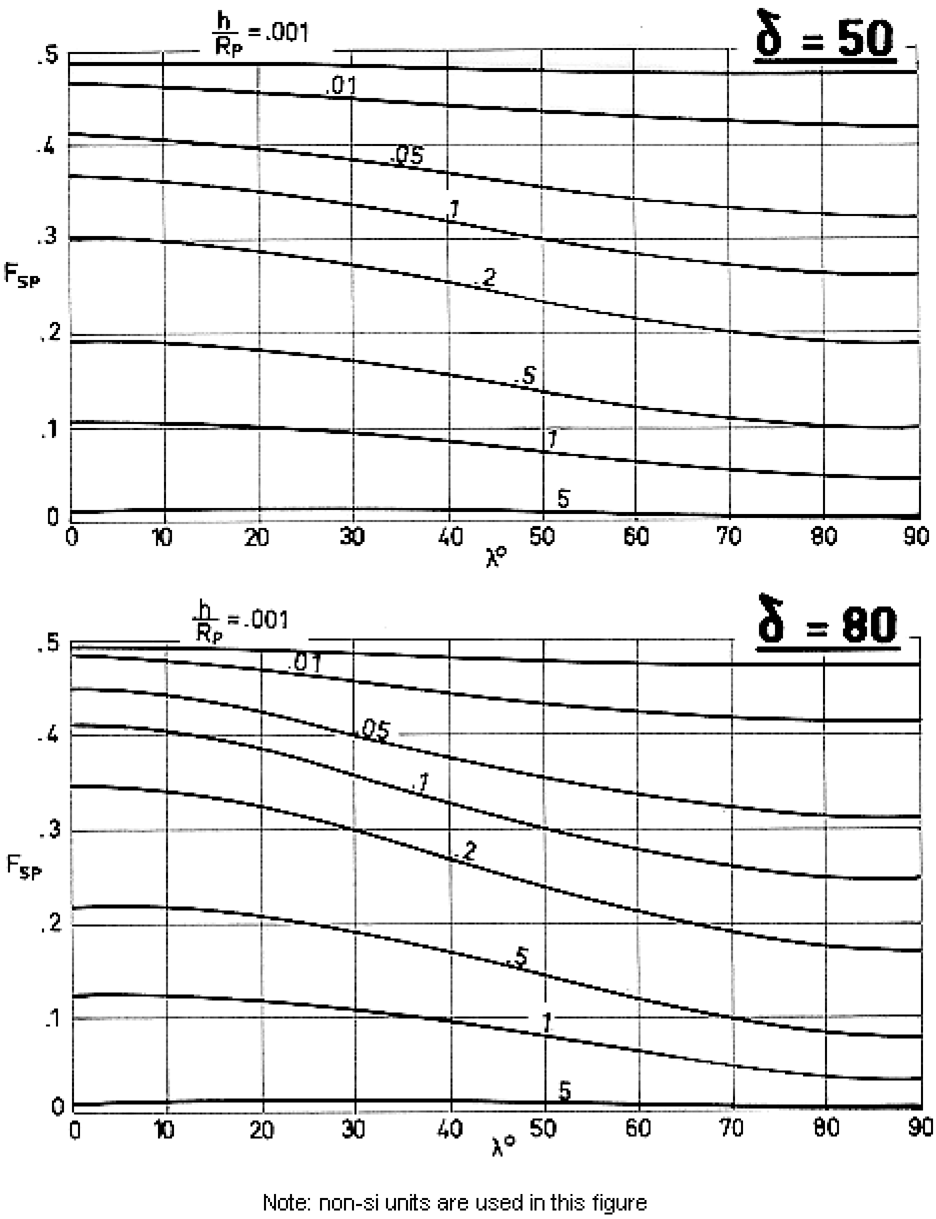

Figure 5-20: F_{SP} as a function of λ in the case of a finite height circular cone. Calculated by the compiler.

6 Albedo radiation

6.1 General

Albedo radiation is that part of the solar radiation incident upon the planet which is reflected or scattered by the planet surface and atmosphere (if existent).

Data on the equilibrium temperature of a satellite, heated by the albedo radiation from a planet, and cooled by radiation to the outer space, are presented in this Clause. These data are based on the assumptions a,b,d and e listed in clause 5.1. In addition, the planet is supposed to be a diffusely reflecting sphere.

The Spacecraft Albedo Radiation Equilibrium Temperature, T_{RA}, as given by

$T_{RA} = [(\alpha/\varepsilon)FT_A^4 + T_s^4]^{1/4}$

Where T_s is assumed to be zero as it has been indicated repeatedly. Values of T_{RA}/T_A vs. α/ε for arbitrary values of the albedo view factor, F, from spacecraft to planet are given in Figure 6-1. These values can be also used to estimate the effect on a sub satellite of the solar radiation reflected or scattered by a large satellite, provided that the above assumption hold.

T_{RA} as function of T_{RA}/T_A for albedo radiation from several planets is given in Figure 6-2. Albedo radiation from the Earth is considered in Figure 6-3. Finally, values of F in three simple cases are presented.

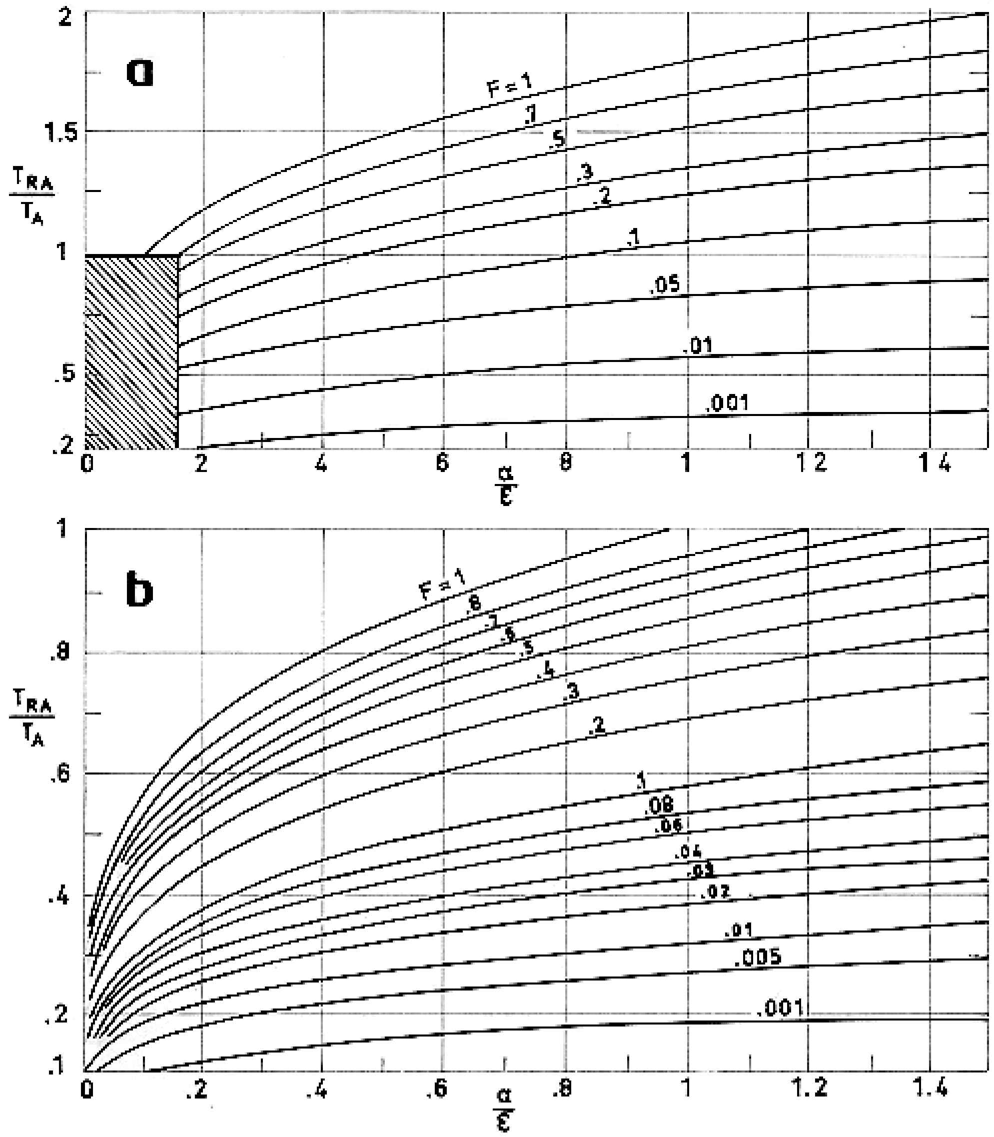

Note: non-si units are used in this figure

Figure 6-1: The ratio T_{RA} / T_A vs. the optical characteristics of the surface for different values of *F*. Shaded zone of *a* is enlarged in *b*. Calculated by the compiler.

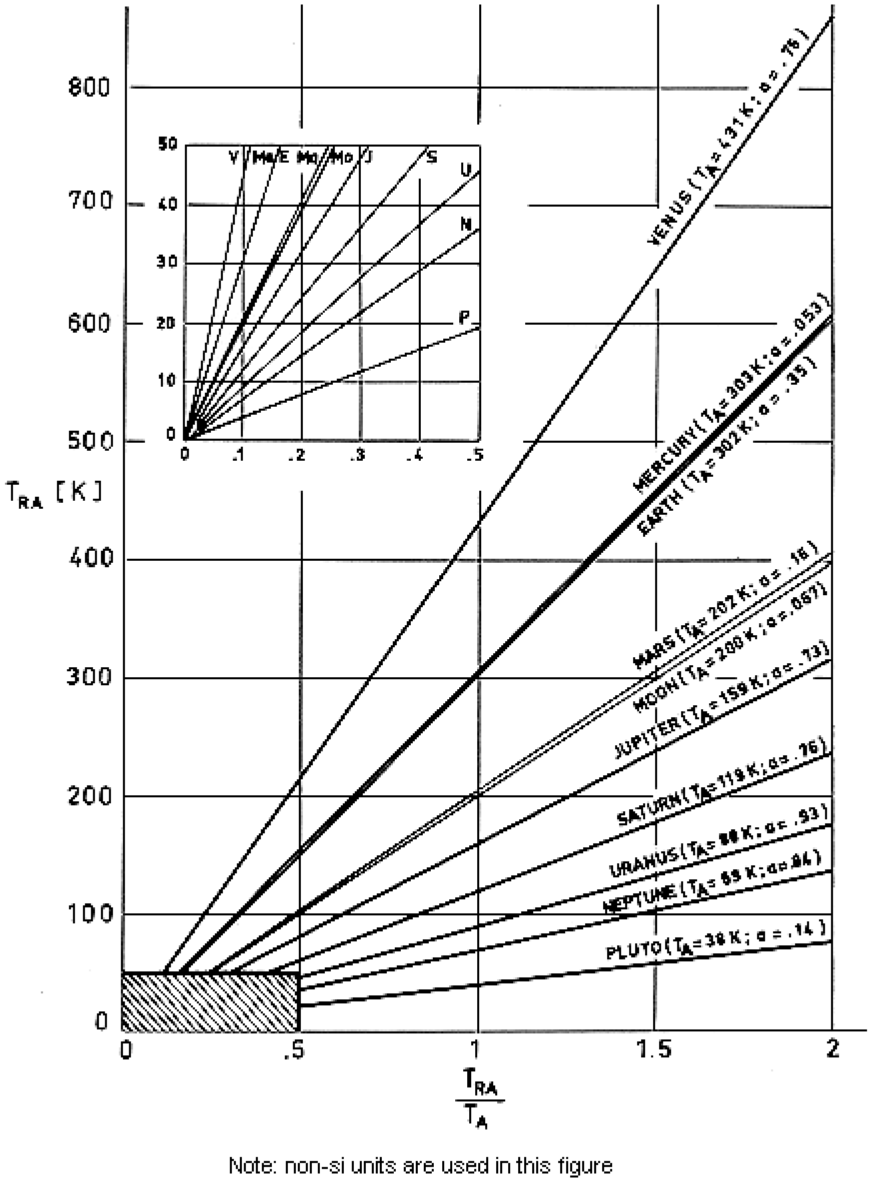

Figure 6-2: Albedo equilibrium temperature, T_{RA}, vs. dimensionless ratio T_{RA} / T_A. Incoming albedo from different planets. After Anderson (1969) [1].

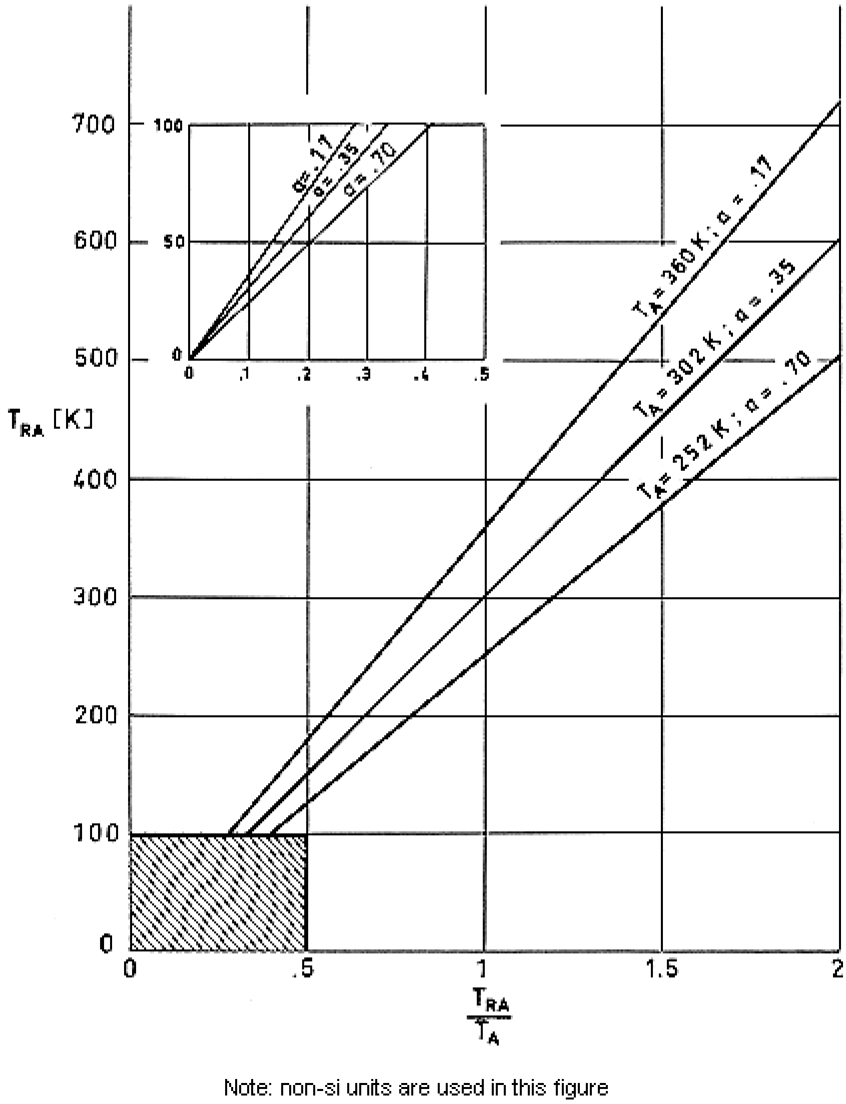

Figure 6-3: Different estimates of albedo equilibrium temperature T_{RA} ,vs. T_{RA} / T_A in case of the Earth. Calculated by the compiler.

Table 6-1: Relevant data on the Planets and the Moon.

	Distance to the sun $x10^{-9}$ [m]	Distance to the sun in AU	Radius of the planet $x10^{-3}$ [m]	Planet to earth radius ratio	Solar constant [$W.m^{-2}$]	Mean albedo
MERCURY	57,9	0,387	2330	0,3659	9034	0,053
VENUS	108,1	0,723	6100	0,9580	2588	0,76
EARTH	149,5	1,0	6367,5	1,0	1353	0,35
MARS	227,4	1,521	3415	0,5363	585	0,16
JUPITER	773,3	5,173	71375	11,2093	51	0,73
SATURN	1425,7	9,536	60500	9,5014	15	0,76
URANUS	2880,7	19,269	24850	3,9026	3,6	0,93
NEPTUNE	4490,1	30,034	25000	3,9262	1,5	0,84
PLUTO	5841,9	39,076	2930	0,4600	0,89	0,14
MOON	149,5	1,0	1738	0,2729	1353	0,067

NOTE 1 References: Kreith (1962) [10], Wolverton (1963) [13], Anderson (1969) [1].

6.2 Infinitely conductive planar surfaces

6.2.1 Flat plate absorbing and emitting on one side

Sketch:

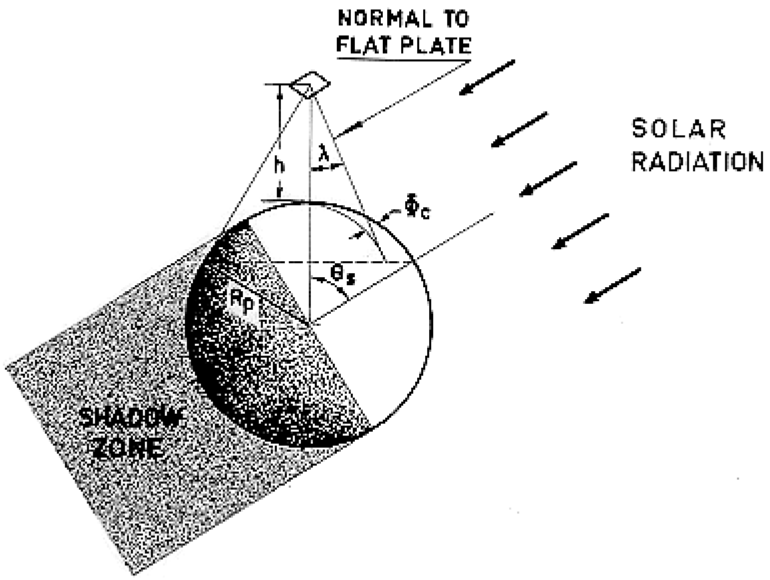

Formula: All results in the literature are obtained numerically.

Reference: Bannister (1965) [2].

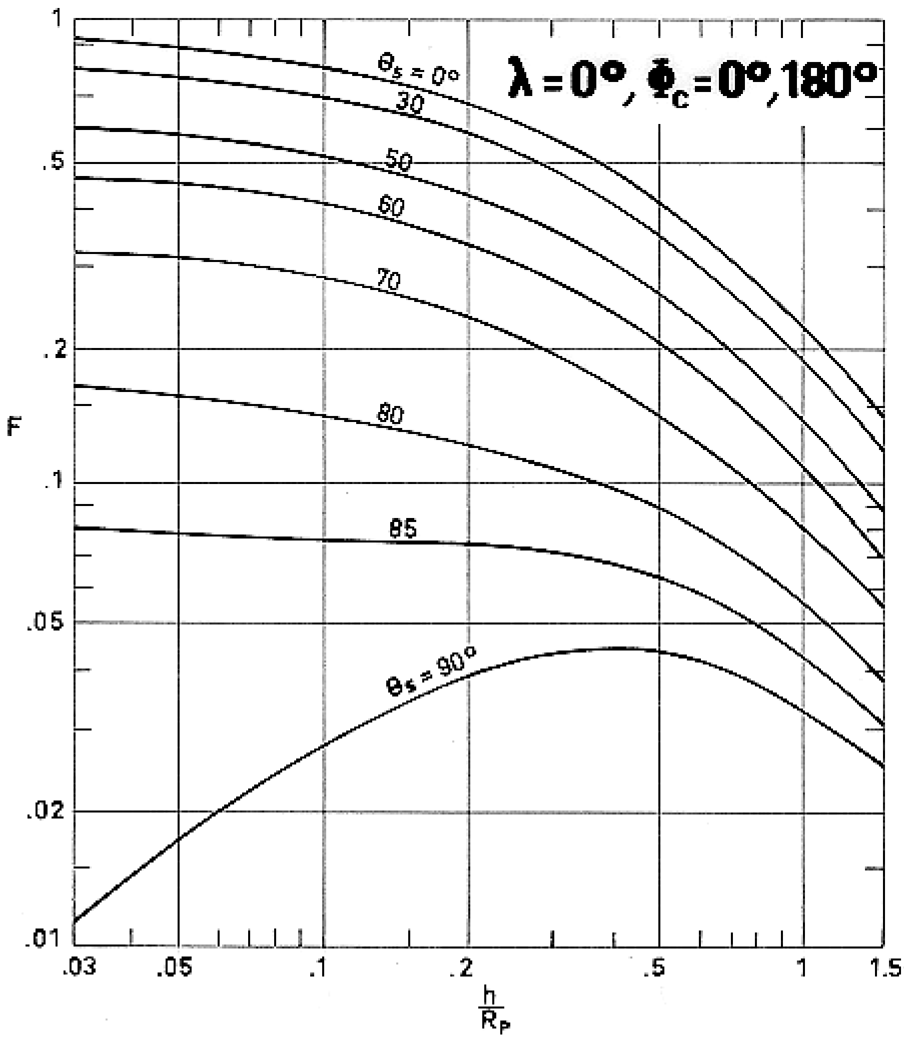

Note: non-si units are used in this figure

Figure 6-4: Albedo view factor *F* vs. h / R_P for different values of θ_s in the case of a flat plate ($\lambda = 0°$, $\phi_c = 180°$). From Bannister (1965) [2].

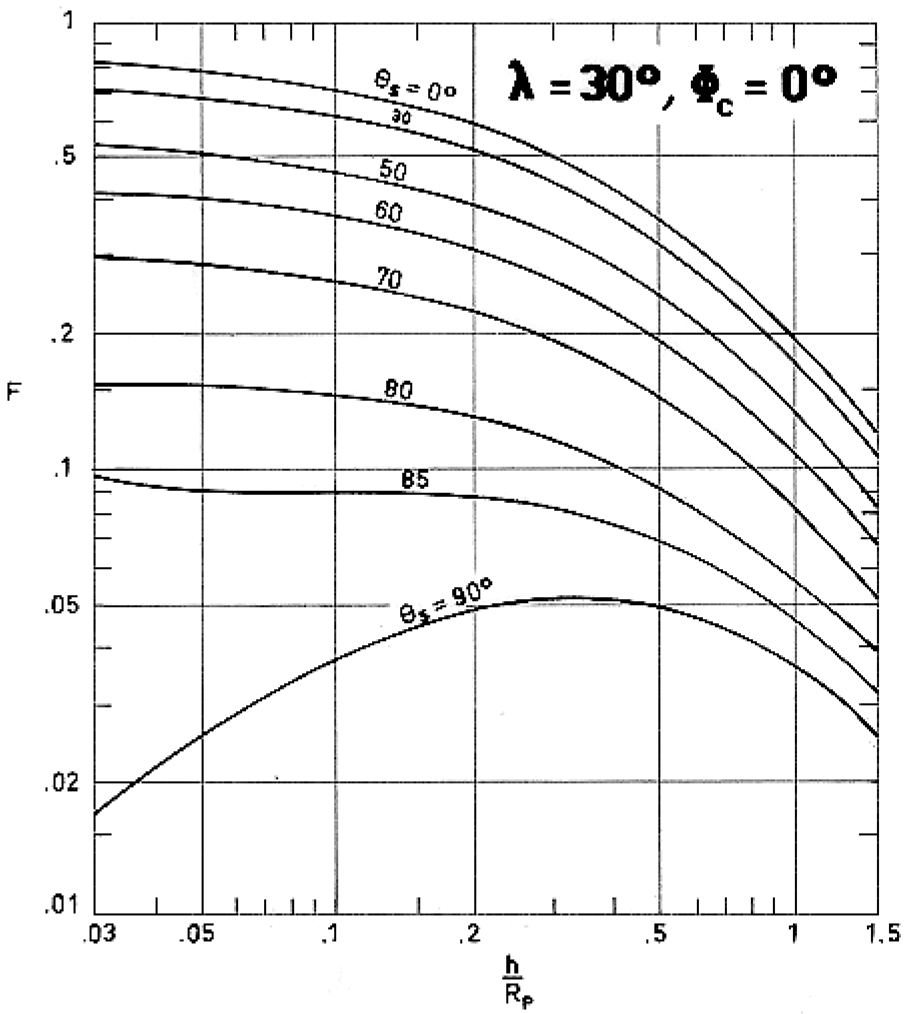

Note: non-si units are used in this figure

Figure 6-5: Albedo view factor *F* vs. *h* / R_P for different values of θ_s in the case of a flat plate (λ = 30°, ϕ_c = 0°). From Bannister (1965) [2].

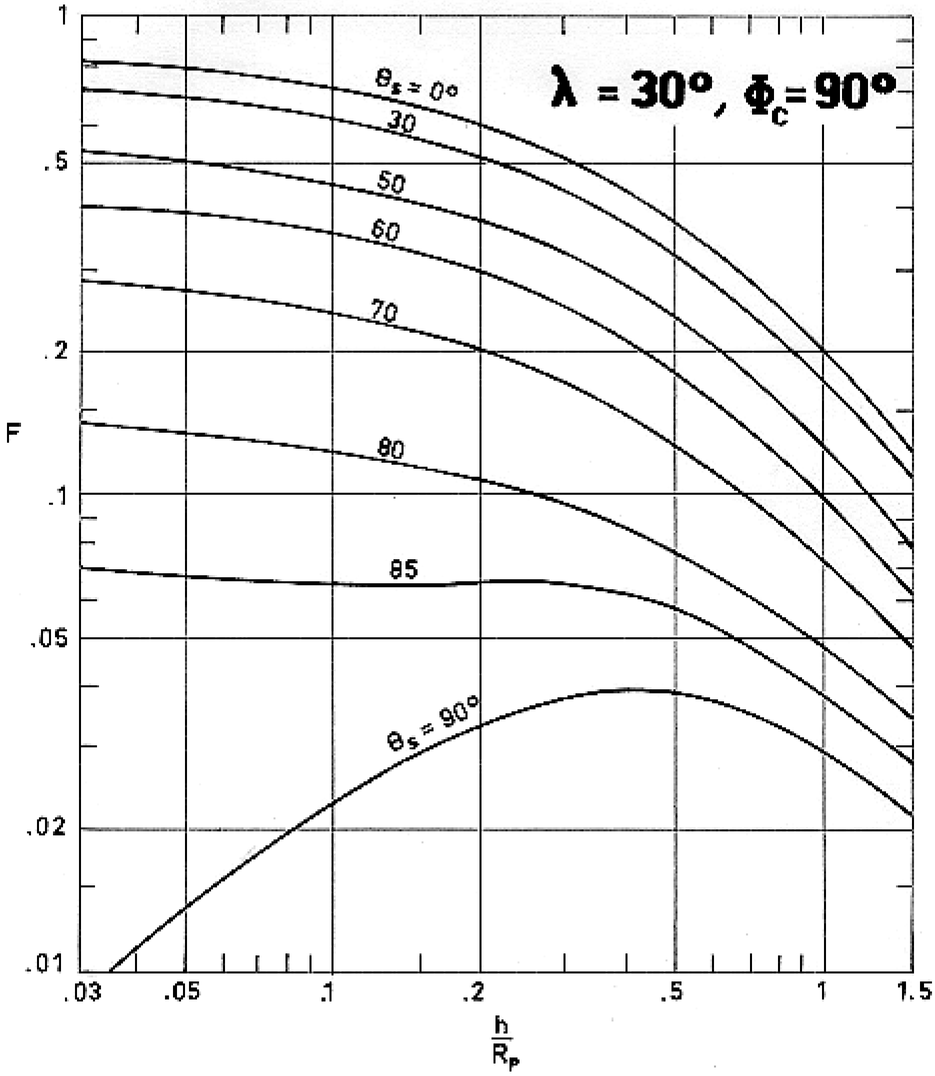

Note: non-si units are used in this figure

Figure 6-6: Albedo view factor *F* vs. h / R_P for different values of θ_S in the case of a flat plate (λ = 30°, ϕ_c = 90°). From Bannister (1965) [2].

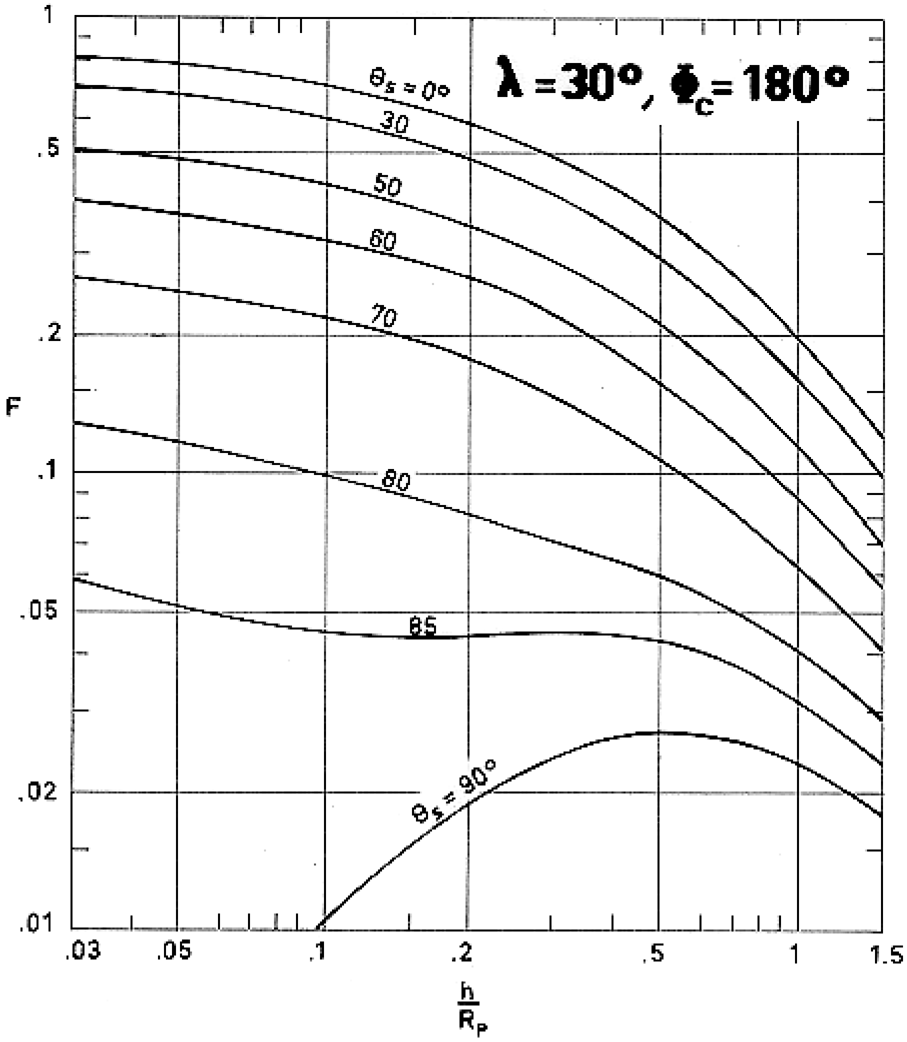

Note: non-si units are used in this figure

Figure 6-7: Albedo view factor *F* vs. h / R_P for different values of θ_S in the case of a flat plate (λ = 30°, ϕ_c = 180°). From Bannister (1965) [2].

6.3 Infinitely conductive spherical surfaces

6.3.1 Sphere

Sketch:

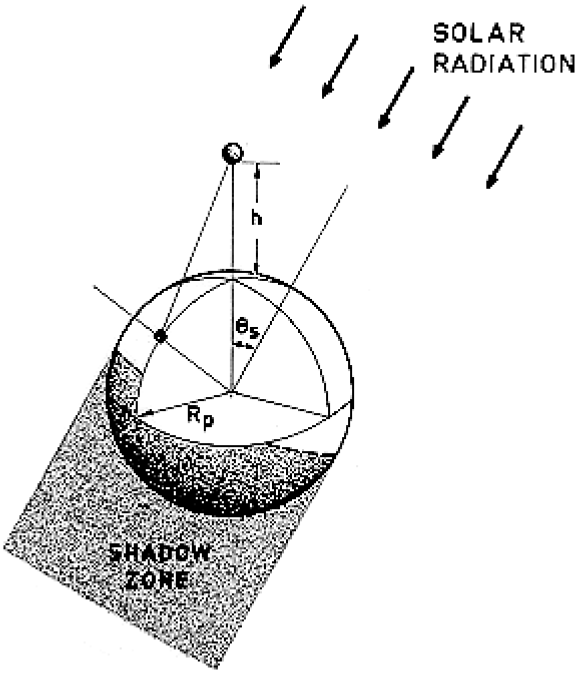

Formula: All results in the literature are obtained numerically.

Reference: Cunningham (1961) [6].

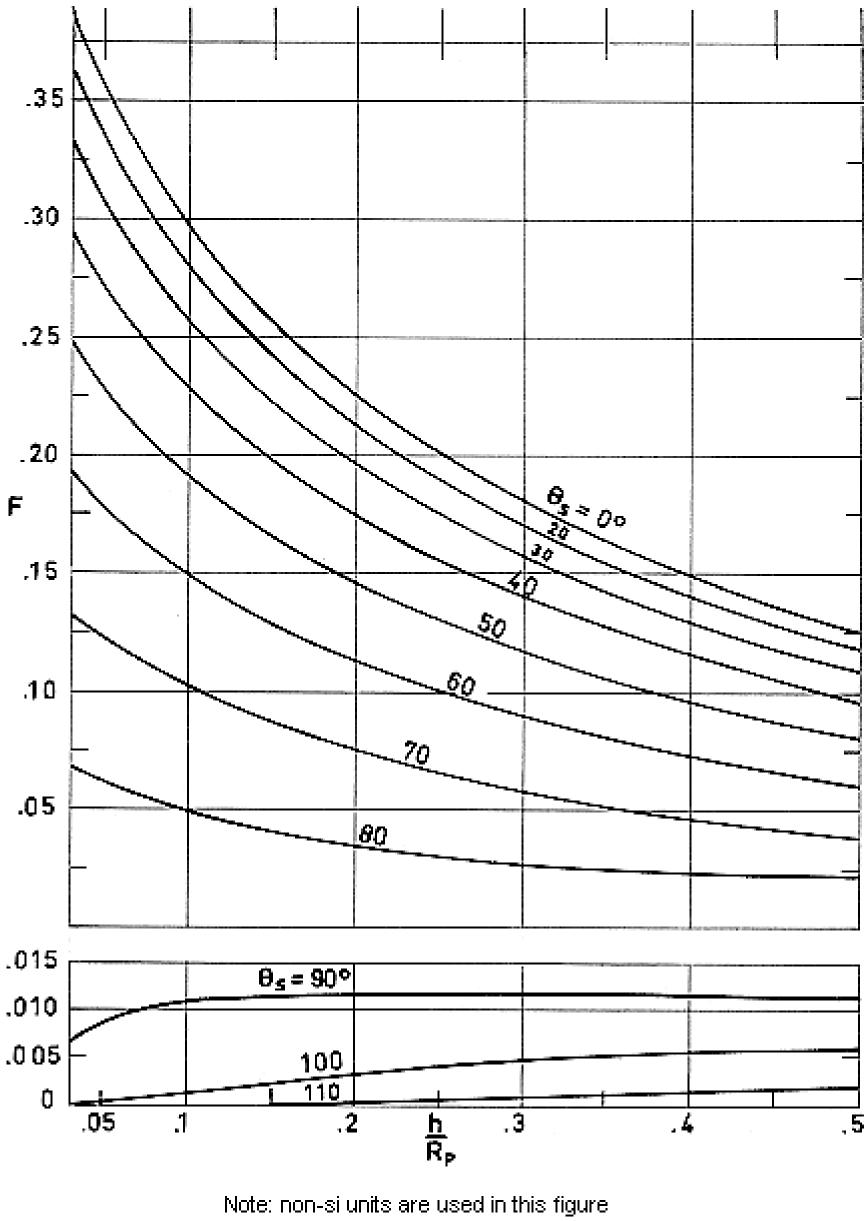

Figure 6-8: Albedo view factor *F* vs. *h* / R_P for different values of θ_S in the case of a sphere. From Cunningham (1961) [6].

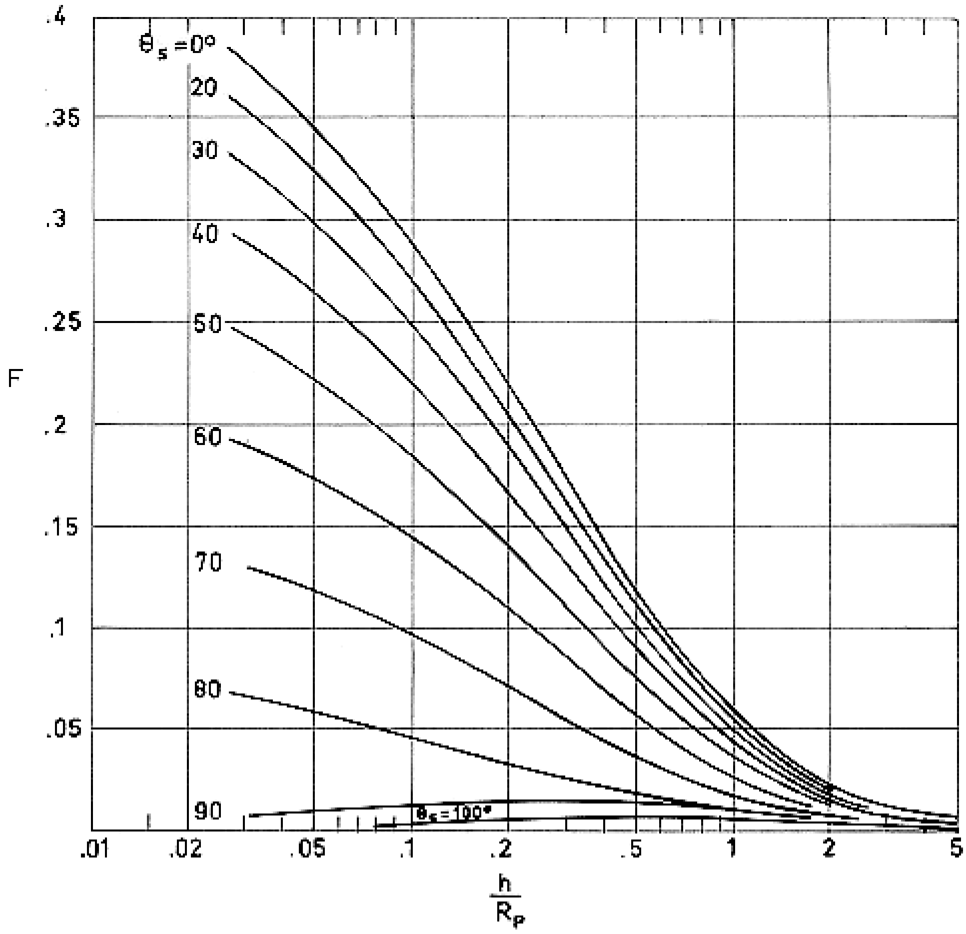

Note: non-si units are used in this figure

Figure 6-9: Albedo view factor *F* vs. *h* / R_P for different values of θ_S in the case of a sphere. From Cunningham (1961) [6].

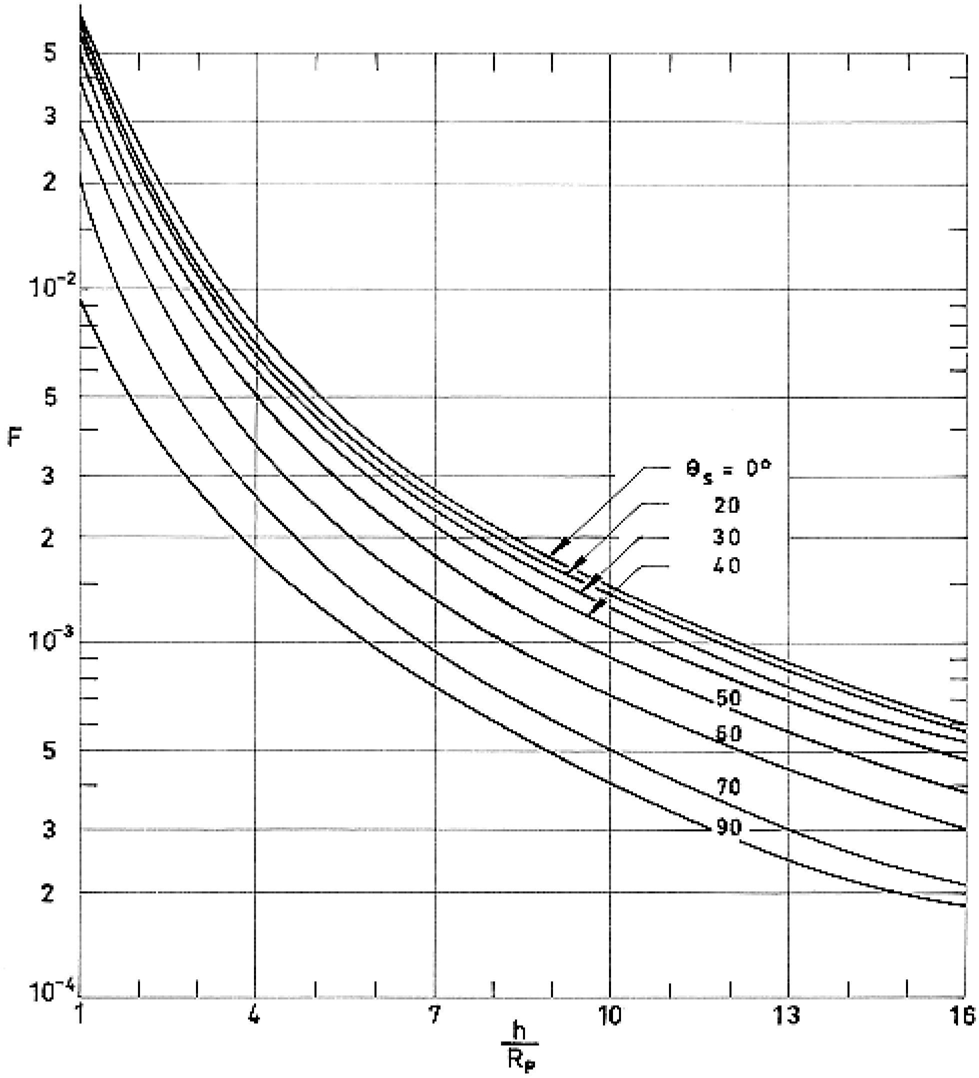

Figure 6-10: Albedo view factor F vs. h / R_P for different values of θ_S in the case of a sphere. Calculated by the compiler.

6.4 Infinitely conductive cylindrical surfaces

6.4.1 Circular cylinder with insulated bases

Sketch:

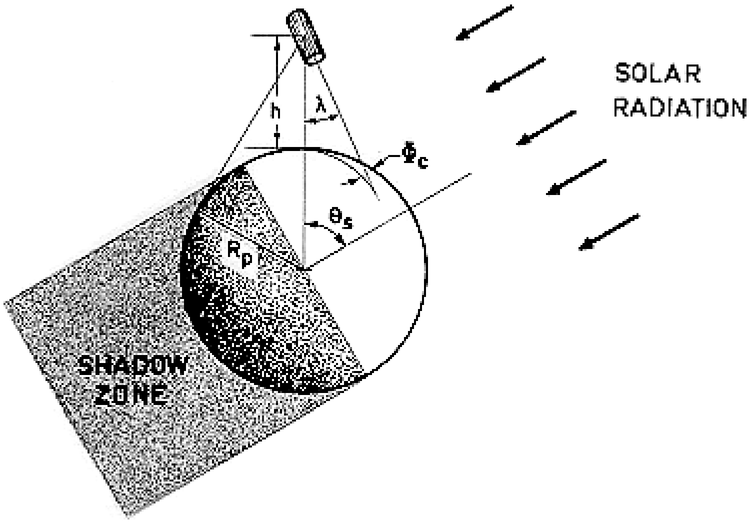

Formula: All results in the literature are obtained numerically.

Reference: Bannister (1965) [2].

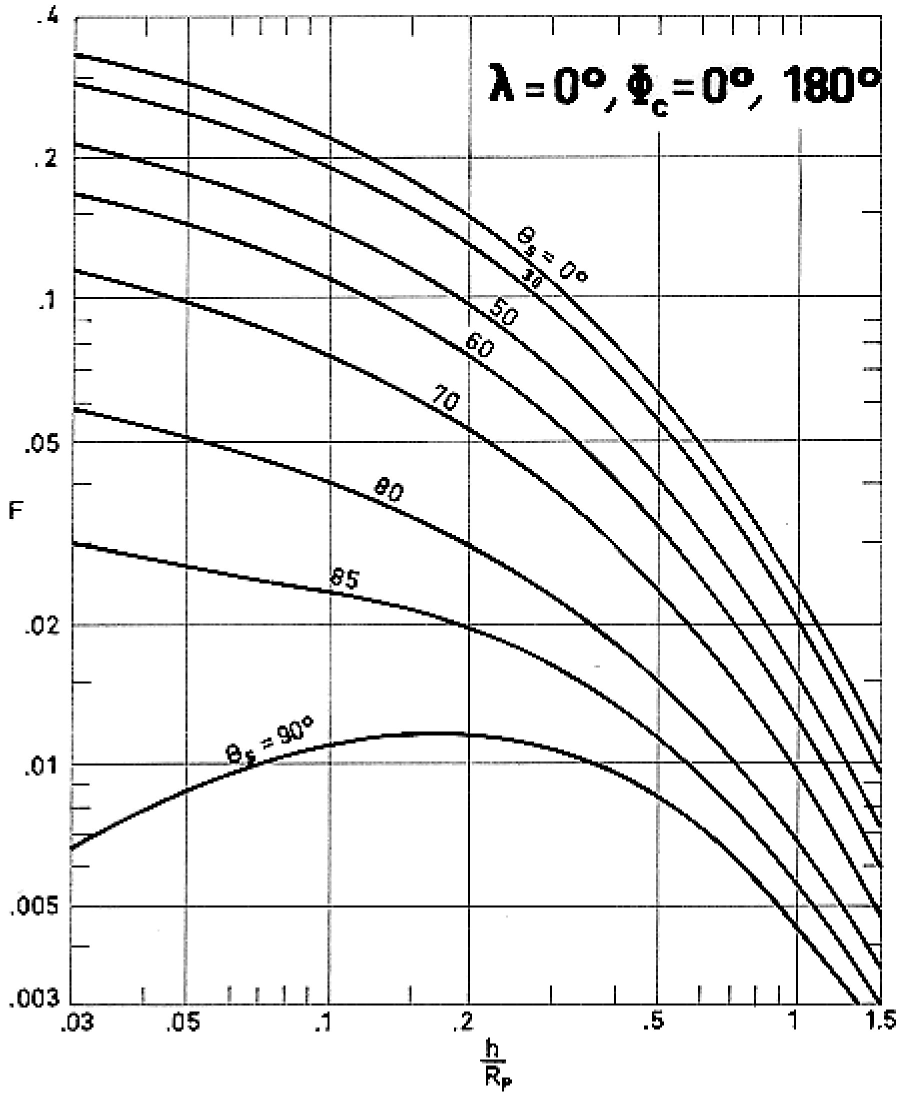

Note: non-si units are used in this figure

Figure 6-11: Albedo view factor *F* vs. *h* / R_P for different values of θ_S in the case of a cylinder (λ = 0°, ϕ_c = 0°, 180°). From Bannister (1965) [2].

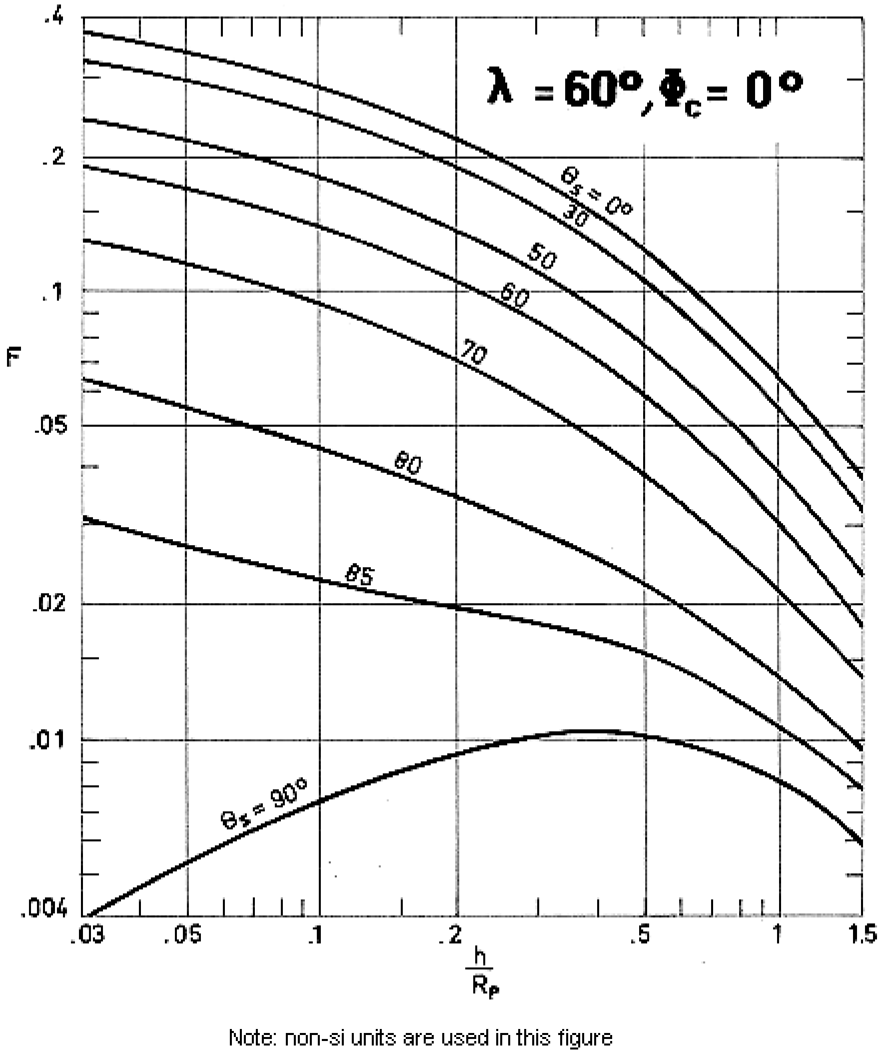

Figure 6-12: Albedo view factor F vs. h / R_P for different values of θ_S in the case of a cylinder (λ = 60°, ϕ_c = 0°). From Bannister (1965) [2].

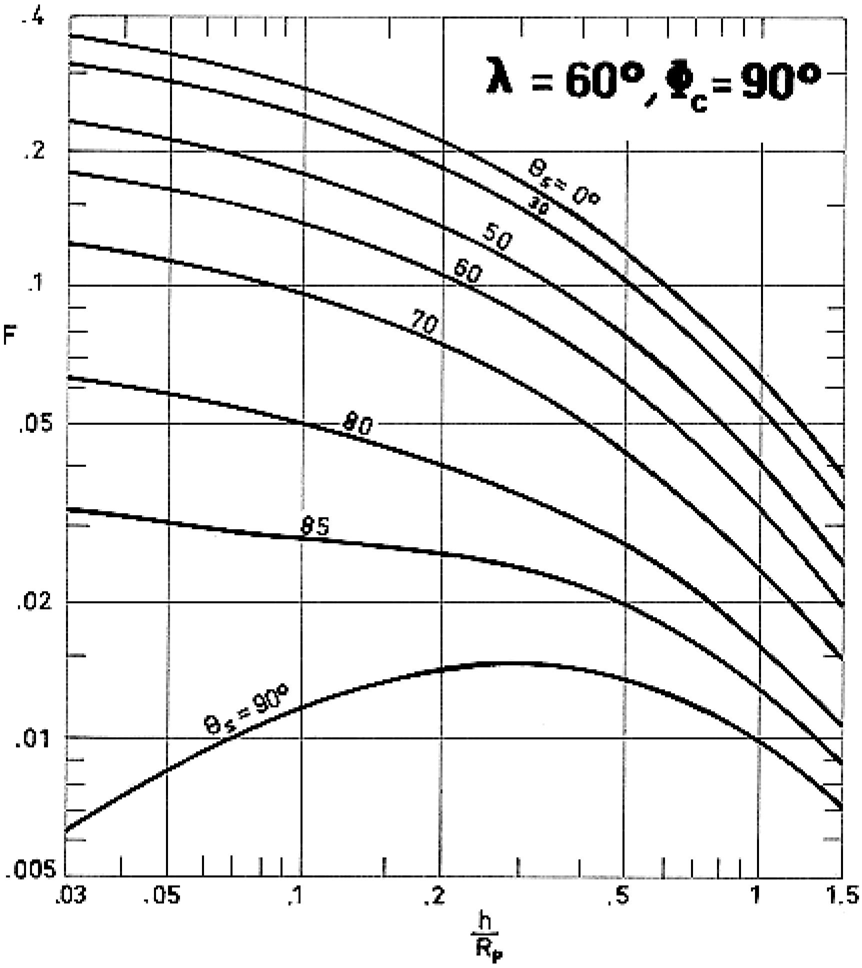

Note: non-si units are used in this figure

Figure 6-13: Albedo view factor *F* vs. h / R_P for different values of θ_S in the case of a cylinder ($\lambda = 60°$, $\phi_c = 90°$). From Bannister (1965) [2].

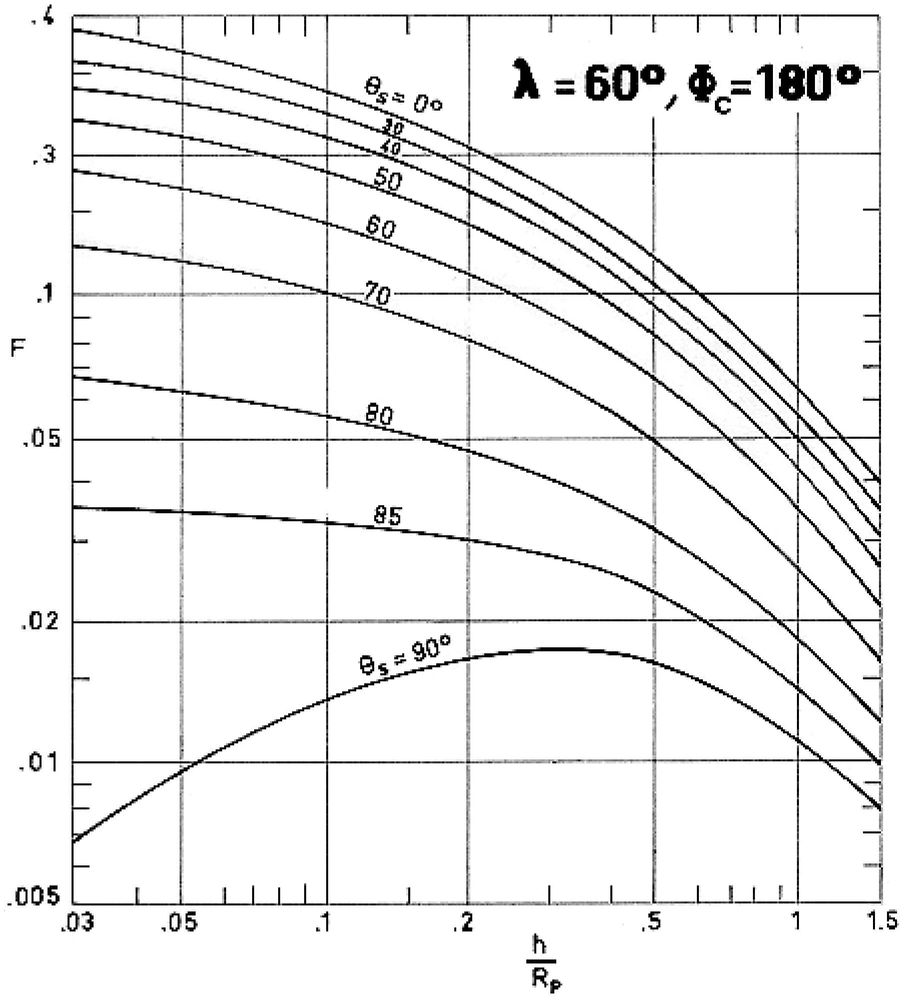

Note: non-si units are used in this figure

Figure 6-14: Albedo view factor F vs. h / R_P for different values of θ_S in the case of a cylinder (λ = 60°, ϕ_c = 180°). From Bannister (1965) [2].

Bibliography

[1] Anderson, A.D., "Nonpenetrating Radiations", in "Space Materials Handbook", J.B. Rittenhouse & J.B. Singletary, Eds., 3rd Edition, NASA SP-3051, 1969, pp. 25-35.

[2] Bannister, T.C., "Radiation Geometry Factor between the Earth and a Satellite", NASA TN D-2750, July 1965.

[3] Camack, W.G., "Albedo and Earth Radiation", in "Space Materials Handbook", C.G. Goetzel, J.B. Rittenhouse & J.B. Singletary, Eds., Addison-Wesley Publishing Co. Inc., Mass., 1965, pp. 31-49.

[4] Charnes, A., Raynor, S., "Solar Heating of a Rotating Cylindrical Space Vehicle", ARS Journal, Vol. 30, No. 5, May 1960, pp. 479-484.

[5] Clark, L.G., Anderson, E.C., "Geometric Shape Factors for Planetary-Thermal and Planetary-Refected radiation Incident upon Spinning and Non-Spinning Spacecraft", NASA TN D-2835, May 1965.

[6] Cunninghan, F.G., "Earth Reflected Solar Radiation Input to Spherical Satellites", NASA TN D-1099, October 1961.

[7] Fontana, A., "The Effect of Planetary Albedo on Solar Orientation of Spacecraft", NASA TN D-4133, September 1967.

[8] Gast, P.R., "Insolation of the Upper Atmosphere and of a Satellite", in "Scientific Uses of Earth Satellites", J.A. Van Allen, Ed., 2nd Edition, The University of Michigan Press, Ann Arbor, 1965.

[9] Johnson, F.S., "Solar Radiation", in "Satellite Environment Handbook", F.S. Johnson, Ed., 2nd Edition, Stanford University Press, Stanford, California, 1966, pp. 95-105.

[10] Kreith, F., "Radiation Heat Transfer for Spacecraft and Solar Power Plant Design", International Textbook Co., Scranton, Pennsylvania, 1962, pp. 57-79.

[11] Nichols, L.D., "Surface-Temperature Distribution on Thin-Walled Bodies Subjected to Solar Radiation in Interplanetary Space", NASA TN D-584, 1961.

[12] Watts, R.G., "Radiant Heat Transfer to Earth Satellites", Journal of Heat Transfer, Vol. 87c, No. 3, August 1965, pp. 369-373.

[13] Wolverton, R., "Flight Performance Handbook for Orbital Operations", John Wiley & Sons, Inc., New York, 1963, pp. B-14/B-15.